THE ELECTROMAGNETIC RADIATION FROM SIMPLE SOURCES IN THE PRESENCE OF A HOMOGENEOUS DIELECTRIC SPHERE

by

V. Bradford Mason

A dissertation submitted in partial fulfillment
of the requirements for the degree of
Doctor of Philosophy
(Electrical Engineering)
in The University of Michigan
1972

Doctoral Committee:

Professor Chen-To Tai, Chairman
Professor Chiao-Min Chu
Associate Professor Jack L. Goldberg
Professor Thomas B. A. Senior
Professor Charles B. Sharpe

RL-562 = RL-562

ABSTRACT

THE ELECTROMAGNETIC RADIATION FROM SIMPLE SOURCES IN THE PRESENCE OF A HOMOGENEOUS DIELECTRIC SPHERE

by

V. Bradford Mason

Chairman: Chen-To Tai

In this research the effect of a homogeneous dielectric sphere on the electromagnetic radiation from simple sources is treated as a boundary-value problem, and the solution is obtained by the technique of dyadic Green's functions. Exact representations of the electric fields in the various regions due to a source located inside, outside, or on the surface of a dielectric sphere are formulated.

Particular attention is given to the effect of sphere size, source location, dielectric constant, and dielectric loss on the radiation patterns and directivity of small spheres (less than 5 wavelengths in diameter) using the Huygens' source excitation. The computed results are found to closely agree with those measured for waveguide-excited plexiglas spheres. Radiation patterns for an extended Huygens' source and for curved electric dipoles located on the sphere's surface are also presented.

The resonance phenomenon associated with the dielectric sphere is studied in terms of the modal representation of the radiated fields. It is found that when the sphere is excited at certain frequencies, much of the energy is radiated into the sidelobes. The addition of a moderate amount of dielectric loss, however, quickly attenuates this resonance effect.

The methods of geometrical optics are used to interpret many of the results.

A computer program which may be used to calculate the directivity and radiation pattern of a Huygens' source located inside or on the surface of a lossy dielectric sphere is listed in the Appendix.

ACKNOWLEDGMENTS

The author wishes to express his gratitude to all the members of his Doctoral Committee for their helpful comments and criticisms. The author is particularly indebted to his Chairman, Professor Chen-To Tai, for his invaluable guidance and encouragement. Special thanks are due to William F. Croswell for providing the experimental measurements used in this research. The author also wishes to express his thanks to Marcia P. Neeley for reading the draft and making helpful suggestions, and to Catherine Rader for typing the manuscript.

Finally, the author wishes to express his appreciation to his wife, Louise, for her support and encouragement throughout this investigation.

TABLE OF CONTENTS

Table of Contents (cont.)

LIST OF TABLES

LIST OF ILLUSTRATIONS

List of Illustrations (cont.)

List of Illustrations (cont.)

LIST OF APPENDICES

Chapter I

INTRODUCTION

Recent investigation by Croswell and Chatterjee (1972) has shown that a small homogeneous dielectric sphere may be used to focus the radiation from an open-ended waveguide into a relatively directive beam, and hence would be useful as an antenna.

Historically, large spherical lenses have been of interest for microwave antennas because their symmetry permits the formation of beams in any direction by displacement of source alone. Perhaps the best known lens of this type was introduced by Luneberg (1944). It has a radially varying dielectric constant and will focus rays emanating from a point source on the surface into a collimated beam of parallel rays at the opposite side of the lens. The Luneberg lens, however, is difficult to fabricate in practice. A survey of other inhomogeneous spherical lenses is given by Johnson (1964).

The imaging properties of the homogeneous dielectric sphere has been investigated by Bekefi and Farnell (1956), using the methods of geometrical optics and the diffraction theory of optical aberrations. Their results suggested that spheres of small refractive index, less than 30 wavelengths in diameter, may be used to produce good diffraction images of point sources.

Assaly (1958) measured patterns for heptane ($\epsilon_r = 1.94$) filled spherical shells 13.3 and 33.3 wavelengths in diameter In this experiment, the lens was supported by a conducting screen and illuminated by a waveguide displaced several wavelengths from the sphere. Data for a 12.4-wavelength diameter sphere ($\epsilon_r = 2.34$) has also been presented by Cheston and Luoma (1963). Their results confirmed that the homogeneous dielectric sphere may be used to produce desirable radiation patterns despite the presence of a large amount of spherical aberration.

Using a somewhat different arrangement, Meinke (1970) measured patterns and gain for a monopole formed on a small hemisphere (less than 1-1/4 wavelengths in diameter) over a ground plane. In his work, using dielectric constants

between 2.2 and 11.5, Meinke noted that the gain tended to oscillate around that which could be obtained using a uniformly excited circular aperture, due to resonances inside the hemisphere.

The far-zone antenna patterns for spheres ranging from about 2 - 4 wavelengths in diameter have been calculated by Ryan and Cain (1971), using ray optics and the radiation integral. Their results for the homogeneous sphere were fairly close to those of the Luneberg lens. Extensive measurements have also been made on a fused silica ($\epsilon_r = 3.5$) lens (Ryan and Cain, 1972).

Finally, recent measurements by Croswell and Chatterjee, some of which have been published (1972), have shown that waveguide excited plexiglas ($\epsilon_r = 2.57$) spheres 2 - 4 wavelengths in diameter exhibit properties desirable for feed antennas used to illuminate paraboloidal reflectors.

Although considerable attention has been given to the study and measurement of scattering from dielectric spheres (see, for example, Inada and Plonus, 1970; Barrick, 1970), no rigorous treatment using electromagnetic theory has been given to the spherical homogeneous dielectric lens as an antenna element.

In this presentation, the radiation from a source in the presence of a dielectric sphere is treated as a boundary-value problem, and the solution is obtained using the dyadic Green's function technique. Particular emphasis is placed on the Huygens' source which is used to model the waveguide excitation of spheres.

Throughout this work the source, together with the dielectric sphere, is considered as an antenna, and hence the properties such as radiation resistance, directivity, and antenna efficiency are studied as well as the radiation pattern.

Chapter II

DYADIC GREEN'S FUNCTIONS PERTAINING TO A SOURCE IN THE PRESENCE OF A DIELECTRIC SPHERE

2.1. Introduction

The effect of a dielectric sphere on the radiation from an antenna may be investigated as a boundary-value problem under the assumption that the current distribution is a known function of position. The solution to this problem may be obtained by the technique of the dyadic Green's functions.

In this chapter, the boundary conditions are first presented. Then, starting with the free-space dyadic Green's function in the spherical system, the functions of the third kind, $\overline{\overline{G}}_3$, are formulated using the method of scattering superposition. Subsequently the dyadic Green's functions of the fourth kind, $\overline{\overline{G}}_4$, are derived from $\overline{\overline{G}}_3$ using the principal of duality. In the next chapter, $\overline{\overline{G}}_3$ and $\overline{\overline{G}}_4$ will be used to obtain expressions for the fields due to electric and magnetic current sources, respectively.

Although the functions presented here form the groundwork for the derivation of the fields in Chapter III, they should also find application to most problems dealing with dielectric spheres.

2.2. The Dyadic Green's Functions Pertaining to an Electric Current Source in the Presence of a Dielectric Sphere

Figure 2-1 shows the geometry of a dielectric sphere with an externally located electric current source. The regions exterior and interior to the sphere are characterized by different constitutive parameters and, therefore, different propagation constants k_1 and k_2, where

$$k_1 = \omega\sqrt{\mu_1\epsilon_1} \qquad \text{(Region I, } R > a\text{)}$$

$$k_2 = \omega\sqrt{\mu_2\epsilon_2} \qquad \text{(Region II, } R < a\text{)}.$$

Here μ_2 and ϵ_2 denote, respectively, the permeability and permittivity of the sphere, which may be complex. For most applications, Region I will be free space, and hence $\mu_1 = \mu_0$ and $\epsilon_1 = \epsilon_0$.

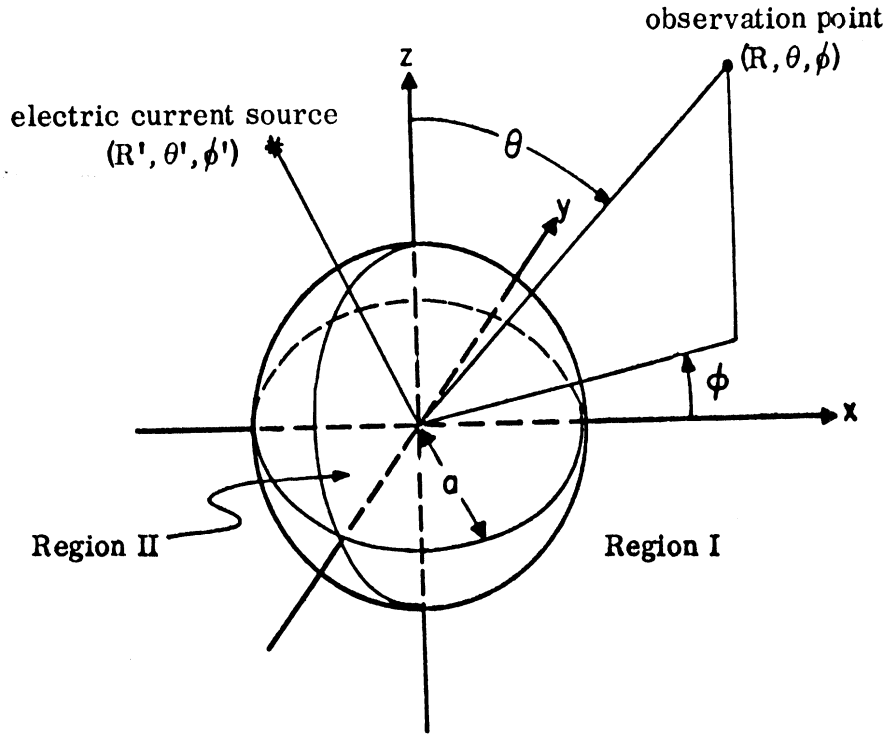

FIG. 2-1: GEOMETRY FOR A CURRENT SOURCE IN THE PRESENCE OF A DIELECTRIC SPHERE.

With the electric current source $\bar{J}(\bar{R}')$ located in Region I, the electric fields in Regions I and II may be expressed by

$$\bar{E}(\bar{R}) = i\omega\mu_1 \iiint \bar{\bar{G}}_3^{(11)}(\bar{R}|\bar{R}') \cdot \bar{J}(\bar{R}')dV' \qquad \text{Region I} \qquad (2.1)$$

$$\bar{E}(\bar{R}) = i\omega\mu_1 \iiint \bar{\bar{G}}_3^{(21)}(\bar{R}|\bar{R}') \cdot \bar{J}(\bar{R}')dV' \qquad \text{Region II} \qquad (2.2)$$

where $\bar{\bar{G}}_3(\bar{R}|\bar{R}')$ is the dyadic Green's function of the third kind and the harmonic time factor $e^{-i\omega t}$ has been suppressed. The first and second numbers in the superscripts of the Green's functions in the above equations denote the regions of the observation and source points, respectively. Those functions are solutions to the vector wave equations

$$\nabla \times \nabla \times \bar{\bar{G}}_3 - k_1^2 \bar{\bar{G}}_3 = \bar{\bar{I}} \delta(\bar{R} - \bar{R}') \quad , \qquad R \geq a$$

$$\nabla \times \nabla \times \bar{\bar{G}}_3 - k_2^2 \bar{\bar{G}}_3 = 0 \quad , \qquad R \leq a \quad . \tag{2.3}$$

Besides satisfying the radiation condition at infinity,

$$\lim_{R \to \infty} R\left[\nabla \times \bar{\bar{G}}_3(\bar{R}|\bar{R}') - ik\hat{R} \times \bar{\bar{G}}_3(\bar{R}|\bar{R}')\right] = 0 \quad ,$$

$\bar{\bar{G}}_3$ also satisfies the boundary conditions at the surface of the sphere

$$\hat{n} \times \bar{\bar{G}}_3(\bar{R}|\bar{R}')\Big|_{R=a_-} = \hat{n} \times \bar{\bar{G}}_3(\bar{R}|\bar{R}')\Big|_{R=a_+}$$

$$\frac{1}{\mu_1} \hat{n} \times \nabla \times \bar{\bar{G}}_3(\bar{R}|\bar{R}')\Big|_{R=a_-} = \frac{1}{\mu_2} \hat{n} \times \nabla \times \bar{\bar{G}}_3(\bar{R}|\bar{R}')\Big|_{R=a_+} \quad . \tag{2.4}$$

The simplest way to find $\bar{\bar{G}}_3(\bar{R}|\bar{R}')$ is to use the method of scattering superposition in which we let the fields consist of a sum of incident and scattered waves. With this method, the form of the scattered waves are first constructed using eigenfunctions which will satisfy the boundary conditions at the sphere surface as well as having the proper form at $R = 0$ and $R = \infty$. The coefficients of the scattered waves are then determined by matching the boundary conditions on the surface of the sphere.

Thus $\bar{\bar{G}}_3(\bar{R}|\bar{R}')$ is treated as consisting of two parts

$$\bar{\bar{G}}_3^{(11)}(\bar{R}|\bar{R}') = \bar{\bar{G}}_0(\bar{R}|\bar{R}') + \bar{\bar{G}}_{3s}(\bar{R}|\bar{R}') \quad , \qquad R \geq a \tag{2.5}$$

$$\bar{\bar{G}}_3^{(21)}(\bar{R}|\bar{R}') = G_{3s}^{(21)}(\bar{R}|\bar{R}') \quad , \qquad R \leq a \quad . \tag{2.6}$$

Here $\bar{\bar{G}}_0(\bar{R}|\bar{R}')$ denotes the free space Green's function pertaining to an infinite region with the same constitutive parameters as Region I, and $\bar{\bar{G}}_{3s}(\bar{R}|\bar{R}')$ represents the part of the wave scattered from the sphere. $\bar{\bar{G}}_{3s}^{(21)}(\bar{R}|\bar{R}')$ is used to denote the Green's function internal to the sphere since only a scattered field will be present in this region.

The free space Green's function for this problem is given by Tai (1971)

as:

$$\bar{\bar{G}}_0(\bar{R}|\bar{R}') = \frac{ik_1}{4\pi}\sum_{n=1}^{\infty}\sum_{m=0}^{n}(2-\delta_0)\frac{2n+1}{n(n+1)}\frac{(n-m)!}{(n+m)!}$$

$$\begin{cases} \bar{M}^{(1)}_{\substack{e\\o}mn}(k_1)\bar{M}'_{\substack{e\\o}mn}(k_1)+\bar{N}^{(1)}_{\substack{e\\o}mn}(k_1)\bar{N}'_{\substack{e\\o}mn}(k_1) \ , & R>R' \\ \bar{M}_{\substack{e\\o}mn}(k_1)\bar{M}'^{(1)}_{\substack{e\\o}mn}(k_1)+\bar{N}_{\substack{e\\o}mn}(k_1)\bar{N}'^{(1)}_{\substack{e\\o}mn}(k_1) \ , & R<R' \end{cases} \qquad (2.7)$$

where $$\delta_0 = \begin{cases} 1, & m=0 \\ 0, & m\neq 0 \end{cases}$$

and

$$\bar{M}_{\substack{e\\o}mn}(k) = j_n(kR)\left[\mp\frac{m}{\sin\theta}P_n^m(\cos\theta)\begin{matrix}\sin\\\cos\end{matrix}m\phi\hat{\theta} - \frac{\partial P_n^m(\cos\theta)}{\partial\theta}\begin{matrix}\cos\\\sin\end{matrix}m\phi\hat{\phi}\right] \qquad (2.8)$$

$$\bar{N}_{\substack{e\\o}mn}(k) = \frac{n(n+1)}{kR}j_n(kR)P_n^m(\cos\theta)\begin{matrix}\cos\\\sin\end{matrix}m\phi\hat{R} + \frac{1}{kR}\frac{\partial}{\partial R}\left[Rj_n(kR)\right]\cdot$$

$$\left[\frac{\partial P_n^m(\cos\theta)}{\partial\theta}\begin{matrix}\cos\\\sin\end{matrix}m\phi\hat{\theta} \mp m\frac{P_n^m(\cos\theta)}{\sin\theta}m\phi\hat{\phi}\right] . \qquad (2.9)$$

The two sets of spherical vector wave functions, represented by $\bar{M}$ and $\bar{N}$ in (2.8) and (2.9), are solutions to the homogeneous vector wave equation

$$\nabla\times\nabla\times\bar{F} - k^2F = 0$$

as shown by Stratton (1941, p. 415), and also satisfy the symmetrical relations

$$\bar{N}_{\substack{e\\o}mn}(k) = \frac{1}{k}\nabla\times\bar{M}_{\substack{e\\o}mn}(k)$$

$$\bar{M}_{\substack{e\\o}mn}(k) = \frac{1}{k}\nabla\times\bar{N}_{\substack{e\\o}mn}(k) . \qquad (2.10)$$

In (2.8) and (2.9), $j_n(kR)$ is used to denote the spherical Bessel function of order n, and $P_n^m(\cos\theta)$ represents the associated Legendre function of degree

n and order m. The expressions in (2.7) with superscript (1) are obtained from (2.8) and (2.9) by replacing the spherical Bessel functions with spherical Hankel functions of the first kind, $h_n^{(1)}(kR)$. A prime is used on a function to denote that it is defined with respect to the primed coordinate variables (R', θ', ϕ') pertaining to the $\bar{R}'$ vector.

In constructing $\bar{\bar{G}}_3(\bar{R}|\bar{R}')$ from the wave functions we make the following observations:

1. For the source located exterior to the sphere, the posterior parts of $\bar{\bar{G}}_{3s}^{(11)}(\bar{R}|\bar{R}')$ and $\bar{\bar{G}}_{3s}^{(21)}(\bar{R}|\bar{R}')$ must be the same as $\bar{\bar{G}}_0(\bar{R}|\bar{R}')$ evaluated at $R < R'$. This is necessary for us to match the boundary conditions at the sphere surface.
2. The propagation constants k_1 and k_2 must be used in the anterior parts of $\bar{\bar{G}}_{3s}^{(11)}(\bar{R}|\bar{R}')$ and $\bar{\bar{G}}_{3s}^{(21)}(\bar{R}|\bar{R}')$, respectively, because of the regions in which the observations points are located.
3. The spherical Hankel functions must be used in the anterior parts of $\bar{\bar{G}}_{3s}^{(11)}(\bar{R}|\bar{R}')$ because these functions represent outward traveling waves.
4. Finally, since the fields are finite at the origin, the anterior parts of $\bar{\bar{G}}_{3s}^{(21)}(\bar{R}|\bar{R}')$ must be constructed using the spherical Bessel functions.

In keeping with these requirements we let

$$\bar{\bar{G}}_{3s}^{(11)}(\bar{R}|\bar{R}') = \frac{ik_1}{4\pi} \sum_{n=1}^{\infty} \sum_{m=0}^{n} (2-\delta_0) \frac{2n+1}{n(n+1)} \frac{(n-m)!}{(n+m)!}$$

$$\left[a_{\substack{e\\o}mn}^{(1)} \bar{M}_{\substack{e\\o}mn}^{(1)}(k_1) \bar{M}'^{(1)}_{\substack{e\\o}mn}(k_1) + b_{\substack{e\\o}mn}^{(1)} \bar{N}_{\substack{e\\o}mn}^{(1)}(k_1) \bar{N}'^{(1)}_{\substack{e\\o}mn}(k_1) \right] \qquad (2.11)$$

and

$$\overline{\overline{G}}_{3s}^{(21)}(\bar{R}|\bar{R}') = \frac{ik_1}{4\pi}\sum_{n=1}^{\infty}\sum_{m=0}^{n}(2-\delta_0)\,\frac{2n+1}{n(n+1)}\,\frac{(n-m)!}{(n+m)!}$$

$$\left[c_{\substack{e\\o}mn}^{(1)}\,\bar{M}_{\substack{e\\o}mn}(k_2)\bar{M}'^{(1)}_{\substack{e\\o}mn}(k_1)+d_{\substack{e\\o}mn}^{(1)}\,\bar{N}_{\substack{e\\o}mn}(k_2)\bar{N}'^{(1)}_{\substack{e\\o}mn}(k_1)\right] . \qquad (2.12)$$

The scattering coefficients a, b, c and d in the above equations, in general, will be complex quantities and represent the magnitude and phase of the sphere's contribution to the total fields. The superscript (1) on these coefficients denotes that they are defined for the source located in Region I, and should not be confused with the meaning of a superscript on a spherical wave function.

Since the tangential components of the resulting $\bar{E}$ and $\bar{H}$ fields must be continuous across the sphere surface, we apply the boundary conditions (2.4) which for our problem become

$$\left.\begin{aligned}\hat{R}\times\overline{\overline{G}}_3^{(11)}(\bar{R}|\bar{R}') &= \hat{R}\times\overline{\overline{G}}_3^{(21)}(\bar{R}|\bar{R}')\\ \frac{1}{\mu_1}\hat{R}\times\nabla\times\overline{\overline{G}}_3^{(11)}(\bar{R}|\bar{R}') &= \frac{1}{\mu_2}\hat{R}\times\overline{\overline{G}}_3^{(21)}(\bar{R}|\bar{R}')\end{aligned}\right\} R = a . \qquad (2.13)$$

Solving the above equations for the coefficients, we find $a_{\substack{e\\o}mn}^{(1)} = a_n^{(1)}$, $b_{\substack{e\\o}mn}^{(1)} = b_n^{(1)}$, $c_{\substack{e\\o}mn}^{(1)} = c_n^{(1)}$ and $d_{\substack{e\\o}mn}^{(1)} = d_n^{(1)}$, where

$$a_n^{(1)} = \frac{\frac{k_2}{\mu_2}\frac{\left[\rho_2 j_n(\rho_2)\right]'}{\rho_2} - \frac{k_1}{\mu_1}\frac{\left[\rho_1 j_n(\rho_1)\right]'}{\rho_1}\,j_n(\rho_2)}{\frac{k_1}{\mu_1}\frac{\left[\rho_2 j_n(\rho_2)\right]'}{\rho_1}\,j_n(\rho_2) - \frac{k_2}{\mu_2}\frac{\left[\rho_2 j_n(\rho_2)\right]'}{\rho_2}\,h_n(\rho_1)}$$

$$b_n^{(1)} = \frac{\frac{k_1}{\mu_1}\frac{\left[\rho_2 j_n(\rho_2)\right]'}{\rho_2}\,j_n(\rho_1) - \frac{k_2}{\mu_2}\frac{\left[\rho_1 j_n(\rho_1)\right]'}{\rho_1}\,j_n(\rho_2)}{\frac{k_2}{\mu_2}\frac{\left[\rho_1 h_n(\rho_1)\right]'}{\rho_1}\,j_n(\rho_2) - \frac{k_1}{\mu_1}\frac{\left[\rho_2 j_n(\rho_2)\right]'}{\rho_2}\,h_n(\rho_1)}$$

$$c_n^{(1)} = \frac{\frac{k_1}{\mu_1}\frac{[\rho_1 h_n(\rho_1)]'}{\rho_1} j_n(\rho_1) - \frac{k_1}{\mu_1}\frac{[\rho_1 j_n(\rho_1)]'}{\rho_1} h_n(\rho_1)}{\frac{k_1}{\mu_1}\frac{[\rho_1 h_n(\rho_1)]'}{\rho_1} j_n(\rho_2) - \frac{k_2}{\mu_2}\frac{[\rho_2 j_n(\rho_2)]'}{\rho_2} h_n(\rho_2)}$$

$$d_n^{(1)} = \frac{\frac{k_1}{\mu_1}\frac{[\rho_1 h_n(\rho_1)]'}{\rho_1} j_n(\rho_1) - \frac{k_1}{\mu_1}\frac{[\rho_1 j_n(\rho_1)]'}{\rho_1} h_n(\rho_1)}{\frac{k_2}{\mu_2}\frac{[\rho_1 h_n(\rho_1)]'}{\rho_1} j_n(\rho_2) - \frac{k_1}{\mu_1}\frac{[\rho_2 j_n(\rho_2)]'}{\rho_2} h_n(\rho_1)} \quad . \qquad (2.14)$$

Here,

$$\rho_1 = k_1 a$$

$$\rho_2 = k_2 a$$

$$[\rho z_n(\rho)]' = \frac{\partial}{\partial \rho}[\rho z_n(\rho)] \, ,$$

where $z_n(\rho)$ is either $j_n(\rho)$ or $h_n(\rho)$. Also, $h_n(\rho)$ denotes $h_n^{(1)}(\rho)$, since only the spherical Hankel functions of the first kind will appear in this work.

For a dielectric sphere in free space,

$$\mu_1 = \mu_2 = \mu_0 \, ,$$

$$\epsilon_1 = \epsilon_0 \, ,$$

$$\epsilon_2/\epsilon_0 = \epsilon_r \, ,$$

where ϵ_r is the relative dielectric constant and may be complex. Equations (2.14) for this case become

$$a_n^{(1)} = \frac{[\rho_2 j_n(\rho_2)]' j_n(\rho_1) - [\rho_1 j_n(\rho_1)]' j_n(\rho_2)}{[\rho_1 h_n(\rho_1)]' j_n(\rho_2) - [\rho_2 j_n(\rho_2)]' h_n(\rho_1)}$$

$$b_n^{(1)} = \frac{\left[\rho_2 j_n(\rho_2)\right]' j_n(\rho_1) - \epsilon_r \left[\rho_1 j_n(\rho_1)\right]' j_n(\rho_2)}{\epsilon_r \left[\rho_1 h_n(\rho_1)\right]' j_n(\rho_2) - \left[\rho_2 j_n(\rho_2)\right]' h_n(\rho_1)}$$

$$c_n^{(1)} = \frac{\left[\rho_1 h_n(\rho_1)\right]' j_n(\rho_1) - \left[\rho_1 j_n(\rho_1)\right]' h_n(\rho_1)}{\left[\rho_1 h_n(\rho_1)\right]' j_n(\rho_2) - \left[\rho_2 j_n(\rho_2)\right]' h_n(\rho_1)}$$

$$d_n^{(1)} = \frac{\sqrt{\epsilon_r}\left[\rho_1 h_n^{(1)}(\rho_1)\right]' j_n(\rho_1) - \sqrt{\epsilon_r}\left[\rho_1 j_n(\rho_1)\right]' h_n(\rho_1)}{\epsilon_r \left[\rho_1 h_n^{(1)}(\rho_1)\right]' j_n(\rho_2) - \left[\rho_2 j_n(\rho_2)\right]' h_n(\rho_1)} . \tag{2.15}$$

Substitution of equations (2.7), (2.11) and (2.12) into (2.5) and (2.6) gives us the desired Green's functions for the configuration of Fig. 2-1. They are

Source in Region I, Observation Point in Region I

$$\bar{\bar{G}}_3^{(11)}(\bar{R}|\bar{R}) = \frac{ik_1}{4\pi} \sum_{n=1}^{\infty} \sum_{m=0}^{n} (2-\delta_0) \frac{2n+1}{n(n+1)} \frac{(n-m)!}{(n+m)!} \cdot$$

$$\cdot \left\{ \bar{M}_{\substack{e\\o}mn}^{(1)}(k_1) \left[\bar{M}_{\substack{e\\o}mn}'(k_1) + a_n^{(1)} \bar{M}_{\substack{e\\o}mn}'^{(1)}(k_1) \right] \right.$$

$$\left. + \bar{N}_{\substack{e\\o}mn}^{(1)}(k_1) \left[\bar{N}_{\substack{e\\o}mn}'(k_1) + b_n^{(1)} \bar{N}_{\substack{e\\o}mn}'^{(1)}(k_1) \right] \right\} \quad , \quad R > R' \tag{2.16}$$

$$\bar{\bar{G}}_3^{(11)}(\bar{R}|\bar{R}') = \frac{ik_1}{4\pi} \sum_{n=1}^{\infty} \sum_{m=0}^{n} (2-\delta_0) \frac{2n+1}{n(n+1)} \frac{(n-m)!}{(n+m)!} \cdot$$

$$\cdot \left\{ \left[\bar{M}_{\substack{e\\o}mn}(k_1) + a_n^{(1)} \bar{M}_{\substack{e\\o}mn}^{(1)}(k_1) \right] \bar{M}_{\substack{e\\o}mn}'^{(1)}(k_1) \right.$$

$$\left. + \left[\bar{N}_{\substack{e\\o}mn}(k_1) + b_n^{(1)} \bar{N}_{\substack{e\\o}mn}^{(1)}(k_1) \right] \bar{N}_{\substack{e\\o}mn}'^{(1)}(k_1) \right\} \quad , \quad a \leq R < R' \tag{2.17}$$

Source in Region I, Observation Point in Region II

$$\bar{\bar{G}}_3^{(21)}(\bar{R}|\bar{R}') = \frac{ik_1}{4\pi}\sum_{n=1}^{\infty}\sum_{m=0}^{n}(2-\delta_0)\frac{2n+1}{n(n+1)}\frac{(n-m)!}{(n+m)!}\cdot$$

$$\cdot\left[c_n^{(1)}\bar{M}_{e_{omn}}(k_2)\bar{M}'^{(1)}_{e_{omn}}(k_1)+d_n^{(1)}\bar{N}_{e_{omn}}(k_2)\bar{N}'^{(1)}_{e_{omn}}(k_1)\right], \quad R \le a . \tag{2.18}$$

For the source located inside the dielectric sphere, again consider the geometry of Fig. 2-1, but now with $R' \le a$. We let $\bar{\bar{G}}_0^{(22)}(\bar{R}|\bar{R}')$ represent the free space Green's function in an infinite region with the same constitutive parameters as that of Region II. From (2.7) we have

$$\bar{\bar{G}}_0^{(22)}(\bar{R}|\bar{R}') = \frac{ik_2}{4\pi}\sum_{n=1}^{\infty}\sum_{m=0}^{n}(2-\delta_0)\frac{2n+1}{n(n+1)}\frac{(n-m)!}{(n+m)!}\cdot$$

$$\begin{cases} \bar{M}^{(1)}_{e_{omn}}(k_2)\bar{M}'_{e_{omn}}(k_2)+\bar{N}^{(1)}_{e_{omn}}(k_2)\bar{N}'_{e_{omn}}(k_2), & R > R' \\ \bar{M}_{e_{omn}}(k_2)\bar{M}'^{(1)}_{e_{omn}}(k_2)+\bar{N}_{e_{omn}}(k_2)\bar{N}'^{(1)}_{e_{omn}}(k_2), & R < R' . \end{cases} \tag{2.19}$$

Using the method of scattering superposition, $\bar{\bar{G}}_3^{(22)}(\bar{R}\ \bar{R}')$ is treated as consisting of two parts,

$$\bar{\bar{G}}_3^{(22)}(\bar{R}|\bar{R}') = \bar{\bar{G}}_0^{(22)}(\bar{R}|\bar{R}')+\bar{\bar{G}}_{3s}^{(22)}(\bar{R}|\bar{R}'), \quad R \le a$$

$$\bar{\bar{G}}_3^{(12)}(\bar{R}|\bar{R}') = \bar{\bar{G}}_{3s}^{(12)}(\bar{R}|\bar{R}'), \quad R \ge a . \tag{2.20}$$

Here $\bar{\bar{G}}_{3s}^{(22)}$ is used to represent the portion of $\bar{\bar{G}}_3$ which is scattered from the inside surface of the dielectric sphere, and $\bar{\bar{G}}_3^{(12)}$ is the transmitted field. We note that $\bar{\bar{G}}_{3s}^{(22)}$ must be finite at the origin, $\bar{\bar{G}}_3^{(12)}$ must satisfy the radiation condition at infinity, and the boundary conditions must be met at the sphere surface. Thus,

$$\bar{\bar{G}}_{3s}^{(12)}(\bar{R}|\bar{R}') = \frac{ik_2}{4\pi}\sum_{n=1}^{\infty}\sum_{m=0}^{n}(2-\delta_0)\frac{2n+1}{n(n+1)}\frac{(n-m)!}{(n+m)!}\cdot$$

$$\cdot\left[a^{(2)}_{\substack{e\\o}mn}\bar{M}^{(1)}_{\substack{e\\o}mn}(k_1)\bar{M}'_{\substack{e\\o}mn}(k_2)+b^{(2)}_{\substack{e\\o}mn}\bar{N}^{(1)}_{\substack{e\\o}mn}(k_1)\bar{N}'_{\substack{e\\o}mn}(k_2)\right], \qquad R > a \tag{2.21}$$

and

$$\bar{\bar{G}}_{3s}^{(22)}(\bar{R}|\bar{R}') = \frac{ik_2}{4\pi}\sum_{n=1}^{\infty}\sum_{m=0}^{n}(2-\delta_0)\frac{2n+1}{n(n+1)}\frac{(n-m)!}{(n+m)!}\cdot$$

$$\cdot\left[c^{(2)}_{\substack{e\\o}mn}\bar{M}_{\substack{e\\o}mn}(k_2)\bar{M}'_{\substack{e\\o}mn}(k_2)+d^{(2)}_{\substack{e\\o}mn}\bar{N}_{\substack{e\\o}mn}(k_2)\bar{N}'_{\substack{e\\o}mn}(k_2)\right], \qquad R < a \tag{2.22}$$

where the superscript (2) on the scattering coefficients denote they pertain to the source located in Region II.

The coefficients are now found by applying the boundary conditions at the sphere surface, namely

$$\left.\begin{aligned}\hat{R}\times\bar{\bar{G}}_3^{(12)}(\bar{R}|\bar{R}') &= \hat{R}\times\bar{\bar{G}}_3^{(22)}(\bar{R}|\bar{R}')\\ \frac{1}{\mu_1}\hat{R}\times\nabla\times\bar{\bar{G}}_3^{(12)}(\bar{R}|\bar{R}') &= \frac{1}{\mu_2}\hat{R}\times\nabla\times\bar{\bar{G}}_3^{(22)}(\bar{R}|\bar{R}')\end{aligned}\right\} R = a.$$

We again find $a^{(2)}_{\substack{e\\o}mn} = a^{(2)}_n$, $b^{(2)}_{\substack{e\\o}mn} = b^{(2)}_n$, $c^{(2)}_{\substack{e\\o}mn} = c^{(2)}_n$ and $d^{(2)}_{\substack{e\\o}mn} = d^{(2)}_n$, where

$$a_n^{(2)} = \frac{\left[\rho_2 j_n(\rho_2)\right]' h_n(\rho_2) - \left[\rho_2 h_n(\rho_2)\right]' j_n(\rho_2)}{\left[\rho_2 j_n(\rho_2)\right]' h_n(\rho_1) - \frac{\mu_2}{\mu_1}\left[\rho_1 h_n(\rho_1)\right]' j_n(\rho_2)}$$

$$b_n^{(2)} = \frac{\left[\rho_2 j_n(\rho_2)\right]' h_n(\rho_2) - \left[\rho_2 h_n(\rho_2)\right]' j_n(\rho_2)}{\frac{k_1\mu_2}{k_2\mu_1}\left[\rho_2 j_n(\rho_2)\right]' h_n(\rho_1) - \frac{k_2}{k_1}\left[\rho_1 h_n(\rho_1)\right]' j_n(\rho_2)}$$

$$c_n^{(2)} = \frac{\frac{\mu_2}{\mu_1}\left[\rho_1 h_n(\rho_1)\right]' h_n(\rho_2) - \left[\rho_2 h_n(\rho_2)\right]' h_n(\rho_1)}{\left[\rho_2 j_n(\rho_2)\right]' h_n(\rho_1) - \frac{\mu_2}{\mu_1}\left[\rho_1 h_n(\rho_1)\right]' j_n(\rho_2)}$$

$$d_n^{(2)} = \frac{\left(\frac{k_2}{k_1}\right)^2 \left[\rho_1 h_n(\rho_1)\right]' h_n(\rho_2) - \frac{\mu_2}{\mu_1}\left[\rho_2 h_n(\rho_2)\right]' h_n(\rho_1)}{\frac{\mu_2}{\mu_1}\left[\rho_2 j_n(\rho_2)\right]' h_n(\rho_1) - \left(\frac{k_2}{k_1}\right)^2 \left[\rho_1 h_n(\rho_1)\right]' j_n(\rho_2)} \quad . \tag{2.23}$$

For the case where $\mu_1 = \mu_2$, these equations become

$$a_n^{(2)} = \frac{\left[\rho_2 j_n(\rho_2)\right]' h_n(\rho_2) - \left[\rho_2 h_n(\rho_2)\right]' j_n(\rho_2)}{\left[\rho_2 j_n(\rho_2)\right]' h_n(\rho_1) - \left[\rho_1 h_n(\rho_1)\right]' j_n(\rho_2)}$$

$$b_n^{(2)} = \frac{\left[\rho_2 j_n(\rho_2)\right]' h_n(\rho_2) - \left[\rho_2 h_n(\rho_2)\right]' j_n(\rho_2)}{\frac{1}{\sqrt{\epsilon_r}}\left[\rho_2 j_n(\rho_2)\right]' h_n(\rho_1) - \sqrt{\epsilon_r}\left[\rho_1 h_n(\rho_1)\right]' j_n(\rho_2)}$$

$$c_n^{(2)} = \frac{\left[\rho_1 h_n(\rho_1)\right]' h_n(\rho_2) - \left[\rho_2 h_n(\rho_2)\right]' h_n(\rho_1)}{\left[\rho_2 j_n(\rho_2)\right]' h_n(\rho_1) - \left[\rho_1 h_n(\rho_1)\right]' j_n(\rho_2)}$$

$$d_n^{(2)} = \frac{\epsilon_r\left[\rho_1 h_n(\rho_1)\right]' h_n(\rho_2) - \left[\rho_2 h_n(\rho_2)\right]' h_n(\rho_1)}{\left[\rho_2 j_n(\rho_2)\right]' h_n(\rho_1) - \left[\rho_1 h_n(\rho_1)\right]' j_n(\rho_2)\epsilon_r} \quad . \tag{2.24}$$

Substitution of equations (2.19), (2.21) and (2.22) into (2.20) yields the desired Green's functions for the internally located electric current source as follows:

Source in Region II, Observation Point in Region I

$$\bar{\bar{G}}_3^{(12)}(\bar{R}|\bar{R}') = \frac{ik_2}{4\pi}\sum_{n=1}^{\infty}\sum_{m=0}^{n}(2-\delta_0)\frac{2n+1}{n(n+1)}\frac{(n-m)!}{(n+m)!}\cdot$$

$$\cdot\left[a_n^{(2)}\bar{M}_{\substack{e\\o}mn}^{(1)}(k_1)\bar{M}_{\substack{e\\o}mn}'(k_2)+b_n^{(2)}\bar{N}_{\substack{e\\o}mn}^{(1)}(k_1)\bar{N}_{\substack{e\\o}mn}'(k_2)\right], \quad R > a \qquad (2.25)$$

Source in Region II, Observation Point in Region II

$$\bar{\bar{G}}_3^{(22)}(\bar{R}|\bar{R}') = \frac{ik_2}{4\pi}\sum_{n=1}^{\infty}\sum_{m=0}^{n}(2-\delta_0)\frac{2n+1}{n(n+1)}\frac{(n-m)!}{(n+m)!}\cdot$$

$$\cdot\left\{\left[\bar{M}_{\substack{e\\o}mn}^{(1)}(k_2)+c_n^{(2)}\bar{M}_{\substack{e\\o}mn}(k_2)\right]\bar{M}_{\substack{e\\o}mn}'(k_2)\right.$$

$$\left.+\left[\bar{N}_{\substack{e\\o}mn}^{(1)}(k_2)+d_n^{(2)}\bar{N}_{\substack{e\\o}mn}(k_2)\right]\bar{N}_{\substack{e\\o}mn}'(k_2)\right\}, \quad a \geq R > R' \qquad (2.26)$$

$$\bar{\bar{G}}_3^{(22)}(\bar{R}|\bar{R}') = \frac{ik_2}{4\pi}\sum_{n=1}^{\infty}\sum_{m=0}^{n}(2-\delta_0)\frac{2n+1}{n(n+1)}\frac{(n-m)!}{(n+m)!}\cdot$$

$$\left\{\bar{M}_{\substack{e\\o}mn}(k_2)\left[\bar{M}_{\substack{e\\o}mn}'^{(1)}(k_2)+c_n^{(2)}\bar{M}_{\substack{e\\o}mn}'(k_2)\right]\right.$$

$$\left.+\bar{N}_{\substack{e\\o}mn}(k_2)\left[\bar{N}_{\substack{e\\o}mn}'^{(1)}(k_2)+d_n^{(2)}\bar{N}_{\substack{e\\o}mn}'(k_2)\right]\right\}, \quad R < R'. \qquad (2.27)$$

2.3 Duality Principle Applied to $\bar{\bar{G}}_3$ and $\bar{\bar{G}}_4$

When dealing with magnetic current sources, it will be convenient to use the dyadic Green's functions of the fourth kind, $\bar{\bar{G}}_4$, to obtain the magnetic field. The symmetry which exists in Maxwell's equations provides a simple means of obtaining these functions from those of the third kind which were derived in Section 2.2.

Consider the following sets of Maxwell's equations:

$$\nabla \times \bar{E} = i\omega\mu \bar{H}$$

$$\nabla \times \bar{H} = -i\omega\epsilon \bar{E} + \bar{J}$$

$$\nabla \cdot \bar{J} = i\omega\rho \tag{2.28}$$

$$\nabla \times \bar{E}' = i\omega\mu \bar{H}' - \bar{J}_m$$

$$\nabla \times \bar{H}' = -i\omega\epsilon \bar{E}'$$

$$\nabla \cdot \bar{J}_m = i\omega\rho_m \tag{2.29}$$

where $\bar{J}_m$ and ρ_m are the magnetic current and charge densities. Here, the primed and unprimed fields are due to electric and magnetic sources respectively.

As shown in detail by Papas (1965), a duality exists in the above equation sets. This principle, however, may be extended to include the dyadic Green's functions of the third and fourth kinds by considering the inhomogeneous vector wave equations derived from (2.28) and (2.29) and their solutions. Thus,

$$\nabla \times \nabla \times \bar{E} - k^2 \bar{E} = i\omega\mu \bar{J}$$

$$\nabla \times \nabla \times \bar{H} - k^2 \bar{H} = i\omega\epsilon \bar{J}_m \tag{2.30}$$

and

$$\bar{E} = i\omega\mu \iiint \bar{\bar{G}}_3(\bar{R}|\bar{R}') \cdot \bar{J} dV'$$

$$\bar{H}' = i\omega\epsilon \iiint \bar{\bar{G}}_4(\bar{R}|\bar{R}') \cdot \bar{J}_m dV' \tag{2.31}$$

or

$$\bar{E} = i\omega\mu \iint \bar{\bar{G}}_3(\bar{R}|\bar{R}') \cdot \bar{K} dS'$$

$$\bar{H}' = i\omega\epsilon \iint \bar{\bar{G}}_4(\bar{R}|\bar{R}') \cdot \bar{K}_m dS' \tag{2.32}$$

where the surface electric and magnetic current densities are given by

$$\bar{K}_m = -\hat{n} \times \bar{E}'$$

$$\bar{K} = \hat{n} \times \bar{H} \quad . \tag{2.33}$$

To change from a system of fields excited by electric sources to one excited by magnetic sources, or vice versa, we see from equations (2.28) to (2.33), it is only necessary to replace the quantities by their duals as summarized in Table 2-1.

Table 2-1: Dual Quantities

$\bar{E}$	$\bar{H}$	$\bar{\bar{G}}_3$	$\bar{J}$	$\bar{K}$	ρ	μ	ϵ	k
$\bar{H}'$	$-\bar{E}'$	$\bar{\bar{G}}_4$	$\bar{J}_m$	$\bar{K}_m$	ρ_m	ϵ	μ	k

It also should be noted that besides satisfying the radiation condition, $\bar{\bar{G}}_4$ also satisfies the boundary conditions at the surface of the sphere,

$$\hat{n} \times \bar{\bar{G}}_4(\bar{R}|\bar{R}')\Big|_{R=a_-} = \hat{n} \times \bar{\bar{G}}_4(\bar{R}|\bar{R}')\Big|_{R=a_+}$$

$$\frac{1}{\epsilon_1} \hat{n} \times \nabla \times \bar{\bar{G}}_4(\bar{R}|\bar{R}')\Big|_{R=a_-} = \frac{1}{\epsilon_2} \hat{n} \times \nabla \times \bar{\bar{G}}_4(\bar{R}|\bar{R}')\Big|_{R=a_+} \tag{2.34}$$

which are the dual of (2.4).

2.4. The Dyadic Green's Functions Pertaining to a Magnetic Source in the Presence of a Dielectric Sphere.

Since the propagation constant k is its own dual, it can be seen from (2.8) and (2.9) that the spherical wave functions will remain invariant in the transformation from $\bar{\bar{G}}_3$ to $\bar{\bar{G}}_4$. The only difference, therefore, will be manifest in the scattering coefficients a_n, b_n, c_n, d_n, and once these coefficients have been determined, it is possible to list the various Green's functions of the fourth kind.

To obtain the coefficients for $\bar{\bar{G}}_4$ from those previously derived for $\bar{\bar{G}}_3$ we let

$$a_n'(\mu,\epsilon) = a_n(\epsilon,\mu)$$

$$b_n'(\mu,\epsilon) = b_n(\epsilon,\mu)$$

$$c_n'(\mu,\epsilon) = c_n(\epsilon,\mu)$$

$$d_n'(\mu,\epsilon) = d_n(\epsilon,\mu)$$

where the primed coefficients are used in $\overline{\overline{G}}_4$ and a_n, b_n, c_n, d_n are defined by (2.14) or (2.23) depending on the source location. Equations (2.15) and (2.24) were not used for the unprimed coefficients in this case because μ_1 cannot be set equal to μ_2 until after the duality principle has been applied.

From (2.14) for the external source we find

$$a_n^{(1)'} = \frac{\left[\rho_2 j_n(\rho_2)\right]' j_n(\rho_1) - \epsilon_r \left[\rho_1 j_n(\rho_1)\right]' j_n(\rho_2)}{\epsilon_r \left[\rho_1 h_n(\rho_1)\right]' j_n(\rho_2) - \left[\rho_2 j_n(\rho_2)\right]' h_n(\rho_1)}$$

$$b_n^{(1)'} = \frac{\left[\rho_2 j_n(\rho_2)\right]' j_n(\rho_1) - \mu_r \left[\rho_1 j_n(\rho_1)\right]' j_n(\rho_2)}{\mu_r \left[\rho_1 h_n(\rho_1)\right]' j_n(\rho_2) - \left[\rho_2 j_n(\rho_2)\right]' h_n(\rho_1)}$$

$$c_n^{(1)'} = \frac{\epsilon_r \left[\rho_1 h_n(\rho_1)\right]' j_n(\rho_1) - \epsilon_r \left[\rho_1 j_n(\rho_1)\right]' h_n(\rho_1)}{\epsilon_r \left[\rho_1 h_n(\rho_1)\right]' j_n(\rho_2) - \left[\rho_2 j_n(\rho_2)\right]' h_n(\rho_1)}$$

$$d_n^{(1)'} = \frac{k_1 k_2 \epsilon_r \left[\rho_1 h_n(\rho_1)\right]' j_n(\rho_1) - k_1 k_2 \epsilon_r \left[\rho_1 j_n(\rho_1)\right]' h_n(\rho_1)}{k_2^2 \left[\rho_1 h_n(\rho_1)\right]' j_n(\rho_2) - k_1^2 \epsilon_r \left[\rho_2 j_n(\rho_2)\right]' h_n(\rho_1)} \tag{2.35}$$

where we have used the fact that $k_1/\rho_1 = k_2/\rho_2$, and let $\mu_r = \mu_2/\mu_1$. For the case when $\mu_1 = \mu_2$, equations (2.35) may be further simplified; it is found that

$$a_n^{(1)'} = b_n^{(1)}$$

$$b_n^{(1)'} = a_n^{(1)}$$

$$c_n^{(1)'} = \sqrt{\epsilon_r}\, d_n^{(1)}$$

$$d_n^{(1)'} = \sqrt{\epsilon_r}\, c_n^{(1)} \quad . \tag{2.36}$$

Proceeding in a similar manner for the internally located magnetic source, it is found from (2.23)

$$a_n^{(2)'} = \frac{\left[\rho_2 j_n(\rho_2)\right]' h_n(\rho_2) - \left[\rho_2 h_n(\rho_2)\right]' j_n(\rho_2)}{\left[\rho_2 j_n(\rho_2)\right]' h_n(\rho_1) - \epsilon_r \left[\rho_1 h_n(\rho_1)\right]' j_n(\rho_2)}$$

$$b_n^{(2)'} = \frac{\left[\rho_2 j_n(\rho_2)\right]' h_n(\rho_2) - \left[\rho_2 h_n(\rho_2)\right]' j_n(\rho_2)}{\frac{k_1}{k_2}\epsilon_r \left[\rho_2 j_n(\rho_2)\right]' h_n(\rho_1) - \frac{k_2}{k_1}\left[\rho_1 h_n(\rho_1)\right]' j_n(\rho_2)}$$

$$c_n^{(2)'} = \frac{\epsilon_r \left[\rho_1 h_n(\rho_1)\right]' h_n(\rho_2) - \left[\rho_2 h_n(\rho_2)\right]' h_n(\rho_1)}{\left[\rho_2 j_n(\rho_2)\right]' h_n(\rho_1) - \epsilon_r \left[\rho_1 h_n(\rho_1)\right]' j_n(\rho_2)}$$

$$d_n^{(2)'} = \frac{\left(\frac{k_2}{k_1}\right)^2 \left[\rho_1 h_n(\rho_1)\right]' h_n(\rho_2) - \epsilon_r \left[\rho_2 h_n(\rho_2)\right]' h_n(\rho_1)}{\epsilon_r \left[\rho_2 j_n(\rho_2)\right]' h_n(\rho_1) - \left(\frac{k_2}{k_1}\right)^2 \left[\rho_1 h_n(\rho_1)\right]' j_n(\rho_2)} \quad . \tag{2.37}$$

By letting $\mu_1 = \mu_2$, it is apparent from the above equations that

$$a_n^{(2)'} = \frac{1}{\sqrt{\epsilon_r}}\, b_n^{(2)}$$

$$b_n^{(2)'} = \frac{1}{\sqrt{\epsilon_r}}\, a_n^{(2)}$$

$$c_n^{(2)'} = d_n^{(2)}$$

$$d_n^{(2)'} = c_n^{(2)} \tag{2.38}$$

where the unprimed coefficients are given by (2.24).

It is now a simple matter to list the dyadic Green's functions of the fourth kind by making the appropriate substitution of the scattering coefficients in equations (2.16) to (2.18) and (2.25) to (2.27). These functions are listed below for the various regions of source and observation points.

Source in Region I, Observation Point in Region I

$$\bar{\bar{G}}_4^{(11)}(\bar{R}|\bar{R}') = \frac{ik_1}{4\pi}\sum_{n=1}^{\infty}\sum_{m=0}^{n}(2-\delta_0)\frac{2n+1}{n(n+1)}\frac{(n-m)!}{(n+m)!}\cdot$$

$$\cdot\left\{\bar{M}_{o_{emn}}^{(1)}(k_1)\left[\bar{M}'_{o_{emn}}(k_1)+b_n^{(1)}\bar{M}'^{(1)}_{o_{emn}}(k_1)\right]\right.$$

$$\left.+\bar{N}_{o_{emn}}^{(1)}(k_1)\left[\bar{N}'_{o_{emn}}(k_1)+a_n^{(1)}\bar{N}'^{(1)}_{o_{emn}}(k_1)\right]\right\}, \quad R>R'$$

$$\bar{\bar{G}}_4^{(11)}(\bar{R}|\bar{R}') = \frac{ik_1}{4\pi}\sum_{n=1}^{\infty}\sum_{m=0}^{n}(2-\delta_0)\frac{2n+1}{n(n+1)}\frac{(n-m)!}{(n+m)!}\cdot$$

$$\cdot\left\{\left[\bar{M}_{o_{emn}}(k_1)+b_n^{(1)}\bar{M}_{o_{emn}}^{(1)}(k_1)\right]\bar{M}'^{(1)}_{o_{emn}}(k_1)\right.$$

$$\left.+\left[\bar{N}_{o_{emn}}(k_1)+a_n^{(1)}\bar{N}_{o_{emn}}^{(1)}(k_1)\right]\bar{N}'^{(1)}_{o_{emn}}(k_1)\right\}, \quad a\le R<R' \qquad (2.39)$$

Source in Region I, Observation Point in Region II

$$\bar{\bar{G}}_4^{(21)}(\bar{R}|\bar{R}') = \frac{ik_2}{4\pi}\sum_{n=1}^{\infty}\sum_{m=0}^{n}(2-\delta_0)\frac{2n+1}{n(n+1)}\frac{(n-m)!}{(n+m)!}\cdot$$

$$\cdot\left[d_n^{(1)}\bar{M}_{o_{emn}}(k_2)\bar{M}'^{(1)}_{o_{emn}}(k_1)+c_n^{(1)}\bar{N}_{o_{emn}}(k_2)\bar{N}'^{(1)}_{o_{emn}}(k_1)\right], \quad R\le a$$

(2.40)

Source in Region II, Observation Point in Region I

$$\bar{\bar{G}}_4^{(12)}(\bar{R}|\bar{R}') = \frac{ik_1}{4\pi}\sum_{n=1}^{\infty}\sum_{m=0}^{n}(2-\delta_0)\frac{2n+1}{n(n+1)}\frac{(n-m)!}{(n+m)!}\cdot$$

$$\cdot\left[b_n^{(2)}\bar{M}_{e_{omn}}^{(1)}(k_1)\bar{M}'_{e_{omn}}(k_2)+a_n^{(2)}\bar{N}_{e_{omn}}(k_1)\bar{N}'_{e_{omn}}(k_2)\right], \quad R>a \tag{2.41}$$

Source in Region II, Observation Point in Region II

$$\bar{\bar{G}}_4^{(22)}(\bar{R}|\bar{R}') = \frac{ik_2}{4\pi}\sum_{n=1}^{\infty}\sum_{m=0}^{n}(2-\delta_0)\frac{2n+1}{n(n+1)}\frac{(n-m)!}{(n+m)!}\cdot$$

$$\left\{\left[\bar{M}_{e_{omn}}^{(1)}(k_2)+d_n^{(2)}\bar{M}_{e_{omn}}(k_2)\right]\bar{M}'_{e_{omn}}(k_2)\;\bar{M}'_{e_{omn}}(k_2)\right.$$

$$\left.+\left[\bar{N}_{e_{omn}}^{(1)}(k_2)+c_n^{(2)}\bar{N}_{e_{omn}}(k_2)\right]\bar{N}'_{e_{omn}}(k_2)\right\}, \quad a>R>R'$$

$$\bar{\bar{G}}_4^{(22)}(\bar{R}|\bar{R}') = \frac{ik_2}{4\pi}\sum_{n=1}^{\infty}\sum_{m=0}^{n}(2-\delta_0)\frac{2n+1}{n(n+1)}\frac{(n-m)!}{(n+m)!}\cdot$$

$$\cdot\left\{\bar{M}_{e_{omn}}(k_2)\left[\bar{M}'^{(1)}_{e_{omn}}(k_2)+d_n^{(2)}\bar{M}'_{e_{omn}}(k_2)\right]\right.$$

$$\left.+\bar{N}_{e_{omn}}(k_2)\left[\bar{N}'^{(1)}_{e_{omn}}(k_2)+c_n^{(2)}\bar{N}'_{e_{omn}}(k_2)\right]\right\}, \quad R<R' \tag{2.42}$$

where we have used the fact that for $\mu_1=\mu_2$, $k_1=k_2/\sqrt{\epsilon_r}$.

This completes the derivation of the dyadic Green's functions, pertaining to a homogeneous dielectric sphere, which will be used in subsequent chapters.

Chapter III

ELECTRIC FIELDS DUE TO SIMPLE POINT SOURCES IN THE PRESENCE OF A DIELECTRIC SPHERE

3.1. Short Horizontal Electric Dipole

Consider an infinitesimal horizontal x-directed electric dipole with current moment C_e located at $R' = b$, $\theta' = 0$, $\phi' = 0$ as shown in Fig. 3-1.

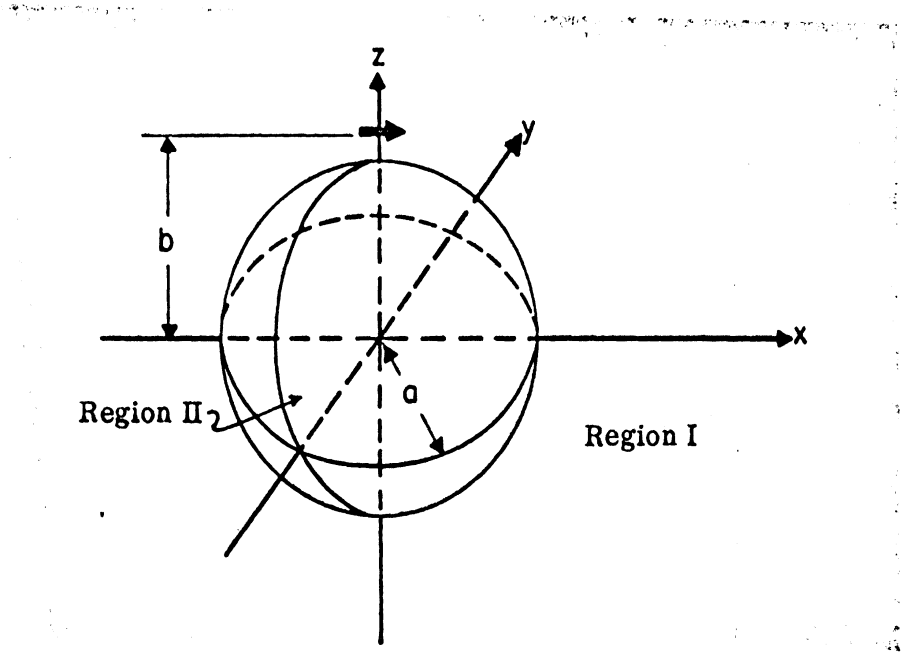

FIG. 3-1: HORIZONTAL ELECTRIC DIPOLE IN THE PRESENCE OF A DIELECTRIC SPHERE.

We let the electric current density be represented by

$$\bar{J}(\bar{R}') = C_e \frac{\delta(R'-b)\delta(\theta')\delta(\phi')}{b^2 \sin\theta'} \hat{x} \quad . \tag{3.1}$$

To find the electric fields in the two Regions, (3.1) is substituted into (2.1) and (2.2). Because of the delta functions within the integrand, the following is obtained

$$\bar{E}(\bar{R}) = i\omega\mu_1 C_e \bar{\bar{G}}_3^{(11)}(\bar{R}|\bar{R}') \cdot \hat{x}\Big|_{\substack{R'=b \\ \theta'=0 \\ \phi'=0}}, \quad \text{Region I}$$

$$\bar{E}(\bar{R}) = i\omega\mu_1 C_e \bar{\bar{G}}_3^{(21)}(\bar{R}|\bar{R}') \cdot \hat{x}\Big|_{\substack{R'=b \\ \theta'=0 \\ \phi'=0}}, \quad \text{Region II.} \tag{3.2}$$

The expression $\bar{\bar{G}}_3(\bar{R}|\bar{R}') \cdot \hat{x}$ must now be examined. First, the associated Legendre functions in (2.8) and (2.9) are evaluated at $\theta = 0$.

It is known (Harrington, 1961) that at $\theta = 0$, i.e., $\cos\theta = 1$,

$$P_n^m(1) = \begin{cases} 1, & m = 0 \\ 0, & m \neq 0 \end{cases} .$$

Also, using de l'Hôpital's Rule for the limit,

$$\frac{P_n^m(\cos\theta)}{\sin\theta}\bigg|_{\theta=0} = \begin{cases} \frac{n(n+1)}{2}, & m = 1 \\ 0, & m \neq 1 \end{cases} .$$

These last two equations show that for the point source located at $\theta' = 0$, only those terms in the series expansion corresponding to $m = 1$ will contribute to the fields.

Since in the spherical coordinate system

$$\hat{x} = \sin\theta\cos\phi\hat{R} + \cos\theta\cos\phi\hat{\theta} - \sin\phi\hat{\phi} ,$$

it is apparent that

$$\bar{M}_{emn}(k) \cdot \hat{x}\Big|_{\phi=0} = \bar{N}_{omn}(k) \cdot \hat{x}\Big|_{\phi=0} = 0 ,$$

and hence

$$\bar{M}_{\substack{e \\ o}mn}(k) \cdot \hat{x}\Big|_{(b,0,0)} = \bar{M}_{o1n}(k) \cdot \hat{x}\Big|_{(b,0,0)} = \frac{n(n+1)}{2} j_n(kb)$$

$$\bar{N}_{e_{o}mn}(k)\cdot\hat{x}\Big|_{(b,0,0)} = \bar{N}_{e1n}(k)\cdot\hat{x}\Big|_{(b,0,0)} = \frac{n(n+1)}{2}\,\frac{\left[kbj_n(kb)\right]'}{kb} \tag{3.3}$$

where the $\bar{M}$ and $\bar{N}$ functions are given by (2.8) and (2.9).

Substitution of the dyadic Green's functions given by (2.16) to (2.18) into (3.2), and using the results (3.3), yields the following expressions for the electric fields:

Source in Region I, Observation Point in Region I

$$\bar{E}_e(\bar{R}) = \frac{-k_1\omega\mu C_e}{4\pi}\sum_{n=1}^{\infty}\frac{2n+1}{n(n+1)}\cdot$$

$$\left\{\bar{M}^{(1)}_{o1n}(k_1)\left[j_n(\rho_3)+a_n^{(1)}h_n(\rho_3)\right]+\bar{N}^{(1)}_{e1n}(k_1)\left[\frac{\left[\rho_3 j_n(\rho_3)\right]'}{\rho_3}+b_n^{(1)}\frac{\left[\rho_3 h_n(\rho_3)\right]'}{\rho_3}\right]\right\},$$

$$R > b \tag{3.4}$$

$$\bar{E}_e(\bar{R}) = \frac{-k_1\omega\mu C_e}{4\pi}\sum_{n=1}^{\infty}\frac{2n+1}{n(n+1)}\cdot$$

$$\left\{\left[\bar{M}_{o1n}(k_1)+a_n^{(1)}\bar{M}_{o1n}(k_1)\right]h_n(\rho_3)+\left[\bar{N}_{e1n}(k_1)+b_n^{(1)}\bar{N}_{e1n}(k_1)\right]\frac{\left[\rho_3 h_n(\rho_3)\right]'}{\rho_3}\right\},$$

$$a \le R \le b \tag{3.5}$$

Source in Region I, Observation Point in Region II

$$\bar{E}_e(\bar{R}) = \frac{-k_1\omega\mu C_e}{4\pi}\sum_{n=1}^{\infty}\frac{2n+1}{n(n+1)}\cdot$$

$$\left\{\bar{M}_{o1n}(k_2)c_n^{(1)}h_n(\rho_3)+\bar{N}_{e1n}(k_2)d_n^{(1)}\frac{\left[\rho_3 h_n(\rho_3)\right]'}{\rho_3}\right\}, \quad 0 \le R \le a. \tag{3.6}$$

Here, $\rho_3 = k_1 b$ and the subscript e is used to denote that the field is due to an electric current source

For the current source located inside the dielectric sphere, consider the geometry of Fig. 3-1, but with $b < a$. The electric fields will then be given by

$$\bar{E}(\bar{R}) = i\omega\mu_2 \iiint \bar{\bar{G}}_3^{(12)}(\bar{R}|\bar{R}') \cdot \bar{J}(\bar{R}')dV'$$

or

$$\bar{E}(\bar{R}) = i\omega\mu_2 \iiint \bar{\bar{G}}_3^{(22)}(\bar{R}|\bar{R}') \cdot \bar{J}(\bar{R}')dV' \qquad (3.7)$$

depending on the location of the observation point.

Letting $\mu_1 = \mu_2$ and using the dyadic Green's functions given by (2.25) to (2.27) together with (3.3), the following expressions are obtained.

Source in Region II, Observation Point in Region I

$$\bar{E}_e(\bar{R}) = \frac{-k_2\omega\mu C_e}{4\pi} \sum_{n=1}^{\infty} \frac{2n+1}{n(n+1)} \cdot$$

$$\left\{ a_n^{(2)} j_n(\rho_4) \bar{M}_{o1n}(k_1) + b_n^{(2)} \frac{[\rho_4 j_n(\rho_4)]'}{\rho_4} \bar{N}_{o1n}^{(1)}(k_1) \right\}, \quad R \geq a \qquad (3.8)$$

Source in Region II, Observation Point in Region II

$$\bar{E}_e(\bar{R}) = \frac{-k_2\omega\mu C_e}{4\pi} \sum_{n=1}^{\infty} \frac{2n+1}{n(n+1)} \cdot$$

$$\left\{ \left[\bar{M}_{o1n}^{(1)}(k_2) + c_n^{(2)} \bar{M}_{o1n}(k_2) \right] j_n(\rho_4) + \left[\bar{N}_{e1n}^{(1)}(k_2) + d_n^{(2)} \bar{N}_{o1n}(k_2) \right] \frac{[\rho_4 j_n(\rho_4)]'}{\rho_4} \right\},$$

$$a \geq R > b \qquad (3.9)$$

$$\bar{E}_e(\bar{R}) = \frac{-k_2\omega\mu C_e}{4\pi} \sum_{n=1}^{\infty} \frac{2n+1}{n(n+1)} \cdot$$

$$\left\{ \bar{M}_{o1n}(k_2) \left[h_n(\rho_4) + c_n^{(2)} j_n(\rho_4) \right] + \bar{N}_{e1n}(k_2) \left[\frac{\left[\rho_4 h_n(\rho_4)\right]'}{\rho_4} + d_n^{(2)} \frac{\left[\rho_4 j_n(\rho_4)\right]'}{\rho_4} \right] \right\},$$

$$R < b \qquad (3.10)$$

where $\rho_4 = k_2 b$.

3.2 Short Horizontal Magnetic Dipole

In this section, the radiation from an infinitesimal magnetic dipole located on the $+z$ axis is considered. The source is pointed in the $-\hat{y}$ direction and has a magnetic current moment C_m.

The magnetic field is given in terms of the dyadic Green's functions of the fourth kind for the appropriate regions of source and observation points as follows:

$$\bar{H}(\bar{R}) = i\omega\epsilon_1 \iiint \bar{\bar{G}}_4^{(11)}(\bar{R}|\bar{R}') \cdot \bar{J}_m(\bar{R}')dV'$$

$$\bar{H}(\bar{R}) = i\omega\epsilon_1 \iiint \bar{\bar{G}}_4^{(21)}(\bar{R}|\bar{R}') \cdot \bar{J}_m(\bar{R}')dV'$$

$$\bar{H}(\bar{R}) = i\omega\epsilon_2 \iiint \bar{\bar{G}}_4^{(12)}(\bar{R}|\bar{R}') \cdot \bar{J}_m(\bar{R}')dV'$$

$$\bar{H}(\bar{R}) = i\omega\epsilon_2 \iiint \bar{\bar{G}}_4^{(22)}(\bar{R}|\bar{R}') \cdot \bar{J}_m(\bar{R}')dV' \qquad (3.11)$$

where $\bar{J}_m$ is the magnetic current density, and for this problem is expressed by

$$\bar{J}_m(\bar{R}') = -C_m \frac{\delta(\bar{R}'-b)\delta(\theta')\delta(\phi')}{b^2 \sin\theta'} \hat{y} \quad . \tag{3.12}$$

In the spherical coordinate system,

$$\hat{y} = \sin\theta' \sin\phi' \hat{R}' + \cos\theta' \sin\phi' \hat{\theta}' + \cos\phi' \hat{\phi}' \quad . \tag{3.13}$$

On performing the integration of (3.11), one finds the magnetic field will be given by

$$\bar{H}(\bar{R}) = -i\omega\epsilon \bar{\bar{G}}_4(\bar{R}|\bar{R}') \cdot \hat{y} \Big|_{\substack{R'=b \\ \theta'=0 \\ \phi'=0}} \quad . \tag{3.14}$$

From (2.8) and (2.9), it is seen

$$\bar{M}_{omn}(k) \cdot \hat{y}\Big|_{\phi=0} = \bar{N}_{emn}(k) \cdot \hat{y}\Big|_{\phi=0} = 0 \ ,$$

and thus

$$\begin{aligned} \bar{M}_{\substack{e \\ o}mn}(k) \cdot \hat{y}\Big|_{(b,0,0)} &= \bar{M}_{e1n}(k) \cdot \hat{y}\Big|_{(b,0,0)} = \frac{-n(n+1)}{2} j_n(kb) \\ \bar{N}_{\substack{e \\ o}mn}(k) \cdot \hat{y}\Big|_{(b,0,0)} &= \bar{N}_{o1n}(k) \cdot \hat{y}\Big|_{(b,0,0)} = \frac{n(n+1)}{2} \frac{\left[kbj_n(kb)\right]'}{kb} \ , \end{aligned} \tag{3.15}$$

where we have used the relationships for the associated Legendre functions derived in Section 3.1.

The magnetic fields due to a magnetic point source could now be listed, but it would be more convenient to find the electric fields. In a source-free region,

$$\bar{E} = \frac{i}{\omega\epsilon} \nabla \times \bar{H}.$$

Also, since

$$\nabla \times \bar{M}_{\substack{e \\ o}mn}(k) = k\bar{N}_{\substack{e \\ o}mn}(k)$$

and

$$\nabla \times \bar{N}_{\substack{e \\ o}mn}(k) = k \bar{M}_{\substack{e \\ o}mn}(k) \ ,$$

we simply need to multiply each term by the factor $ik/\omega\epsilon$ appropriate to the region of observation, and interchange the roles of the resulting $\bar{M}$ and $\bar{N}$ functions to obtain the electric fields from the magnetic field expressions.

Using the above result and the Green's functions given by (2.39) to (2.42), we find the electric fields due to an infinitesimal $-\hat{y}$ directed magnetic dipole located at ($R' = 0$, $\theta' = 0$, $\phi' = 0$) may be expressed as follows.

Source in Region I, Observation Point in Region I

$$\bar{E}_m(\bar{R}) = \frac{i\omega k_1 \mu C_m}{4\pi\eta_1} \sum_{n=1}^{\infty} \frac{2n+1}{n(n+1)} \cdot$$

$$\left\{ \bar{M}^{(1)}_{o1n}(k_1) \left[\frac{\left[\rho_3 j_n(\rho_3)\right]'}{\rho_3} + a_n^{(1)} \frac{\left[\rho_3 h_n(\rho_3)\right]'}{\rho_3} \right] - \bar{N}^{(1)}_{e1n}(k_1) \left[j_n(\rho_3) + b_n^{(1)} h_n(\rho_3) \right] \right\} , \quad R > b \tag{3.16}$$

$$\bar{E}_m(\bar{R}) = \frac{i\omega k_1 \mu C_m}{4\pi\eta_1} \sum_{n=1}^{\infty} \frac{2n+1}{n(n+1)} \cdot$$

$$\left\{ \left[\bar{M}_{o1n}(k_1) + a_n^{(1)} \bar{M}^{(1)}_{o1n}(k_1) \right] \frac{\left[\rho_3 h_n(\rho_3)\right]'}{\rho_3} - \left[\bar{N}_{e1n}(k_1) + b_n^{(1)} \bar{N}^{(1)}_{e1n}(k_1) \right] h_n(\rho_3) \right\} ,$$

$$a \leq R < b \tag{3.17}$$

Source in Region I, Observation Point in Region II

$$\bar{E}_m(\bar{R}) = \frac{i\omega k_1 \mu C_m}{4\pi\eta_1} \sum_{n=1}^{\infty} \frac{2n+1}{n(n+1)}$$

$$\left\{ c_n^{(1)} \frac{\left[\rho_3 h_n(\rho_3)\right]'}{\rho_3} \bar{M}_{o1n}(k_2) - d_n^{(1)} h_n(\rho_3) \bar{N}_{e1n}(k_2) \right\} , \quad R \leq a \tag{3.18}$$

Source in Region II, Observation Point in Region I

$$\bar{E}_m(\bar{R}) = \frac{i\omega\mu k_1 \epsilon_r C_m}{4\pi\eta_1} \sum_{n=1}^{\infty} \frac{2n+1}{n(n+1)} \cdot$$

$$\left\{ a_n^{(2)} \frac{\left[\rho_4 j_n(\rho_4)\right]'}{\rho_4} \bar{M}_{o1n}^{(1)}(k_1) - b_n^{(2)} j_n(\rho_4) \bar{N}_{e1n}^{(1)}(k_1) \right\}, \quad R \geq a \qquad (3.19)$$

Source in Region II, Observation Point in Region II

$$\bar{E}_m(\bar{R}) = \frac{i\omega\mu k_1 \epsilon_r C_m}{4\pi\eta_1} \sum_{n=1}^{\infty} \frac{2n+1}{n(n+1)}$$

$$\left\{ \frac{\left[\rho_4 j_n(\rho_4)\right]'}{\rho_4} \left[\bar{M}_{o1n}^{(1)}(k_2) + c_n^{(2)} \bar{M}_{o1n}(k_2)\right] - j_n(\rho_4) \left[\bar{N}_{e1n}^{(1)}(k_2) + d_n^{(2)} \bar{N}_{e1n}(k_2)\right] \right\},$$

$$a \geq R > b \qquad (3.20)$$

$$\bar{E}_m(\bar{R}) = \frac{i\omega\mu k_1 \epsilon_r C_m}{4\pi\eta_1} \sum_{n=1}^{\infty} \frac{2n+1}{n(n+1)} \cdot$$

$$\left\{ \left[\frac{\left[\rho_4 h_n(\rho_4)\right]'}{\rho_4} + c_n^{(2)} \frac{\left[\rho_4 j_n(\rho_4)\right]'}{\rho_4} \right] \bar{M}_{o1n}(k_2) - \left[h_n(\rho_4) + d_n^{(2)} j_n(\rho_4)\right] \bar{N}_{e1n}(k_2) \right\},$$

$$R < b. \qquad (3.21)$$

Here the relation $\eta = \sqrt{\mu/\epsilon}$ is used and again $\rho_3 = k_1 b$ and $\rho_4 = k_2 b$.

Chapter IV

ELECTRIC FIELDS DUE TO A HUYGENS' SOURCE IN THE PRESENCE OF A DIELECTRIC SPHERE

4.1 Introduction

The radiation from a homogeneous dielectric sphere, a few wavelengths in diameter, placed over the aperture of an open-ended waveguide is of considerable practical interest since it has been shown experimentally (Croswell and Chatterjee, 1972) that this device exhibits properties desirable for a feed antenna.

Because it would be exceedingly difficult to solve this problem exactly, we will neglect the scattering from the waveguide and model the exciting fields using a superposition of electric and magnetic dipole currents forming an approximate Huygens' source.

In this chapter, the electric and magnetic current relationship necessary to construct a Huygens' source in free space is first derived, and then the radiation from it is examined. Subsequently, the electric fields are derived for an approximate Huygens' source in the presence of a dielectric sphere, and it is shown that the same results are obtained if the source is allowed to approach the sphere surface from either the inside or outside of the sphere. Finally, the far-zone fields are derived and the results examined for a very small sphere.

4.2 Huygens' Source in Free Space

Consider a small portion of a uniform x-polarized plane wave in free space, incident normally on the $z = 0$ plane as shown in Fig. 4-1. The electric

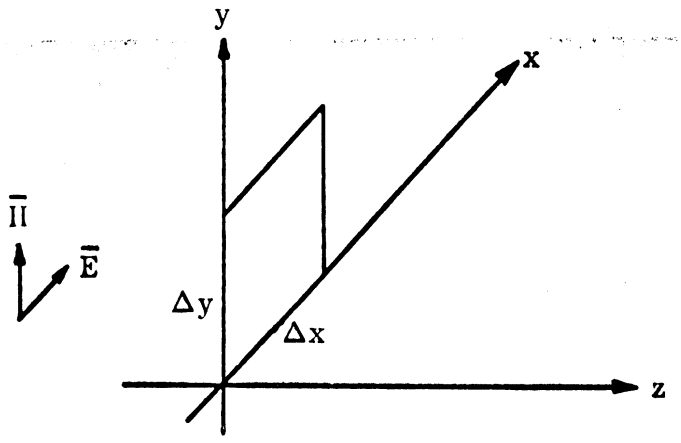

FIG. 4-1: PLANE WAVE GEOMETRY

and magnetic fields across this plane are related by

$$E_x = \eta_0 H_y \quad . \tag{4.1}$$

When the fields to the right of $z = 0$ are of interest, the incident fields may be replaced by fictitious electric and magnetic current sheets,

$$\bar{K}_e = \hat{n} \times \bar{H}$$

$$\bar{K}_m = -\hat{n} \times \bar{E} \quad .$$

For this problem, $\hat{n} = \hat{z}$ and thus

$$\bar{K}_e = -H_y \hat{x}$$

$$\bar{K}_m = -\eta_0 H_y \hat{y} \quad . \tag{4.2}$$

Allowing the portion of the plane wave under consideration to become small, the incident fields may be replaced by the equivalent electric and magnetic dipole current moments $C_e \hat{x}$ and $C_m \hat{y}$, where

$$C_e = \iint K_e \, dS$$

$$C_m = \iint K_m \, dS \quad . \tag{4.3}$$

Substituting (4.2) into (4.3) we find $C_m = \eta_0 C_e$. This double source corresponding to the ratio of electric and magnetic fields of (4.1) is called the "Huygens' source" because Huygens introduced the concept of considering a wavefront as a system of secondary sources.

Let us now derive the far-zone fields radiated from a pair of crossed point electric and magentic dipoles as shown in Fig. 4-2, and then particularize to the special case of the Huygens' source.

For the $\hat{x}$ directed electric dipole, the far-zone electric field is given by

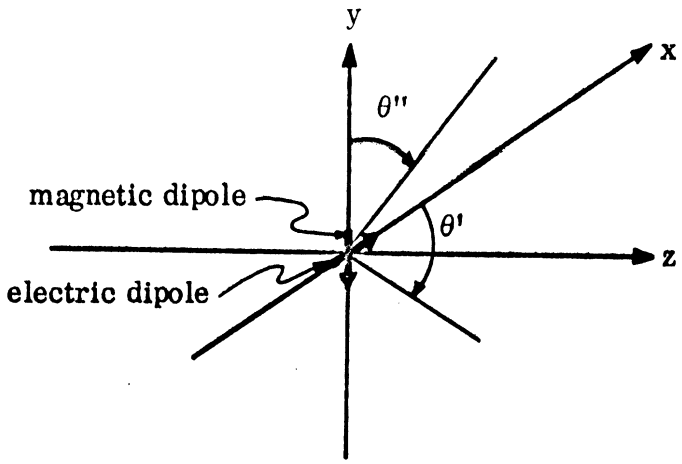

FIG. 4-2: COORDINATE SYSTEM FOR HUYGENS' SOURCE

$$\bar{E}_e = -\frac{i\omega\mu_0}{4\pi} C_e \frac{e^{ikR}}{R} \sin\theta' \hat{\theta}' \tag{4.4}$$

where C_e is the electric current moment of the source and θ' is measured with respect to the x-axis. From duality, Table 2-1, it is found that the magnetic field radiated by a $-\hat{z}$ directed magnetic dipole of current moment C_m is given by

$$\bar{H}_m = \frac{i\omega\epsilon_0 C_m}{4\pi} \frac{e^{ikR}}{R} \sin\theta'' \hat{\theta}'' \,, \tag{4.5}$$

where, in this case, θ'' is measured with respect to the y-axis.

In the far-zone $\hat{R} \times \bar{E} = \eta_0 \bar{H}$, and hence from (4.5)

$$\bar{E}_m = \frac{-i\eta_0\omega\epsilon_0 C_m}{4\pi} \frac{e^{ikR}}{R} \sin\theta'' \hat{\phi}'' \,. \tag{4.6}$$

Using the coordinate transformation

$$\sin\theta'\hat{\theta}' = -\cos\theta\cos\phi\hat{\theta} + \sin\phi\hat{\phi}$$

$$\sin\theta''\hat{\theta}'' = \cos\phi\hat{\theta} - \cos\theta\sin\phi\hat{\phi} ,$$

where θ is measured from the z-axis as is the usual case for the spherical coordinate system, (4.4) and (4.6) become

$$\bar{E}_e = -\frac{i\omega\mu_0 C_e}{4\pi}\frac{e^{ikR}}{R}(-\cos\theta\cos\phi\hat{\theta} + \sin\phi\hat{\phi}) \tag{4.7}$$

$$\bar{E}_m = -\frac{i\omega\eta_0\epsilon_0 C_m}{4\pi}\frac{e^{ikR}}{R}(\cos\phi\hat{\theta} - \cos\theta\sin\phi\hat{\phi}) . \tag{4.8}$$

Letting

$$C_m = \eta C_e , \tag{4.9}$$

where $\eta = \eta_0/\sqrt{\epsilon_r}$, (4.7) and (4.8) may be combined. Thus,

$$\bar{E}_H = \bar{E}_e + \bar{E}_m = -\frac{i\omega\mu_0 C_e}{4\pi}\frac{e^{ikR}}{R}$$
$$\left[\left(\frac{1}{\sqrt{\epsilon_r}} - \cos\theta\right)\cos\phi\hat{\theta} + \left(1 - \frac{\cos\theta}{\sqrt{\epsilon_r}}\right)\sin\phi\hat{\phi}\right] . \tag{4.10}$$

For now the factor $\sqrt{\epsilon_r}$ is simply a constant used in the ratio of the electric and magnetic current sources.

We let $\epsilon_r = 1$ to construct the Huygens' source in free space, and hence (4.10) becomes

$$\bar{E}_H = -\frac{i\omega\mu_0 C_e}{4\pi}\frac{e^{ikR}}{R}(\cos\phi\hat{\theta} + \sin\phi\hat{\phi})(1 - \cos\theta) . \tag{4.11}$$

It is apparent from this equation that the Huygens' source will radiate a linearly polarized cardioid-shaped pattern with a field maximum in the $-\hat{z}$ direction and a null in the $+\hat{z}$ direction.

It is because of this directional characteristic together with its simplicity that the Huygens' source has been chosen to model the waveguide aperture excitation of a dielectric sphere.

4.3 Huygens' Source in the Presence of a Dielectric Sphere

We can only approximate the Huygens' source in the presence of the dielectric sphere because the complex wave impedance η is not known.

Although, in general, η would be a function of the sphere diameter and constitutional parameters as well as the source location, we will let

$$\eta = \begin{cases} \eta_1, & b > a \quad (4.12) \\ \eta_2, & b \leq a \quad (4.13) \end{cases}$$

where $\eta_1 = \sqrt{\mu_1/\epsilon_1}$, $\eta_2 = \sqrt{\mu_2/\epsilon_2}$, and the regions are shown in Fig. 4-3.

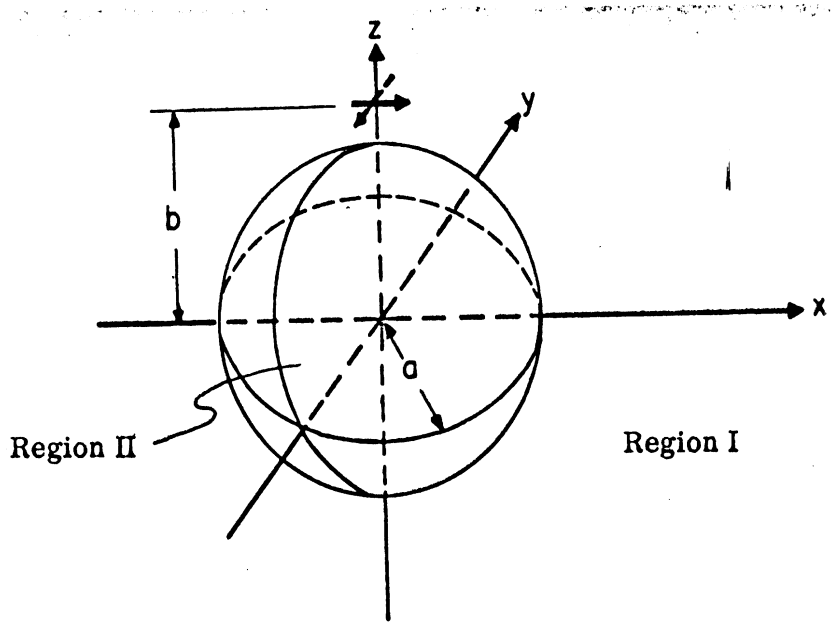

FIG. 4-3: HUYGENS' SOURCE IN THE PRESENCE OF A DIELECTRIC SPHERE.

Equation (4.12) was chosen because it would be valid if $b \gg a$, since for this case the sphere would have little effect on the source. Alternately, (4.13) would be appropriate for the source located within, or on the surface of, a large lossy dielectric sphere. Also, as will be shown in subsequent sections, (4.13) yields a good approximation to the Huygens' source on the surface of small spheres.

To obtain the electric fields due to the source located external to the sphere, let $C_m = \eta_1 C_e$ and combine (3.4) to (3.6) with (3.16) to (3.18). A similar procedure is followed using equations (3.8) to (3.10), (3.19) to (3.21), and letting $C_m = \eta_2 C_e$. The resulting equations for the electric fields in the various regions are given as follows.

Source in Region I, Observation Point in Region I

$$\bar{E}_H(\bar{R}) = \frac{-k_1 \omega \mu C_e}{4\pi} \sum_{n=1}^{\infty} \frac{2n+1}{n(n+1)} \cdot$$

$$\left\{ (A_n^{(1)} + D_n^{(1)}) \bar{M}_{o1n}^{(1)}(k_1) + (B_n^{(1)} + C_n^{(1)}) \bar{N}_{e1n}^{(1)}(k_1) \right\} , \qquad R > b \qquad (4.14)$$

$$\bar{E}_H(\bar{R}) = \frac{-k_1 \omega \mu C_e}{4\pi} \sum_{n=1}^{\infty} \frac{2n+1}{n(n+1)} \cdot$$

$$\left\{ \left[h_n(\rho_3) - i \frac{[\rho_3 h_n(\rho_3)]'}{\rho_3} \right] \left[\bar{M}_{o1n}(k_1) + a_n^{(1)} \bar{M}_{o1n}^{(1)}(k_1) \right] \right.$$
$$\left. + \left[\frac{[\rho_3 h_n(\rho_3)]'}{\rho_3} + i h_n(\rho_3) \right] \left[\bar{N}_{e1n}(k_1) + b_n^{(1)} \bar{N}_{e1n}^{(1)}(k_1) \right] \right\} , \qquad a \le R < b \qquad (4.15)$$

Source in Region I, Observation Point in Region II

$$\bar{E}_H(\bar{R}) = \frac{-k_1 \omega \mu C_e}{4\pi} \sum_{n=1}^{\infty} \frac{2n+1}{n(n+1)} \cdot$$

$$\left\{ \left[h_n(\rho_3) - i [\rho_3 h_n(\rho_3)]' \right] c_n^{(1)} \bar{M}_{o1n}(k_2) + \right.$$
$$\left. + \left[\frac{[\rho_3 h_n(\rho_3)]'}{\rho_3} + i h_n(\rho_3) \right] d_n^{(1)} \bar{N}_{e1n}(k_2) \right\} , \qquad 0 \le R \le a \qquad (4.16)$$

Source in Region II, Observation Point in Region I

$$\bar{E}_H(\bar{R}) = \frac{-k_1\omega\mu C_e}{4\pi}\sum_{n=1}^{\infty}\frac{2n+1}{n(n+1)}\cdot$$

$$\left\{(A_n^{(2)}+D_n^{(2)})\bar{M}_{o1n}^{(1)}(k_1)+(B_n^{(2)}+C_n^{(2)})\bar{N}_{e1n}^{(1)}(k_1)\right\}, \quad R>a \qquad (4.17)$$

Source in Region II, Observation Point in Region II

$$\bar{E}_H(\bar{R}) = \frac{-k_2\omega\mu C_e}{4\pi}\sum_{n=1}^{\infty}\frac{2n+1}{n(n+1)}\cdot$$

$$\left\{\left[j_n(\rho_4)-i\frac{[\rho_4 j_n(\rho_4)]'}{\rho_4}\right]\left[\bar{M}_{o1n}^{(1)}(k_2)+c_n^{(2)}\bar{M}_{o1n}(k_2)\right]\right.$$

$$\left.+\left[\frac{[\rho_4 j_n(\rho_4)]'}{\rho_4}+ij_n(\rho_4)\right]\left[\bar{N}_{e1n}^{(1)}(k_2)+d_n^{(2)}\bar{N}_{e1n}(k_2)\right]\right\}, \quad a\geq R>b \qquad (4.18)$$

$$\bar{E}_H(\bar{R}) = \frac{-k_2\omega\mu C_e}{4\pi}\sum_{n=1}^{\infty}\frac{2n+1}{n(n+1)}\cdot$$

$$\left\{\left[h_n(\rho_4)+c_n^{(2)}j_n(\rho_4)-i\frac{[\rho_4 h_n(\rho_4)]'}{\rho_4}-ic_n^{(2)}\frac{[\rho_4 j_n(\rho_4)]'}{\rho_4}\right]\bar{M}_{o1n}(k_2)\right.$$

$$\left.+\left[\frac{[\rho_4 h_n(\rho_4)]'}{\rho_4}+d_n^{(2)}\frac{[\rho_4 j_n(\rho_4)]'}{\rho_4}+ih_n(\rho_4)+id_n^{(2)}j_n(\rho_4)\right]\bar{N}_{e1n}(k_2)\right\}, \quad R<b \qquad (4.19)$$

where

$$A_n^{(1)} = j_n(\rho_3)+a_n^{(1)}h_n(\rho_3)$$

$$B_n^{(1)} = \frac{[\rho_3 j_n(\rho_3)]'}{\rho_3}+b_n^{(1)}\frac{[\rho_3 h_n(\rho_3)]'}{\rho_3}$$

$$C_n^{(1)} = ij_n(\rho_3) + ib_n^{(1)} h_n(\rho_3)$$

$$D_n^{(1)} = -i \frac{[\rho_3 j_n(\rho_3)]'}{\rho_3} - ia_n^{(1)} \frac{[\rho_3 h_n(\rho_3)]'}{\rho_3} \tag{4.20}$$

and

$$A_n^{(2)} = j_n(\rho_4)\, a_n^{(2)} \sqrt{\epsilon_r}$$

$$B_n^{(2)} = \frac{[\rho_4 j_n(\rho_4)]'}{\rho_4} b_n^{(2)} \sqrt{\epsilon_r}$$

$$C_n^{(2)} = ij_n(\rho_4) b_n^{(2)} \sqrt{\epsilon_r}$$

$$D_n^{(2)} = -i \frac{[\rho_4 j_n(\rho_4)]'}{\rho_4} a_n^{(2)} \sqrt{\epsilon_r} \quad . \tag{4.21}$$

The coefficients in (4. 14) and (4. 17) were combined into A_n, B_n, C_n, D_n since the primary interest here will be the electric field far from the antenna. A_n and B_n represent the field contribution from the electric current source and similarly C_n and D_n were derived from the magnetic source. Again, the superscript on the coefficient denotes the source region.

These coefficients are now simplified for the case where the source is located on the surface of the sphere. The procedure will be to first let the external source approach the sphere surface. Subsequently, we let the internal source approach the surface, and the results are compared as a check on the validity of the expressions.

Since $C_m = \eta_1 C_e$ for the external source, (4. 14) must be modified for the source on the surface where $C_m = \eta_2 C_e$. Thus, (4. 14) becomes

$$\bar{E}_H(\bar{R}) = \frac{-k_1 \omega \mu C_e}{4\pi} \sum_{n=1}^{\infty} \frac{2n+1}{n(n+1)} \cdot$$

$$\left\{ \left(A_n^{(1)} + \frac{D_n^{(1)}}{\sqrt{\epsilon_r}} \right) \bar{M}_{o1n}^{(1)} + \left(B_n^{(1)} + \frac{C_n^{(1)}}{\sqrt{\epsilon_r}} \right) \bar{N}_{e1n}^{(1)} \right\} \Bigg|_{b=a} \qquad (4.22)$$

where the relation $\eta_1 = \eta_2 \sqrt{\epsilon_r}$ has been used.

To evaluate the coefficients, we first insert (2.14) into (4.20) and let $\rho_3 = \rho_1$, i.e., $k_1 b = k_1 a$. The Wronskian relation from Appendix I,

$$j_n(\rho)\left[\rho h_n(\rho)\right]' - h_n(\rho)\left[\rho j_n(\rho)\right]' = i/\rho \ , \qquad (4.23)$$

is then applied to simplify the expressions. After some algebraic manipulation, it is found that for the source on the sphere surface

$$A_n^{(1)} = \frac{i}{\rho_1} \frac{j_n(\rho_2)}{\left[\rho_1 h_n(\rho_1)\right]' j_n(\rho_2) - \left[\rho_2 j_n(\rho_2)\right]' h_n(\rho_1)}$$

$$B_n^{(1)} = \frac{i}{\rho_2^2} \frac{\rho_2 j_n(\rho_2)'}{\epsilon_r \left[\rho_1 h_n(\rho_1)\right]' j_n(\rho_2) - \left[\rho_2 j_n(\rho_2)\right]' h_n(\rho_1)}$$

$$\frac{C_n^{(1)}}{\sqrt{\epsilon_r}} = -\frac{\epsilon_r}{\rho_2} \frac{j_n(\rho_2)}{\epsilon_r \left[\rho_1 h_n(\rho_1)\right]' j_n(\rho_2) - \left[\rho_2 j_n(\rho_2)\right]' h_n(\rho_1)}$$

$$\frac{D_n^{(1)}}{\sqrt{\epsilon_r}} = \frac{1}{\rho_1 \rho_2} \frac{\rho_2 j_n(\rho_2)'}{\left[\rho_1 h_n(\rho_1)\right]' j_n(\rho_2) - \left[\rho_2 j_n(\rho_2)\right]' h_n(\rho_1)} \cdot \qquad (4.24)$$

In a similar manner but with $\rho_4 = \rho_2$ we find from (4.21), (2.24) and (4.23) that

$$\left.\begin{aligned} A_n^{(2)} &= A_n^{(1)} \\ B_n^{(2)} &= B_n^{(1)} \\ C_n^{(2)} &= C_n^{(1)}/\sqrt{\epsilon_r} \\ D_n^{(2)} &= D_n^{(1)}/\sqrt{\epsilon_r} \end{aligned}\right\} \quad \begin{aligned} \rho_1 &= \rho_3 \\ \rho_2 &= \rho_4 \end{aligned} \tag{4.25}$$

In comparing (4.22) with (4.17), it is seen that (4.25) confirms that the same results are obtained if the excitation is allowed to approach the surface from either the inside or outside of the sphere.

4.4. Far-Zone Field

In the far zone, the spherical Hankel functions of the first kind may be replaced by the leading term of their asymptotic expressions. Thus,

$$\begin{aligned} h_n(kR) &\sim (-i)^{n+1} \frac{e^{ikR}}{kR} \\ \frac{1}{kR}\frac{\partial}{\partial R}\left[Rh_n(kR)\right] &\sim (-i)^n \frac{e^{ikR}}{kR} \end{aligned} \quad . \tag{4.26}$$

For large values of kR, the spherical wave functions become

$$\begin{aligned} \bar{M}^{(1)}_{\substack{e\\o}mn}(kR) &\sim (-i)^{n+1} \frac{e^{ikR}}{kR} \bar{m}_{\substack{e\\o}mn} \\ \bar{N}^{(1)}_{\substack{e\\o}mn}(kR) &\sim (-i)^{n} \frac{e^{ikR}}{kR} \bar{n}_{\substack{e\\o}mn} \end{aligned} \quad , \tag{4.27}$$

where

$$\bar{m}_{\substack{e\\o}mn} = \left\{ \mp \frac{m}{\sin\theta} P_n^m(\cos\theta) \begin{matrix}\sin\\ \cos\end{matrix} m\phi\,\hat{\theta} - \frac{\partial P_n^m(\cos\theta)}{\partial\theta} \begin{matrix}\cos\\ \sin\end{matrix} m\phi\,\hat{\phi} \right\} \tag{4.28}$$

and

$$\bar{n}_{\substack{e\\o}mn} = \left\{ \frac{\partial P_n^m(\cos\theta)}{\partial\theta} \begin{matrix}\cos\\ \sin\end{matrix} m\phi\hat{\theta} \mp \frac{P_n^m(\cos\theta)}{\sin\theta} \begin{matrix}\sin\\ \cos\end{matrix} m\phi\hat{\phi} \right\} . \tag{4.29}$$

Using these results in (4.14) and (4.17) we obtain the following far-zone field expressions for the Huygens' source in the presence of a dielectric sphere.

Source in Region I, $C_m = \eta_1 C_e$

$$\bar{E}_H(\bar{R}) = \frac{-\omega\mu_1 C_e}{4\pi} \frac{e^{ik_1 R}}{R} \sum_{n=1}^{\infty} \frac{2n+1}{n(n+1)} (-i)^n \cdot$$

$$\left\{ -i(A_n^{(1)} + D_n^{(1)})\bar{m}_{o1n} + (B_n^{(1)} + C_n^{(1)})\bar{n}_{e1n} \right\} , \tag{4.30}$$

Source in Region II, $C_m = \eta_2 C_e$

$$\bar{E}_H(\bar{R}) = \frac{-\omega\mu_1 C_e}{4\pi} \frac{e^{ik_1 R}}{R} \sum_{n=1}^{\infty} \frac{2n+1}{n(n+1)} (-i)^n$$

$$\left\{ -i(A_n^{(2)} + D_n^{(2)})\bar{m}_{o1n} + (B_n^{(2)} + C_n^{(2)})\bar{n}_{e1n} \right\} , \tag{4.31}$$

where the coefficients are defined by (4.20) and (4.21).

In order to recover the far-zone field expressions due to the electric or magnetic source only, simply let $C_n = D_n = 0$ or $A_n = B_n = 0$ in the above equations.

Now the source is placed on the surface of the dielectric sphere and the diameter is allowed to become very small. The results using $C_m = \eta_1 C_e$ and $C_m = \eta_2 C_e$ are then compared to those of an ideal Huygens' source in free space.

For small arguments only the first term in the ascending series for the spherical Bessel functions is needed. It is found (Abramowitz and Stegun, 1966)

$$j_n(\rho) \sim \frac{1}{1\cdot 3\cdot 5\ldots(2n+1)} \rho^n$$

$$h_n(\rho) \sim 1\cdot 3\cdot 5\ldots(2n-1)(-i)\rho^{-(n+1)} \tag{4.32}$$

hence,

$$\left[\rho j_n(\rho)\right]' \sim \frac{n+1}{1\cdot 3\cdot 5\ldots(2n+1)}\,\rho^n$$

$$\left[\rho h_n(\rho)\right]' \sim 1\cdot 3\cdot 5\ldots(2n-1)\cdot i\cdot n\rho^{-(n+1)} \quad ,$$

and therefore,

$$\left[\rho_1 h_n(\rho_1)\right]' j_n(\rho_2) \sim \frac{in}{2n+1}\,\rho_1^{-(n+1)}\rho_2^n$$

$$\left[\rho_2 j_n(\rho_2)\right]' h_n(\rho_1) \sim \frac{-i(n+1)}{2n+1}\,\rho_1^{-(n+1)}\rho_2^n \quad . \tag{4.33}$$

Using these relations in (4.24),

$$A_n^{(1)} \sim \frac{\rho_1^n}{1\cdot 3\cdot 5\ldots(2n+1)}$$

$$B_n^{(1)} \sim \frac{(2n+1)(n+1)}{(\epsilon_r n+n+1)\cdot 3\cdot 5\ldots(2n+1)}\,\rho_1^{(n-1)}$$

$$C_n^{(1)} \sim \frac{i\epsilon_r(2n+1)}{(\epsilon_r n+n+1)\cdot 3\cdot 5\ldots(2n+1)}\,\rho_1^n$$

$$D_n^{(1)} \sim \frac{-i\rho_1^{(n-1)}}{1\cdot 3\cdot 5\ldots(2n+1)} \quad , \tag{4.34}$$

and therefore in the limit as $\rho \longrightarrow 0$

$$A_n^{(1)} = C_n^{(1)} = 0$$

$$B_n^{(1)} = B_1^{(1)} = \frac{2}{\epsilon_r+2}$$

$$D_n^{(1)} = D_1^{(1)} = -\frac{2i}{3} \quad . \tag{4.35}$$

Inserting (4.35) into (4.30) and evaluating the $\bar{m}$ and $\bar{n}$ functions given by (4.28) and (4.29) we obtain the following expression:

$$\bar{E}_H(\bar{R}) = \frac{-i\omega\mu_1 C_e}{4\pi}\frac{e^{ik_1R}}{R}\cdot$$

$$\left\{\left(1-\frac{3}{\epsilon_r+2}\cos\theta\right)\cos\phi\hat{\theta}+\left(\frac{3}{\epsilon_r+2}-\cos\theta\right)\sin\phi\hat{\phi}\right\}, \qquad (4.36)$$

where the facts that $P_1^1(\cos\theta)/\sin\theta = 1$ and $\frac{\partial}{\partial\theta}P_1^1(\cos\theta) = \cos\theta$ have been used. Had $C_m = \eta_2 C_e$ been used in relating the electric and magnetic current sources, the coefficients would have been related as shown in (4.25) and the following expression for the field would have been obtained:

$$\bar{E}_H(\bar{R}) = \frac{-i\omega\mu_1 C_e}{4\pi}\frac{e^{ik_1R}}{R}\cdot$$

$$\left\{\left(\frac{1}{\sqrt{\epsilon_r}}-\frac{3}{\epsilon_r+2}\cos\theta\right)\cos\phi\hat{\theta}+\left(\frac{3}{\epsilon_r+2}-\frac{\cos\theta}{\sqrt{\epsilon_r}}\right)\sin\phi\hat{\phi}\right\}. \qquad (4.37)$$

Equations (4.36) and (4.37) may be compared to the expression for the far field radiated from an ideal Huygens' source in free space (4.11), repeated here:

$$\bar{E}_H(\bar{R}) = \frac{-i\omega\mu_1 C_e}{4\pi}\frac{e^{ik_1R}}{R}\left\{(1-\cos\theta)\cos\phi\hat{\theta}+(1-\cos\theta)\sin\phi\hat{\phi}\right\}. \qquad (4.38)$$

It is seen from (4.36), derived using $C_m = \eta_1 C_e$, that even a very small sphere has an effect on the radiation pattern. In particular, the contribution from the electric dipole source has an additional factor of $3/(\epsilon_r+2)$ as compared to the free-space case. The magnetic source contribution, however, has remained unchanged. Note that when $\epsilon_r = 1$, equation (4.36) reduces to (4.38), the free-space case, as it should.

The small dielectric sphere apparently behaves like a short electric dipole with a current moment

$$C_e = \frac{3}{\epsilon_r+2} - 1 = \frac{1-\epsilon_r}{\epsilon_r+2} \qquad (4.39)$$

which is independent of the sphere size. This factor also appears in the results found by Stratton (1941, p. 206) for a dielectric sphere within a uniform static electric field.

Let us now look at the deviation of the small dielectric sphere patterns, using $C_m = \eta_1 C_e$ or $C_m = \eta_2 C_e$ for the electric and magnetic current relations, from the pattern radiated by a Huygens' source in free space.

Let

$$\alpha_1 = \frac{3}{\epsilon_r + 2} \qquad \text{and} \qquad \alpha_2 = \frac{3\sqrt{\epsilon_r}}{\epsilon_r + 2} \quad .$$

The first terms of (4.36) and (4.37) then contain the respective factors

$$1 - \alpha_1 \cos\theta$$

$$\frac{1}{\sqrt{\epsilon_r}} (1 - \alpha_2 \cos\theta)$$

and similarly in the second terms we find the factors

$$\alpha_1 - \cos\theta$$

$$\frac{1}{\sqrt{\epsilon_r}} (\alpha_2 - \cos\theta) \quad .$$

For the Huygens' source in free space $\alpha_1 = \alpha_2 = 1$ and a $(1 - \cos\theta)$ pattern remains.

Table 4-1 shows the values of α_1 and α_2 for various values of dielectric constants. The α_2 remains a good deal closer to unity than α_1, and hence using η_2 for the current relations in constructing the Huygens' source on the surface of a small dielectric sphere will yield only a small error. In fact, α_2 differs from unity by only 6 percent at its maximum value corresponding to a dielectric constant of 2.

TABLE 4-1

Approximate Huygens' Source Factors
For Small Spheres

ϵ_r	α_1	α_2
1.0	1.0	1.0
1.5	0.86	1.05
2.0	0.75	1.06
2.5	0.67	1.05
3.0	0.60	1.04
3.5	0.55	1.02
4.0	0.50	1.00
4.5	0.46	0.98
5.0	0.43	0.96

Chapter V

PROPERTIES OF A HUYGENS' SOURCE IN THE PRESENCE OF A DIELECTRIC SPHERE

5.1 Introduction

In this chapter, the orthogonality relationships between the $\bar{n}$ and $\bar{m}$ functions are shown and then an expression for the radiated power is derived. Equations for the radiation resistance and directivity are formulated and compared to the free-space case for small spheres. Finally, an expression is developed for the power dissipated due to the nonzero conductivity of the dielectric material.

5.2 Radiated Power

In the far zone we found (4.30, 4.31) that the electric field radiated by a Huygens' source in the presence of a dielectric sphere may be represented by

$$\bar{E}_H(\bar{R}) = \frac{-\omega\mu_1 C_e}{4\pi} \frac{e^{ik_1 R}}{R} \sum_{n=1}^{\infty} \frac{2n+1}{n(n+1)} (-i)^n (\alpha_n \bar{m}_{o1n} + \beta_n \bar{n}_{e1n}) \qquad (5.1)$$

where

$$\alpha_n = -i(A_n^{(1)} + D_n^{(1)}) \ ,$$

$$\beta_n = B_n^{(1)} + C_n^{(1)}$$

or

$$\alpha_n = -i(A_n^{(2)} + D_n^{(2)}) \ ,$$

$$\beta_n = B_n^{(2)} + C_n^{(2)}$$

for the source located in Regions I or IL respectively. The vector wave functions in (5.1) are found from (4.28) and (4.29) to be

$$\bar{m}_{o1n} = \frac{P_n^1(\cos\theta)}{\sin\theta} \cos\phi\hat{\theta} - \frac{\partial P_n^1(\cos\theta)}{\partial\theta} \sin\phi\hat{\phi}$$

$$\bar{n}_{e1n} = \frac{\partial P_n^1(\cos\theta)}{\partial\theta}\cos\phi\hat{\theta} - \frac{P_n^1(\cos\theta)}{\sin\theta}\sin\phi\hat{\phi} \quad . \tag{5.2}$$

An expression for the total radiated power W may be derived by integrating the total power flow across an infinitely large sphere, centered at the origin, using the relation

$$W = \frac{1}{2\eta_0}\int_0^{2\pi}\int_0^{\pi} \bar{E}\cdot\bar{E}^* R^2 d\Omega \tag{5.3}$$

where $d\Omega = \sin\theta\, d\theta\, d\phi$, and * denotes the complex conjugate.

Let us now investigate the various scalar products which will be formed in (5.3). From (5.2), it can be seen that each term of the product $\bar{m}_{o1n}\cdot\bar{n}_{e1\ell}$ will contain a factor of the form

$$\frac{P_n^1(\cos\theta)}{\sin\theta}\,\frac{\partial P_\ell^1(\cos\theta)}{\partial\theta} \quad .$$

Using the differential relations for the associated Legendre functions (Stratton, 1941, p. 402), it is found

$$\frac{P_n^1(\cos\theta)}{\sin\theta}\,\frac{\partial P_\ell^1(\cos\theta)}{\partial\theta} = \frac{1}{2}\left[\ell(\ell+1)\frac{P_n^1(\cos\theta)}{\sin\theta}P_\ell^0(\cos\theta) - \frac{P_n^1(\cos\theta)}{\sin\theta}P_\ell^2(\cos\theta)\right].$$

It now follows that

$$\int_0^{\pi}\frac{P_n^1(\cos\theta)}{\sin\theta}\,\frac{\partial P_\ell^1(\cos\theta)}{\partial\theta}\sin\theta\, d\theta = 0 \tag{5.4}$$

since

$$\int_0^{\pi} P_n^m(\cos\theta)\, P_n^k(\cos\theta) d\theta = 0 \quad , \qquad m \neq k \quad .$$

Thus $$\iint \bar{m}_{o1n} \cdot \bar{n}_{e1\ell}\, d\Omega \equiv 0 .$$

Also, on performing the integration,

$$\iint \bar{m}_{o1n} \cdot \bar{m}_{o1\ell}\, d\Omega = \iint \bar{n}_{e1n} \cdot \bar{n}_{e1\ell}\, d\Omega = \frac{2\pi n^2 (n+1)^2}{2n+1}\, \delta_{n\ell} , \tag{5.5}$$

where

$$\delta_{n\ell} = \begin{cases} 0, & n \neq \ell \\ 1, & n = \ell \end{cases}$$

and we have used the formula (Stratton, 1941, p. 417)

$$\int_0^{\pi} \left(\frac{dP_n^m}{d\theta} \frac{dP_\ell^m}{d\theta} + m^2 \frac{P_n^m P_\ell^m}{\sin^2\theta} \right) \sin\theta\, d\theta = \frac{2n(n+1)(n+m)!}{(2n+1)(n-m)!}\, \delta_{n\ell} . \tag{5.6}$$

Upon inserting (5.1) into (5.3) and evaluating the integrals with the aid of (5.5), we obtain the desired relation for the radiated power

$$W = \frac{15}{2} k_1^2 C_e^2 \sum_{n=1}^{\infty} (2n+1)(\alpha_n \alpha_n^* + \beta_n \beta_n^*) , \tag{5.7}$$

where $\eta_0 = 120\pi\,\Omega$.

5.3 Radiation Resistance

Suppose that instead of having an infinitesimal point source, the electric current element were of a short length ℓ with a constant magnitude I_0. Then $C_e = I_0 \ell$, and the radiation resistance for this system is easily obtained.

The radiation resistance of an antenna is defined as

$$R = \frac{2W}{|I_0|^2} . \tag{5.8}$$

That is, assuming no losses, a current element with an rms value of I_0 flowing on an antenna with a radiation resistance R will radiate an average power W.

The far-zone electric field of the crossed dipole source in the absence of the dielectric sphere is given by (4. 10). Using this equation together with (5. 3) and (5. 8), the radiation resistance is given by

$$R = 20(k_1 \ell)^2 \left(1 + \frac{1}{\epsilon_r}\right) \quad . \tag{5. 9}$$

It is apparent from this equation that for the Huygens' source in free space, i.e. $\epsilon_r = 1$, the radiation resistance obtains its maximum value of $40(k\ell)^2$ which is twice that of an elementary electric dipole source.

To determine the radiation resistance of the source in the presence of the dielectric sphere (5. 7) is substituted into (5. 8). Hence

$$R = 15(k_1 \ell)^2 \sum_{n=1}^{\infty} (2n+1)(\alpha_n \alpha_n^* + \beta_n \beta_n^*) \quad . \tag{5. 10}$$

Let us now place the source on the surface of the sphere, allow the radius to become small, and see how the resulting radiation resistance compares to the free-space case. Using the relations (4. 35) to evaluate α and β we find for the case when $C_m = \eta_1 C_e$

$$R = 20(k\ell)^2 \left[1 + \left(\frac{3}{\epsilon_r + 2}\right)^2\right] \quad . \tag{5. 11}$$

Had we let $C_m = \eta_2 C_e$ in relating the electric and magnetic current moments, instead of (5. 11) we would have obtained

$$R = 20(k\ell)^2 \left[\frac{1}{\epsilon_r} + \left(\frac{3}{\epsilon_r + 2}\right)^2\right] \quad . \tag{5. 12}$$

In order to compare the radiation resistances for the various sources, (5. 9), (5. 11) and (5. 12) are divided by $(k\ell)^2$ and the results denoted by R_0, R_1 and R_2,

respectively. The results are shown in Table 5-1 for various values of ϵ_r.

TABLE 5-1

Normalized Radiation Resistance
for Sources on Small Spheres

ϵ_r	R_0	R_1	R_2
1	40.0	40.0	40.0
2	30.0	31.2	21.2
3	26.6	27.2	13.8
4	25.0	25.0	10.0
5	24.0	23.6	6.6

It can be seen that the normalized radiation resistance R_1 of the source ($C_m = \eta_1 C_e$) on the surface of a small dielectric sphere closely corresponds to the free-space case, R_0. It should be noted, however, that R_0 does not correspond to the Huygens' source, i.e., $1-\cos\theta$ pattern, unless $\epsilon_r = 1$ in (5.9). The normalized radiation resistance R_2 of the source ($C_m = \eta_2 C_e$) is smaller than R_1 because in the former the magnetic current moment is reduced in order to compensate for the reduction of the electric current moment by the dielectric sphere. In the next chapter, it will be seen that the radiation resistance for larger spheres tends to oscillate about the free-space value.

5.4. Directivity

The directivity in the forward direction relative to an isotropic source is defined by

$$D = \frac{4\pi(\text{radiation intensity in } \theta = 180^\circ \text{ direction})}{\text{total power radiated}}, \qquad (5.13)$$

since for the sphere concentric with the origin, and the source located on the $+z$ axis, we are interested in the relative field intensity in the $-\hat{z}$ ($\theta = 180^\circ$) direction.

From (5.2), it is evident that

$$\bar{m}_{oln}\Big|_{\substack{\theta=\pi \\ \phi=0}} = (-1)^{n+1}\,\frac{n(n+1)}{2}\,\hat{\theta}$$

and

$$\bar{n}_{o\ln}\Big|_{\substack{\theta=\pi \\ \phi=0}} = (-1)^n \frac{n(n+1)}{2}\,\hat{\theta} \tag{5.14}$$

since

$$\frac{P_n^1(\cos\theta)}{\sin\theta}\bigg|_{\theta=\pi} = (-1)^{n+1}\frac{n(n+1)}{2}$$

and

$$\frac{\partial P_n^1(\cos\theta)}{\partial\theta}\bigg|_{\theta=\pi} = (-1)^n \frac{n(n+1)}{2} \quad .$$

Using this result in (5.1), an expression for the radiated power intensity in the -z direction is obtained. Thus,

$$\frac{R^2}{2\eta_0}\,\bar{E}\cdot\bar{E}^*\Big|_{\theta=\pi} = \frac{15k_1^2C_e^2}{4\pi}\left|\sum_{n=1}^{\infty}\frac{2n+1}{2}(i)^n(\alpha_n+\beta_n)\right|^2 \tag{5.15}$$

where $\eta_0 = 120\pi\,\Omega$.

Combining (5.15), (5.7) and (5.13), the desired directivity formula results:

$$D = \frac{\left|\sum_{n=1}^{\infty}\frac{2n+1}{2}(i)^n(\alpha_n+\beta_n)\right|^2}{\sum_{n=1}^{\infty}\frac{2n+1}{2}(\alpha_n\alpha_n^*+\beta_n\beta_n^*)} \quad . \tag{5.16}$$

Again, it is noted that $A_n = B_n = 0$ or $C_n = D_n = 0$ in the expressions for α_n and β_n in Section 5.2, in order to recover the result due to the magnetic or electric source only.

It is found from (5.16) for the small sphere case that

$$D_2 = \frac{\frac{3}{2}\left(\frac{\epsilon_r+2}{3\sqrt{\epsilon_r}}+1\right)^2}{\left(\frac{\epsilon_r+2}{3\sqrt{\epsilon_r}}\right)^2+1} \qquad \text{for } C_m = \eta_2 C_e \,, \tag{5.17}$$

and

$$D_1 = \frac{\frac{3}{2}\left(\frac{\epsilon_r+2}{3}+1\right)^2}{\left(\frac{\epsilon_r+2}{3}\right)^2+1} \qquad \text{for } C_m = \eta_1 C_e \,. \tag{5.18}$$

The results are shown for various values of ϵ_r in Table 5-2.

TABLE 5-2

Directivity of Sources on Small Spheres

ϵ_r	D_1	D_2
1	3.000	3.000
2	2.940	2.997
3	2.824	2.999
4	2.700	3.000
5	2.586	2.999

From (4.11) and (5.13) it can be shown that the directivity of a Huygens' source is 3. From Table 5-2 it is seen that the directivity D_2 remains approximately this value.

In Chapter 6, it will be of interest to compare the directivity of the pattern radiated by the dielectric sphere with that of a uniformly illuminated aperture of the same diameter. The normalized field pattern of a large uniform aperture as shown in Fig. 5-1 can be found by the application of Huygens' principle and is given by Kraus (1950):

$$E(\theta) = \frac{2\lambda}{\pi d}\,\frac{J_1\left(\frac{\pi d}{\lambda}\sin\theta\right)}{\sin\theta} \,. \tag{5.19}$$

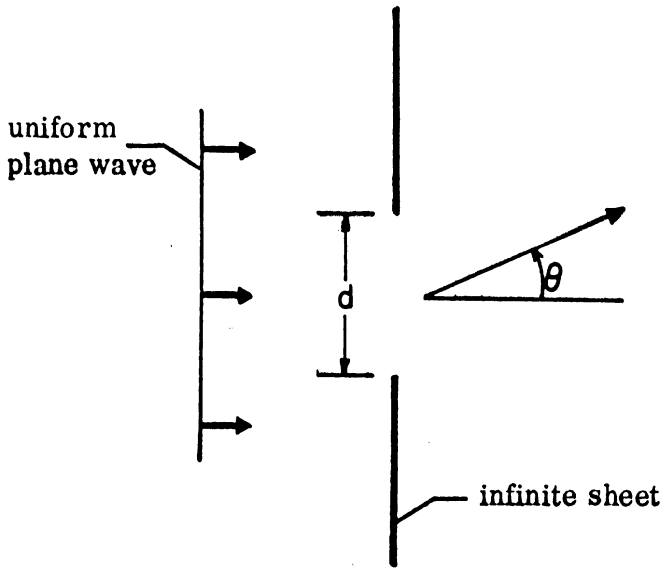

FIG. 5-1: UNIFORMLY ILLUMINATED APERTURE.

For this case, the expression

$$D = \frac{|E(0)|^2}{\frac{1}{4\pi}\int |E(\theta)|^2 d\Omega}$$

is used for the directivity, and hence

$$D = \frac{\pi^2 d^2}{2\lambda^2 \int_0^{\pi/2} \frac{\left[J_1\left(\frac{\pi d}{\lambda}\sin\theta\right)\right]^2}{\sin\theta} d\theta} \quad . \tag{5.20}$$

5.5 Dielectric Loss

For a lossy dielectric ϵ_2 is complex and may be represented by

$$\epsilon_2 = \epsilon' + i\epsilon'' \quad , \tag{5.21}$$

where ϵ' and ϵ'' are the real and imaginary parts of the permittivity

respectively. The conductivity σ is related to ϵ'' by

$$\sigma = \omega\epsilon'' \quad , \tag{5.22}$$

and the loss tangent is defined as

$$\tan\delta = \epsilon''/\epsilon' \quad . \tag{5.23}$$

Equation (5.21), therefore, may be cast in the form

$$\epsilon_2 = \epsilon'(1+i\tan\delta) \quad . \tag{5.24}$$

The propagation constant k_2 will also be complex, being equal to

$$k_2 = k'\sqrt{1+i\tan\delta} \quad . \tag{5.25}$$

Thus, in the previously derived equations, ϵ_2, k_2 and also η_2 are simply replaced by their complex values to account for the dielectric loss.

To find the power dissipated within the sphere, the source is placed in Region I close to the surface of the sphere. With $C_m = \eta_2 C_e$, it is found from (3.6) and (3.18) that the electric field within the sphere is given by

$$\bar{E}_H(\bar{R}) = \frac{-k_1\omega\mu C_e}{4\pi}\sum_{n=1}^{\infty}\frac{2n+1}{n(n+1)}\left\{\nu\bar{M}_{o1n}(k_2)+\xi\bar{N}_{e1n}(k_2)\right\} \quad , \tag{5.26}$$

where

$$\bar{M}_{o1n}(k_2) = j_n(\rho)\left[\frac{P_n^1(\cos\theta)}{\sin\theta}\cos\phi\hat{\theta} - \frac{\partial P_n^1(\cos\theta)}{\partial\theta}\sin\phi\hat{\phi}\right] \tag{5.27}$$

$$\bar{N}_{e1n}(k_2) = \frac{n(n+1)}{\rho}j_n(\rho)P_n^1(\cos\theta)\cos\phi\hat{R} + \frac{1}{\rho}\left[\rho j_n(\rho)\right]'\left[\frac{\partial P_n^1(\cos\theta)}{\partial\theta}\cos\phi\hat{\theta} - \frac{P_n^1(\cos\theta)}{\sin\theta}\sin\phi\hat{\phi}\right] \tag{5.28}$$

$$\rho = k_2 R$$

$$\nu = c_n^{(1)} h_n(\rho_3) - \frac{ic_n^{(1)}}{\sqrt{\epsilon_r}} \frac{[\rho_3 h_n(\rho_3)]'}{\rho_3}$$

$$\xi = d_n^{(1)} \frac{[\rho_3 h_n(\rho_3)]'}{\rho_3} + i \frac{d_n^{(1)}}{\sqrt{\epsilon_r}} h_n(\rho_3)$$

and $c_n^{(1)}$, $d_n^{(1)}$ are given by (2.14).

The power dissipated within a region of conductivity σ is given by the formula

$$P_D = \frac{1}{2} \iiint \sigma \bar{E} \cdot \bar{E}^* dV \quad . \tag{5.29}$$

For a homogeneous sphere of radius a (5.29) becomes

$$P_D = \sigma/2 \int_0^{2\pi} \int_0^{\pi} \int_0^{a} \bar{E}(\bar{R}) \cdot \bar{E}(R)^* R^2 \sin\theta \, dR \, d\theta \, d\phi \, . \tag{5.30}$$

Because of the orthogonality of the associated Legendre functions and their derivatives, shown in Section 5.2,

$$\int_0^{\pi} \bar{M}_{o1n} \cdot \bar{N}_{e1\ell} \sin\theta \, d\theta \equiv 0 \quad .$$

Also, it is easy to show

$$\int_0^{2\pi} \int_0^{\pi} \bar{M}_{o1n}(\rho) \cdot \bar{M}_{o1\ell}^*(\rho) d\Omega = 2\pi n^2 \frac{(n+1)^2}{2n+1} j_n(\rho) j_n^*(\rho) \delta_{n\ell}$$

and

$$\int_0^{2\pi} \int_0^{\pi} \bar{N}_{e1n}(\rho) \cdot \bar{N}_{e1\ell}^*(\rho) \, d\Omega = \frac{2\pi n^2 (n+1)^2}{\rho\rho^* (2n+1)} \Big[n(n+1) j_n(\rho) j_n^*(\rho) + [\rho j_n(\rho)]' [\rho j_n(\rho)]'^* \Big] \delta_{n\ell} \quad , \tag{5.31}$$

where we have used (5.6) and the formula (Stratton, 1941, p. 403)

$$\int_0^{\pi} P_n^m(\cos\theta) P_\ell^m(\cos\theta)\sin\theta\, d\theta = \frac{2}{2n+1}\frac{(n+m)!}{(n-m)!}\,\delta_{n\ell} \quad .$$

With the aid of (5.31) the θ and ϕ integrations are performed and an expression for the dissipated power obtained. Thus,

$$P_D = \frac{\sigma k_1^2 \omega^2 \mu_1^2 C_e^2}{16\pi} \sum_{n=1}^{\infty} (2n+1) \int_0^a \left\{ \nu\nu^* j_n(\rho) j_n(\rho)^* + \frac{\xi\xi^*}{\rho\rho^*} \left[n(n+1) j_n(\rho) j_n^*(\rho) + \left[\rho j_n(\rho)\right]' \left[\rho j_n(\rho)\right]'^* \right] \right\} R^2 dR$$

or

$$P_D = \frac{15\sigma\eta_0 k_1^2 C_e^2}{2|\epsilon_r|} \sum_{n=1}^{\infty} (2n+1) \int_0^a \left\{ \left|\nu\rho j_n(\rho)\right|^2 + n(n+1)\left|\xi j_n(\rho)\right|^2 + \left|\xi\left[\rho j_n(\rho)\right]'\right|^2 \right\} dR \quad . \tag{5.32}$$

Now that expressions for the dissipated power P_D and the radiated power W (5.7) are available, the antenna efficiency may be computed from the relation

$$\frac{\text{Power radiated}}{\text{Total input power}} = \frac{W}{W+P_D} \quad . \tag{5.33}$$

Chapter VI

NUMERICAL RESULTS

6.1 Introduction

Some of the more significant equations derived in Chapters IV and V were programmed and evaluated using the University of Michigan IBM System 360 Model 67 dual-processor computer. The data was then plotted on the CALCOMP 780/763 digital plotter.

In this chapter, the numerical results using a Huygens' source are first compared with measured data for plexiglas spheres placed over the ends of waveguides. Curves are then presented showing the variation of directivity with sphere diameter for various dielectric constants. Subsequently, the resonant modes of the dielectric sphere are studied together with the effect of dielectric loss. Finally, curves are presented which show that directive patterns may be produced with the source located inside the sphere.

6.2 Comparison with Measured Data for the Plexiglas Sphere

The far-zone electric fields radiated from a Huygens' source on the surface of a dielectric sphere (4.31) were calculated numerically for the two principle planes using the computer program listed in Appendix B. Since the series for the far field converges in a manner similar to the spherical Bessel functions it was found that $N = kD+7$ terms provided sufficient accuracy.

The normalized power patterns for various diameter spheres, computed in one degree increments, are presented in Figures 6-1 to 6-4. Here the E and H planes correspond to the $\phi = 0$ and $\phi = \pi/2$ planes, respectively. In each case, a dielectric constant of 2.57 with a loss tangent of .0065 was used, which is typical of plexiglas in the frequency range of interest (von Hippel, 1954). It should be noted that with the source oriented as shown in Fig. 4-3, the maximum radiation occurs in the -z direction, and hence the top of the computed patterns correspond to $\theta = 180$ degrees.

The curves on the left of each figure were measured by Croswell and Chatterjee in the anechoic chamber located at the NASA Langley Research Center. These measurements were made using plexiglas spheres centered against the flange of an open-ended waveguide. The parameters are listed in Table 6-1. It should be noted that no attempt was made to impedance match the waveguide or, in the case of the rectangular guide, to physically fit the aperture to the curved surface of the sphere.

TABLE 6-1

Measurement Parameters

Sphere Diameter (inches)	3	5	5	5
Frequency (GH_z)	5.0	5.0	8.0	10.0
Sphere Diameter (λ_0)	1.27	2.12	3.39	4.23
Waveguide Type	C-band Circular		X-band Rectangular	

From these patterns, Figs. 6-1 to 6-4, it can be seen that the agreement is quite good, particularly for the larger diameter spheres. The theoretical patterns do, however, show sharper nulls in the main beam and stronger back lobes than the measured patterns. These differences may be due to scattering from the waveguide feed structure used in the measurements.

Figure 6-5 shows the directivity of the Huygens' source on the surface of the sphere computed from (5.16). Again, a dielectric constant of 2.57 and loss tangent of .0065 have been used. For comparison, the directivity of a uniformly illuminated circular aperture (5.20) is also shown. The abscissa is measured in aperture diameter or sphere diameter in free-space wavelengths. The small circles and crosses in the figure represent directivities derived from measured patterns for waveguide-excited plexiglas spheres using the empirical formula

$$D = \frac{K}{\theta_1 \theta_2} \quad ,$$

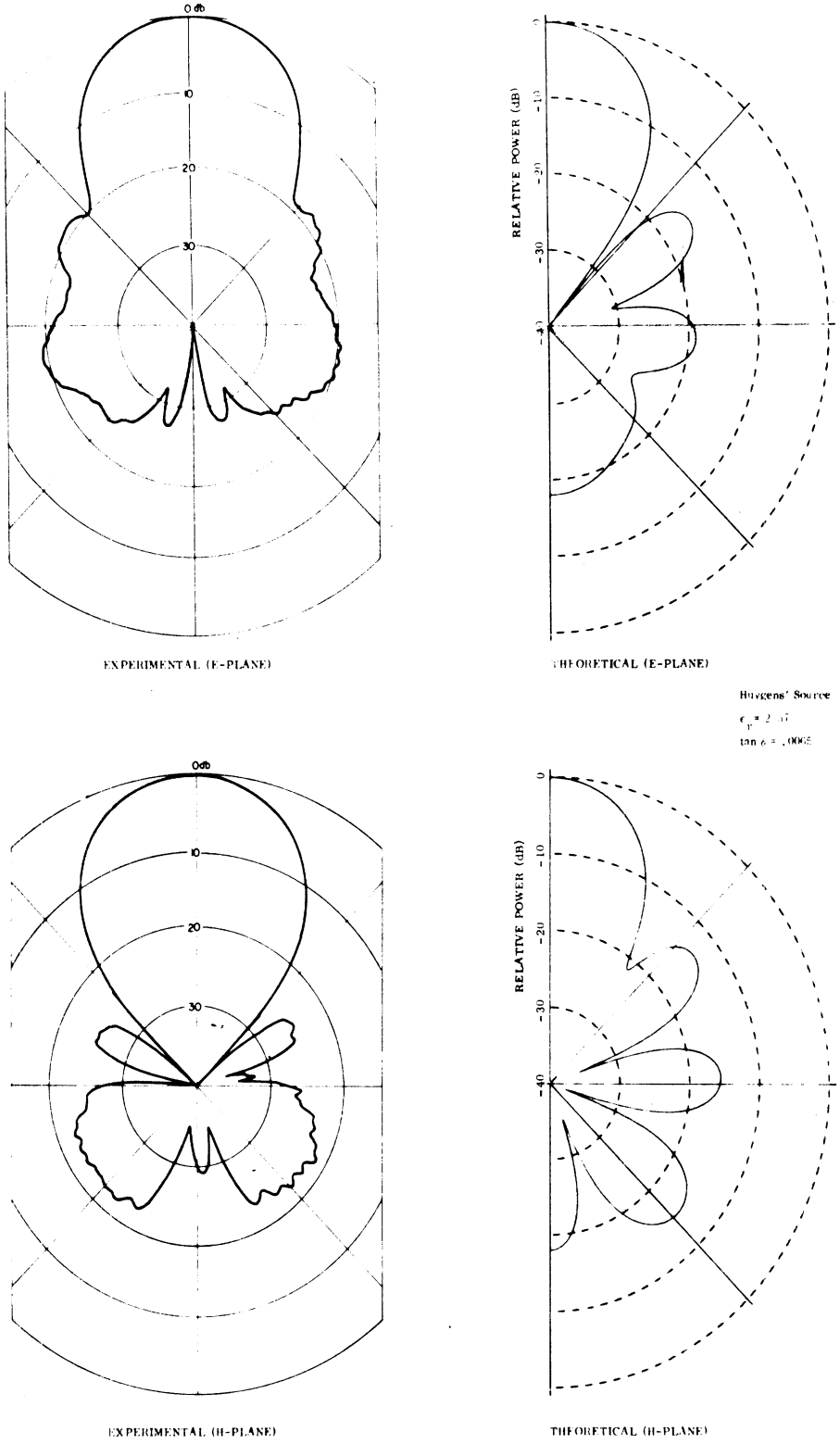

FIG. 6-1: RADIATION PATTERNS FOR PLEXIGLAS SPHERE ($D = 1.27\lambda_o$).

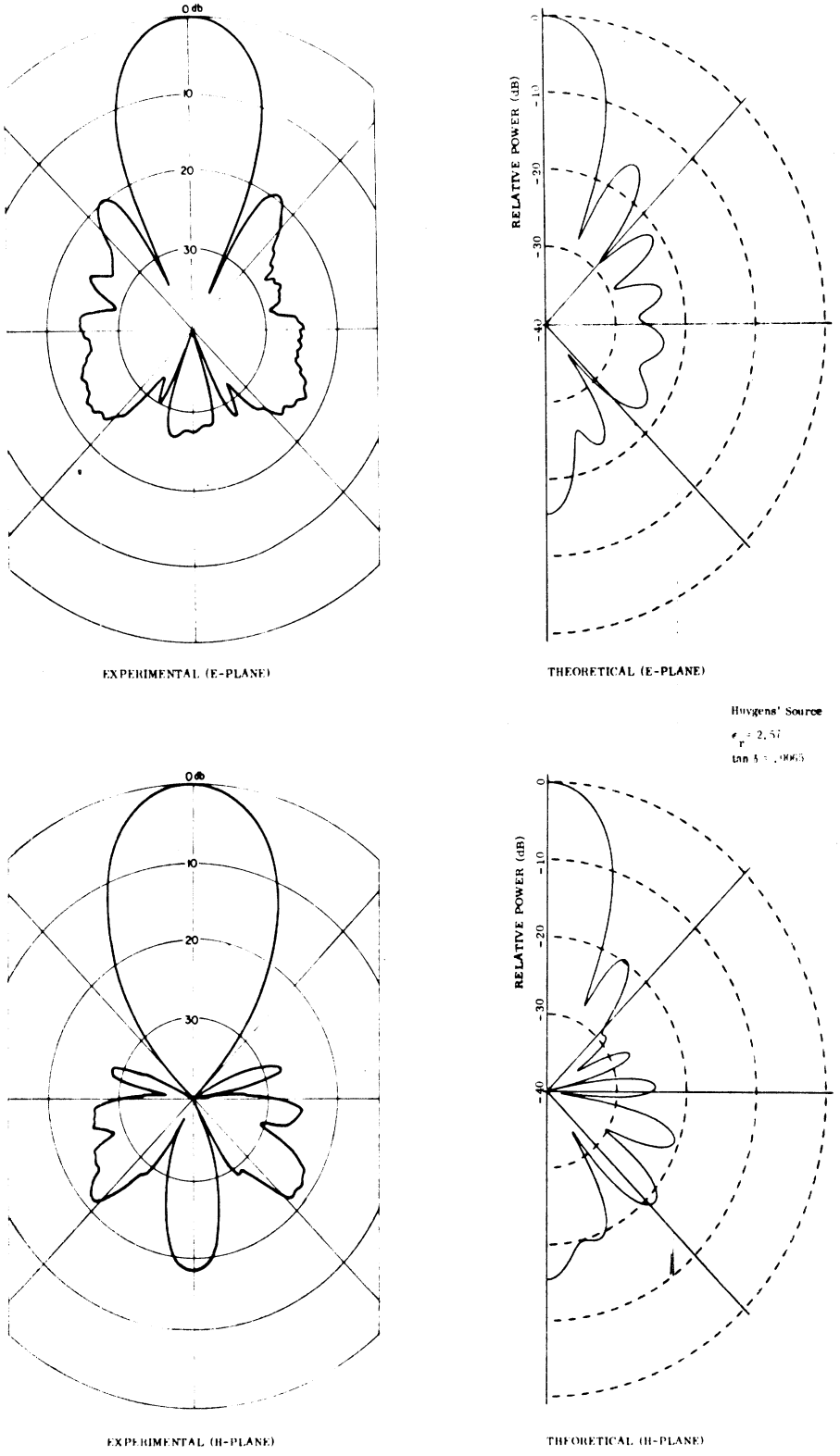

FIG. 6-2: RADIATION PATTERNS FOR PLEXIGLAS SPHERE ($D = 2.12\lambda_o$).

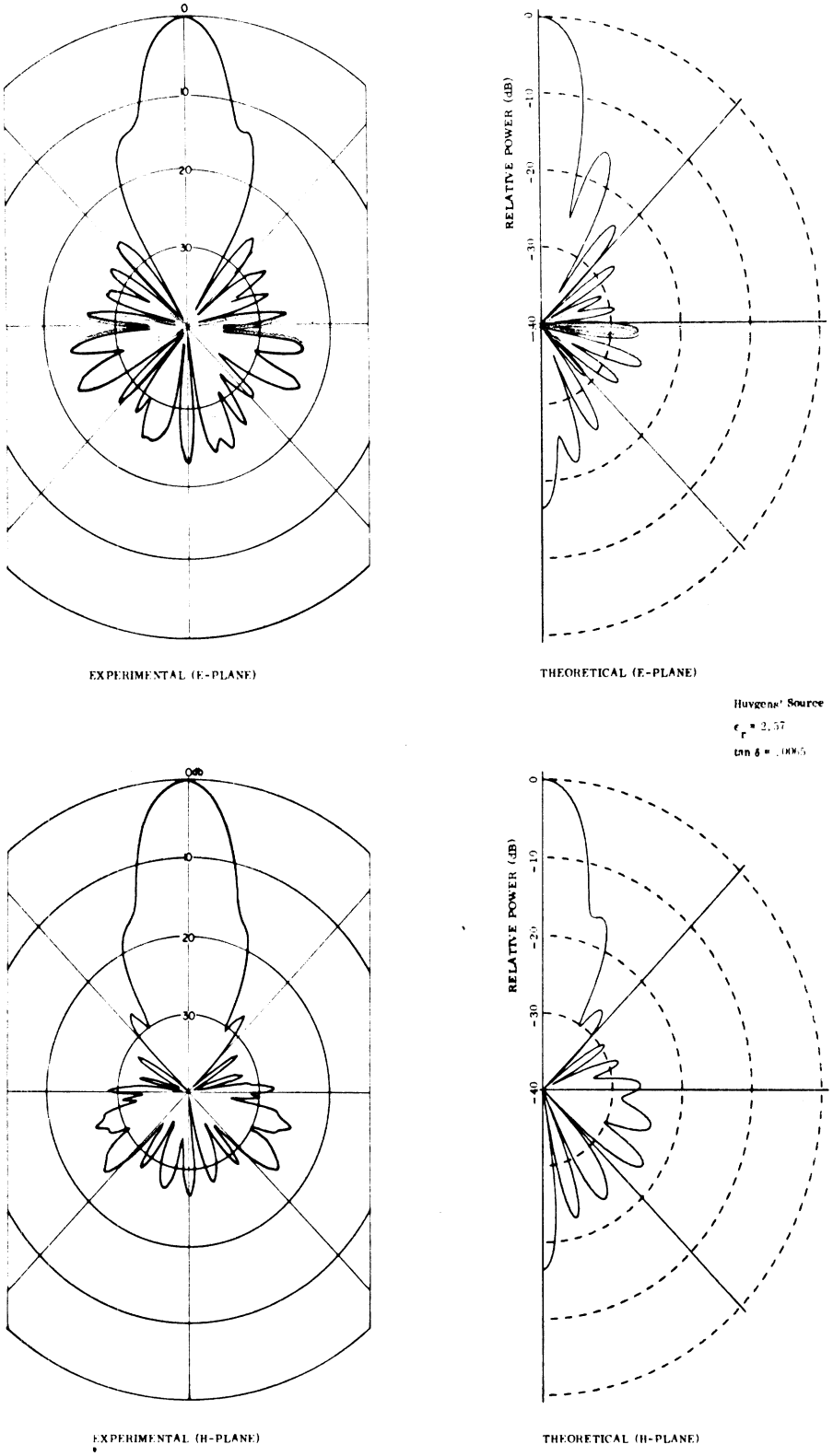

FIG. 6-3: RADIATION PATTERNS FOR PLEXIGLAS SPHERE ($D = 3.39\lambda_o$).

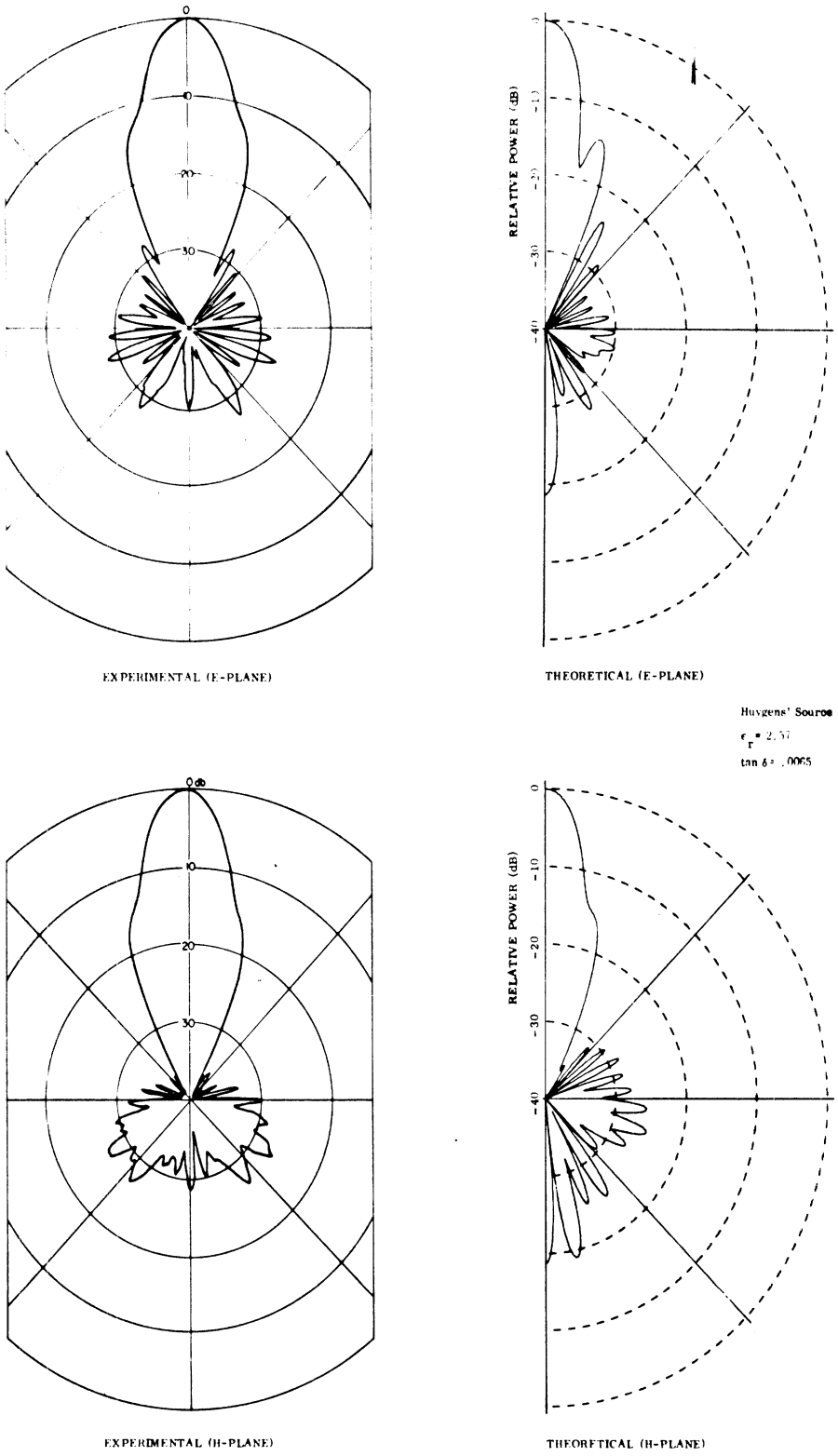

FIG. 6-4: RADIATION PATTERN FOR PLEXIGLAS SPHERE ($D = 4.23\lambda_o$)

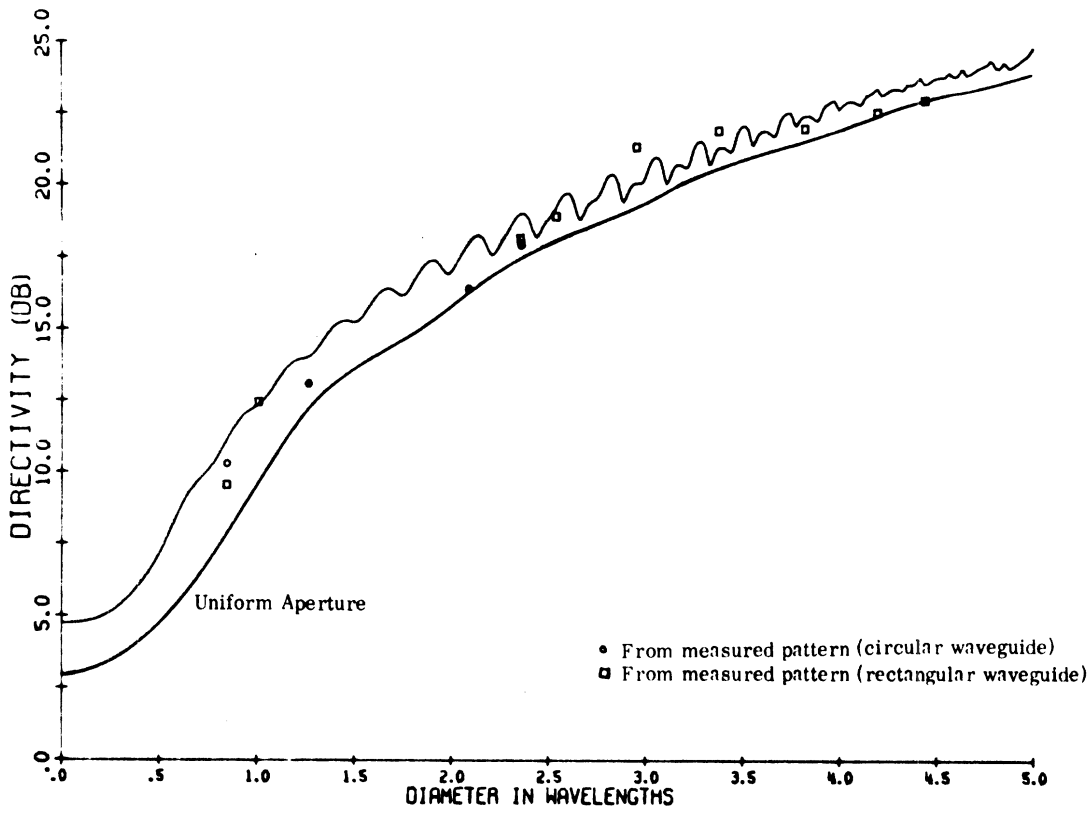

FIG. 6-5: DIRECTIVITY OF PLEXIGLAS SPHERE ($\epsilon_r = 2.57$, $\tan\delta = .0065$).

where K is a constant and θ_1 and θ_2 are the half-power beamwidths in the two principle planes measured in degrees. By comparing the computed directivity with the beamwidths of the Huygens' source patterns, it was found that K = 26,500 yielded an error less than 0.5dB for sphere diameters in the range of interest. Since the measured and computed patterns have the same general shape, this value of K was used in the above formula.

It can be seen from Fig. 6-5 that the experimental and theoretical directivities agree quite favorably with a maximum deviation of 1.7dB occurring at $D = .85\lambda_0$. It is also noted that for the measured data available, the directivity is generally greater than that for a uniformly illuminated aperture.

In Table 6-2, the radiation patterns presented in Fig. 6-3 for the dielectric sphere are compared to that observed for a conical horn of about the same diameter (3.4λ) as given by Jasik (1961). The data is for a horn optimized in the sense that the flare angle has been adjusted to yield a maximum phase deviation of $3/8\lambda$ in the aperture wavefront.

TABLE 6-2

Comparison with Optimum Horn

Parameter	Optimized Horn $D = 3.4\lambda_0$	Plexiglas Sphere, $D = 3.39\lambda_0$	
		Measured	Theoretical
E-plane, 3 dB beamwidth (degrees)	16	12.5	14
H-plane, 3 dB beamwidth (degrees)	19	14	14
First sidelobe level, E-Plane (dB)	-8.5	-13.5	-16
First sidelobe angle from axis, E-plane (degrees)	22	20	22
Directivity (dB)	17.7	23.7	21.0

From this table, one can see that both the measured and theoretical patterns for the plexiglas sphere have lower sidelobes and higher directivity than the optimized conical horn.

Figure 6-6 shows the radiation resistance computed from (5.10) together with power reflection coefficient curves measured for 2 and 3-inch plexiglas spheres.

Here it is noted that both the radiation resistance and the measured curves have strong peaks occurring with a periodicity of about $D = 0.25\lambda_0$ or $(k_2 a) = 1.26$.

The antenna efficiency was computed using (5.33) and is plotted in Fig. 6-7. For this computation, the source was placed $0.01\lambda_0$ from the sphere surface to avoid the problem of infinite loss associated with a point source in contact with a lossy medium (Tai, 1947).

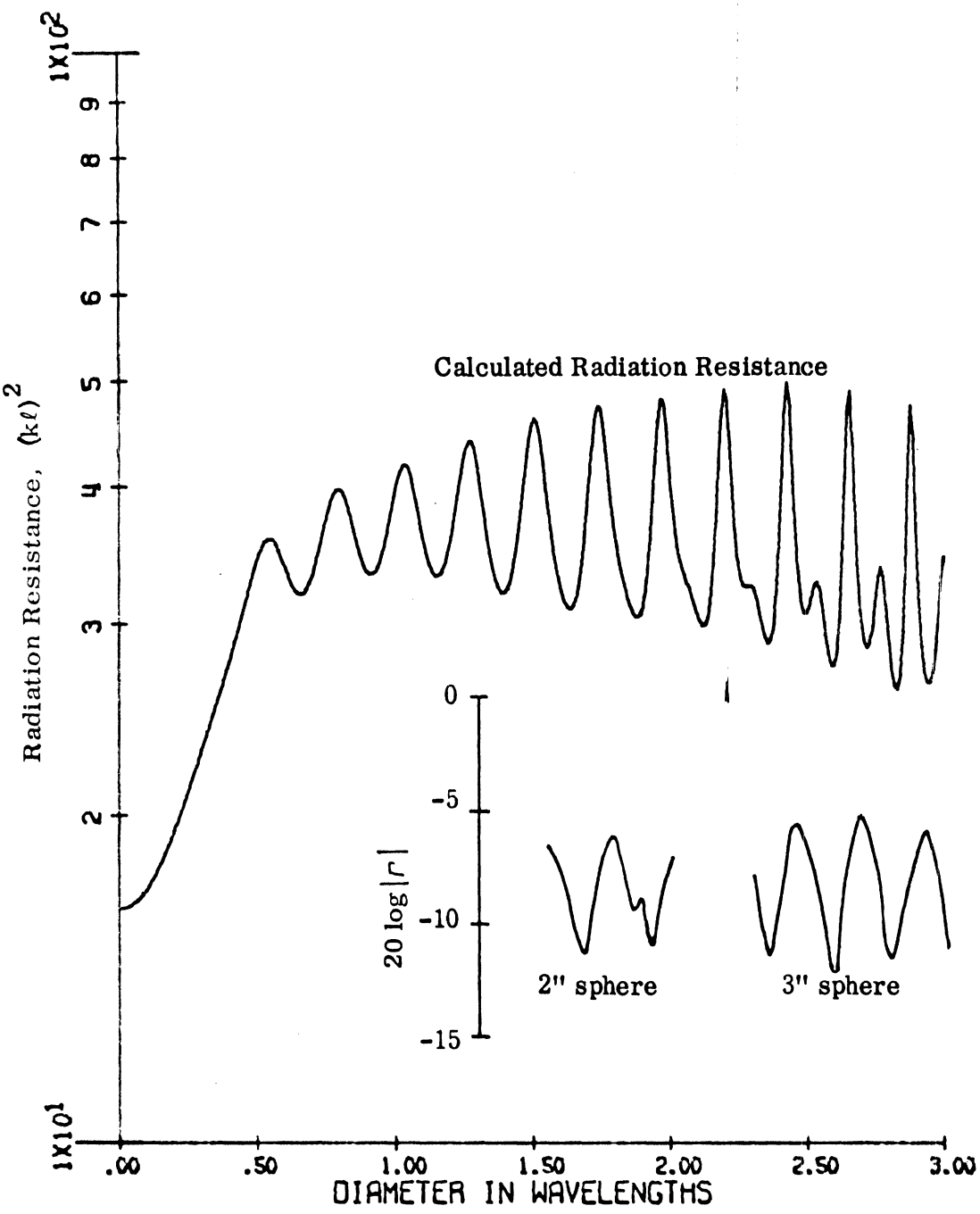

FIG. 6-6: CALCULATED RADIATION RESISTANCE AND MEASURED REFLECTION COEFFICIENTS (dB) FOR PLEXIGLAS SPHERES.

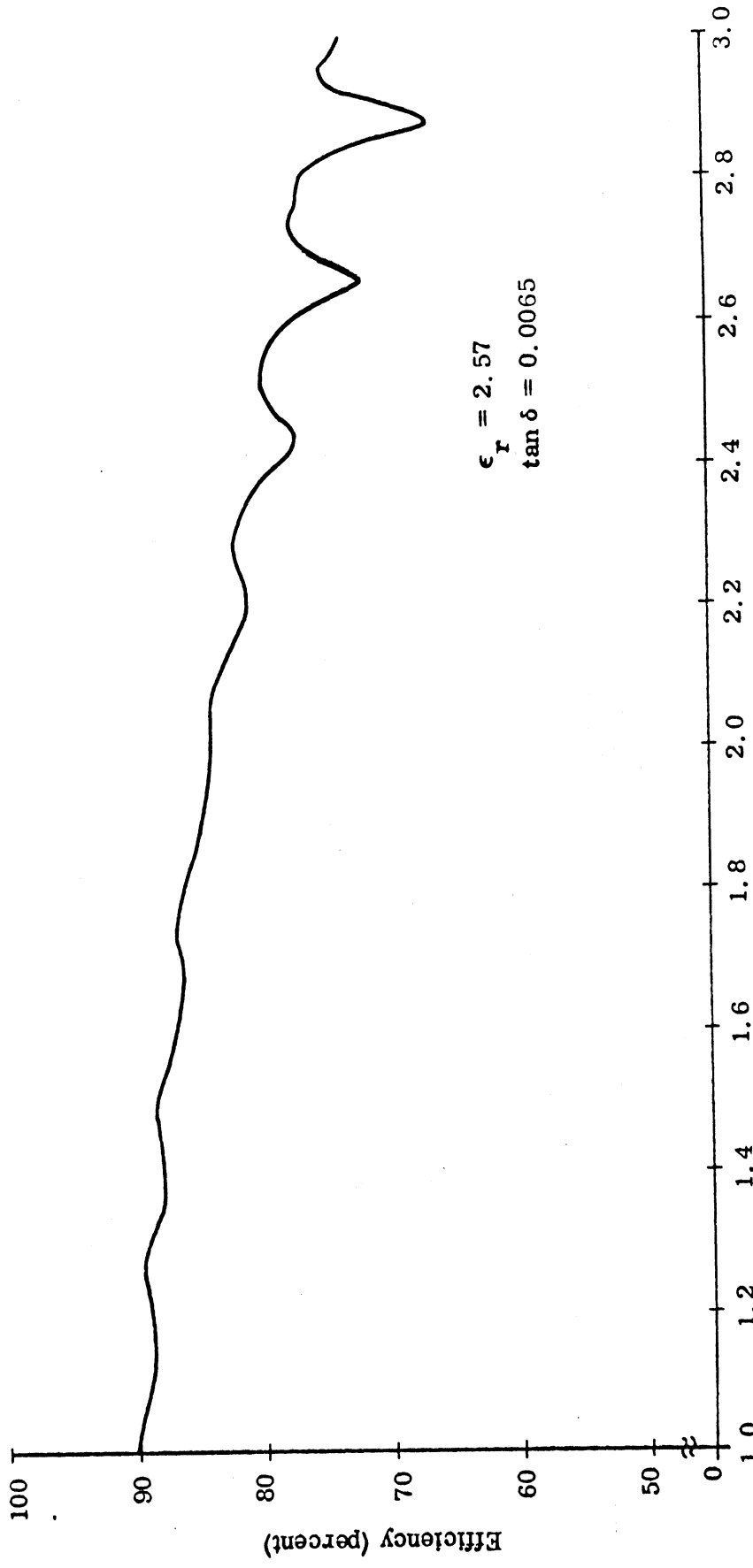

FIG. 6-7: CALCULATED ANTENNA EFFICIENCY OF HUYGENS' SOURCE NEAR A PLEXIGLAS SPHERE.

As one might expect, the antenna efficiency generally decreases with increasing sphere diameter. It is also noted (Fig. 6-7) that for the larger sphere diameters the efficiency curve shows a marked decrease at the same points the radiation resistance (Fig. 6-6) shows sharp peaks.

6.3 Directivity

Since the directivity is an important parameter in antenna design, the value of dielectric constant which maximizes this parameter for a given diameter is of interest.

The directivities for the Huygens' source on the surface of the sphere (5.16) are plotted as a function of sphere diameter for various lossless dielectrics in Fig. 6-8. Since the curves were plotted at only a finite number of points (0.01 diameter interval), it is recognized that some of the fine structure may not be precise. Nevertheless, it is apparent from these figures that as the diameter increases, the directivity becomes frequency-sensitive, with the effect being more pronounced for the higher dielectric spheres. The sharp dips in these curves are due to a resonance effect, discussed in detail in Section 6.4, caused by the dielectric sphere in which much of the energy is radiated into the sidelobes.

The resonance effect was not noted in the relatively smooth curve of Fig. 6-5 because the dielectric loss was included in the calculation. By comparing the directivity curves of Fig. 6-9 which were calculated using a loss tangent of .0065 with the lossless curves of Fig. 6-8, it is noted that the loss tends to attenuate the resonance with the effect being most notable at the larger sphere diameters. The dielectric loss, however, had little effect on the peaks of the curves.

Figure 6-9f was constructed by drawing smooth curves through the maximum points on the directivity curves presented in Figures 6-5 and 6-9. Here it is seen that a dielectric constant of about 3.0 tends to optimize the directivity, particularly for the larger diameter spheres.

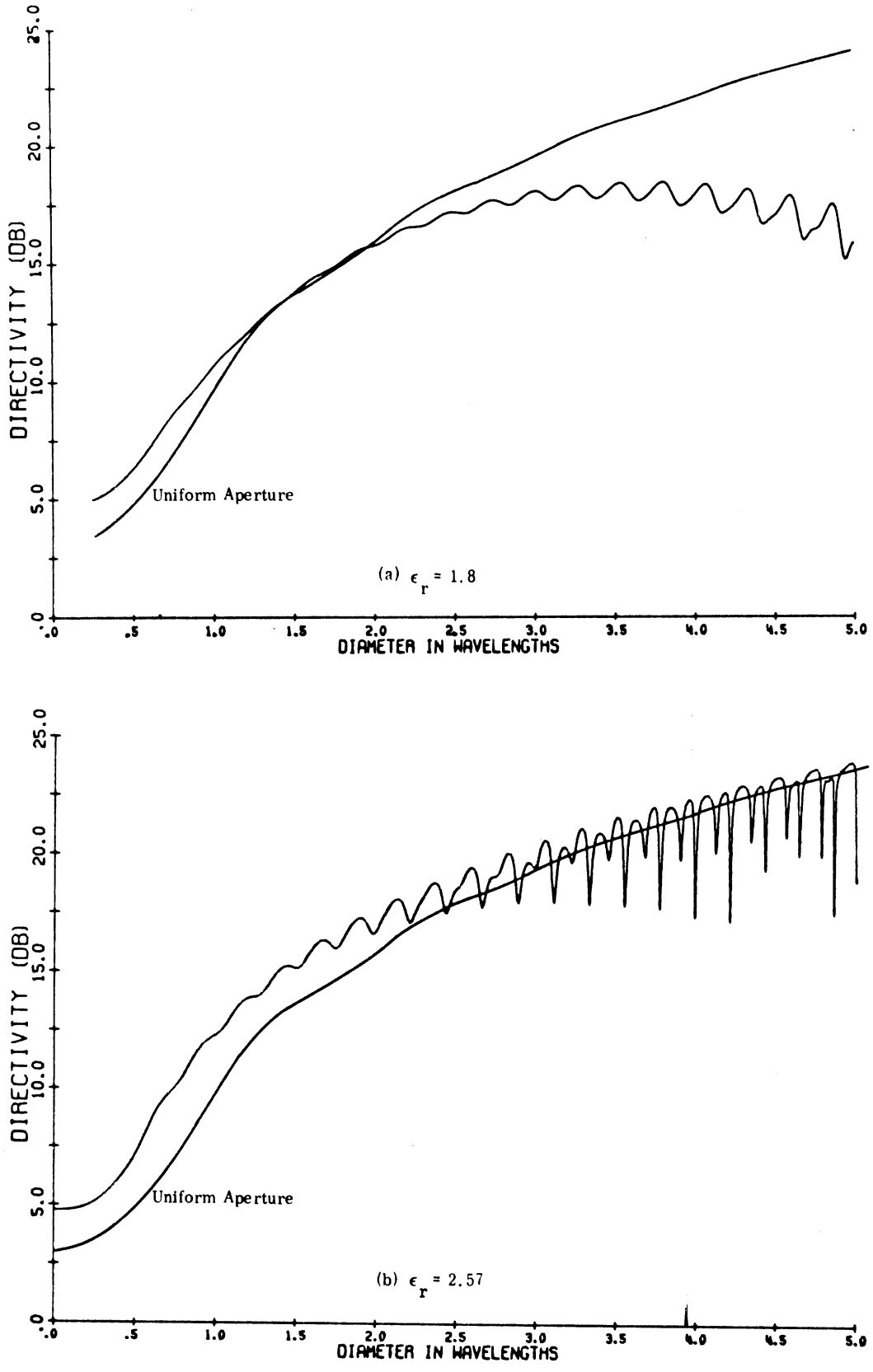

FIG. 6-8: DIRECTIVITY OF LOSSLESS SPHERES.

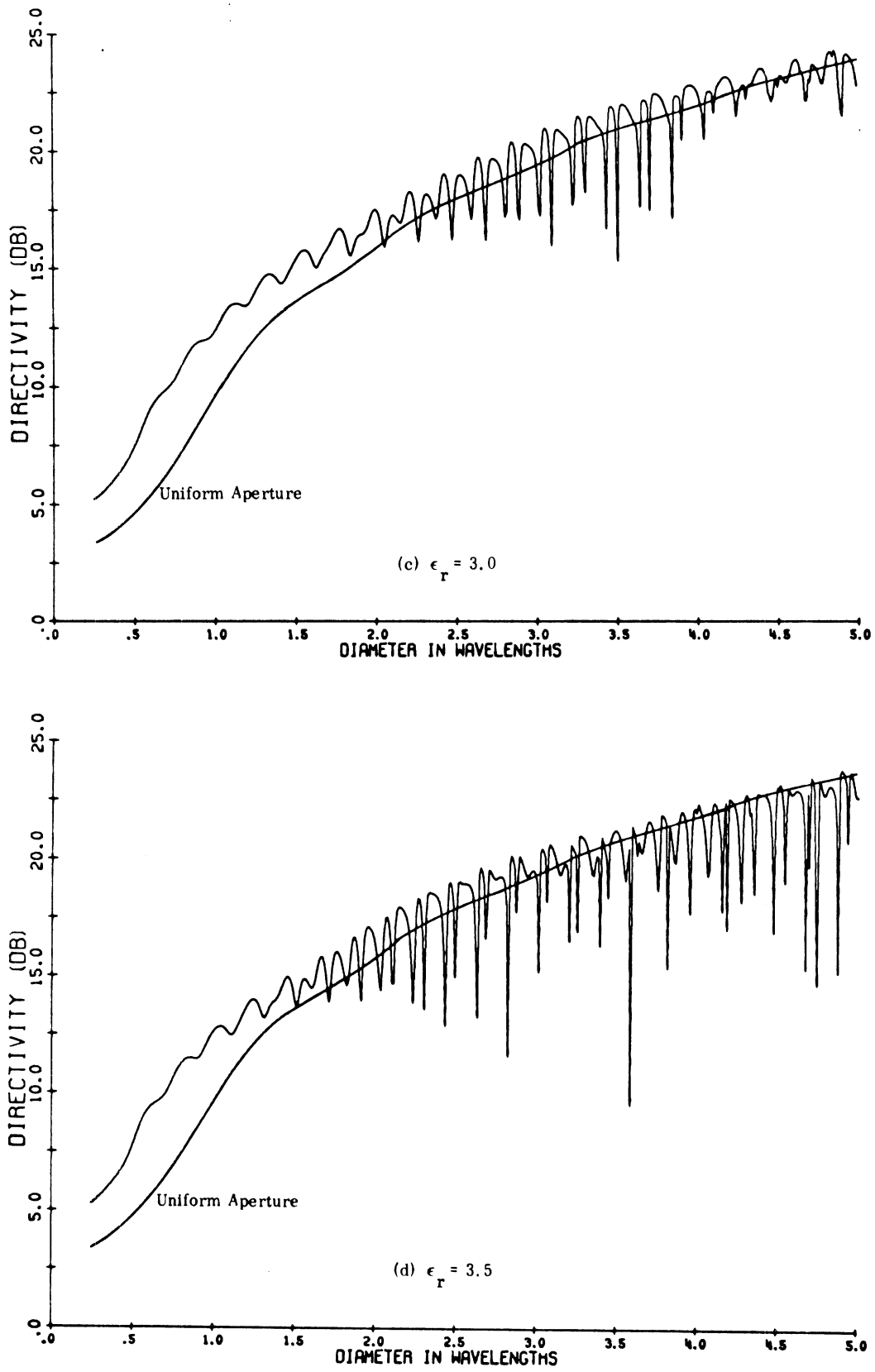

FIG. 6-8: DIRECTIVITY OF LOSSLESS SPHERES.

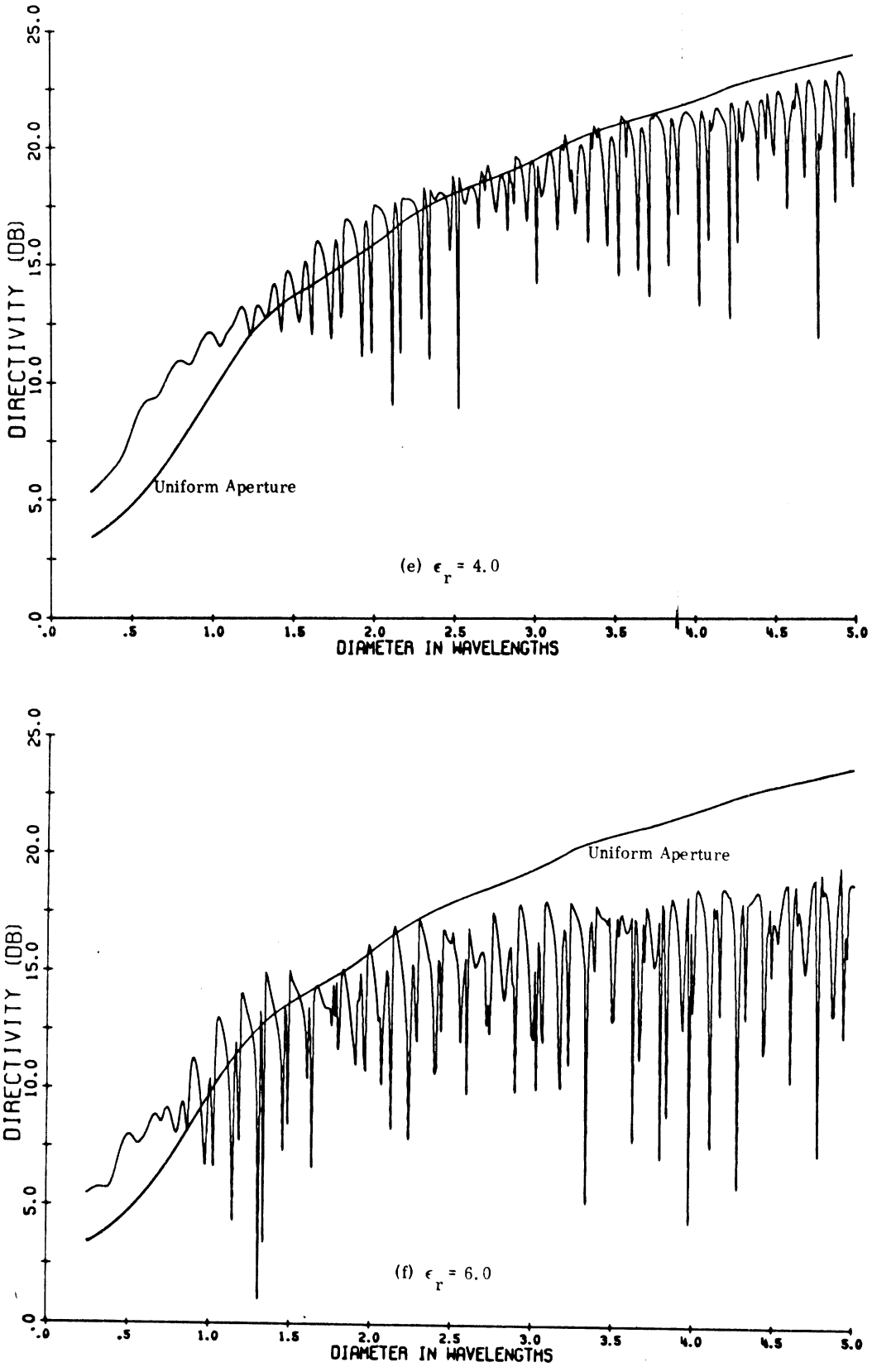

FIG. 6-8: DIRECTIVITY OF LOSSLESS SPHERES.

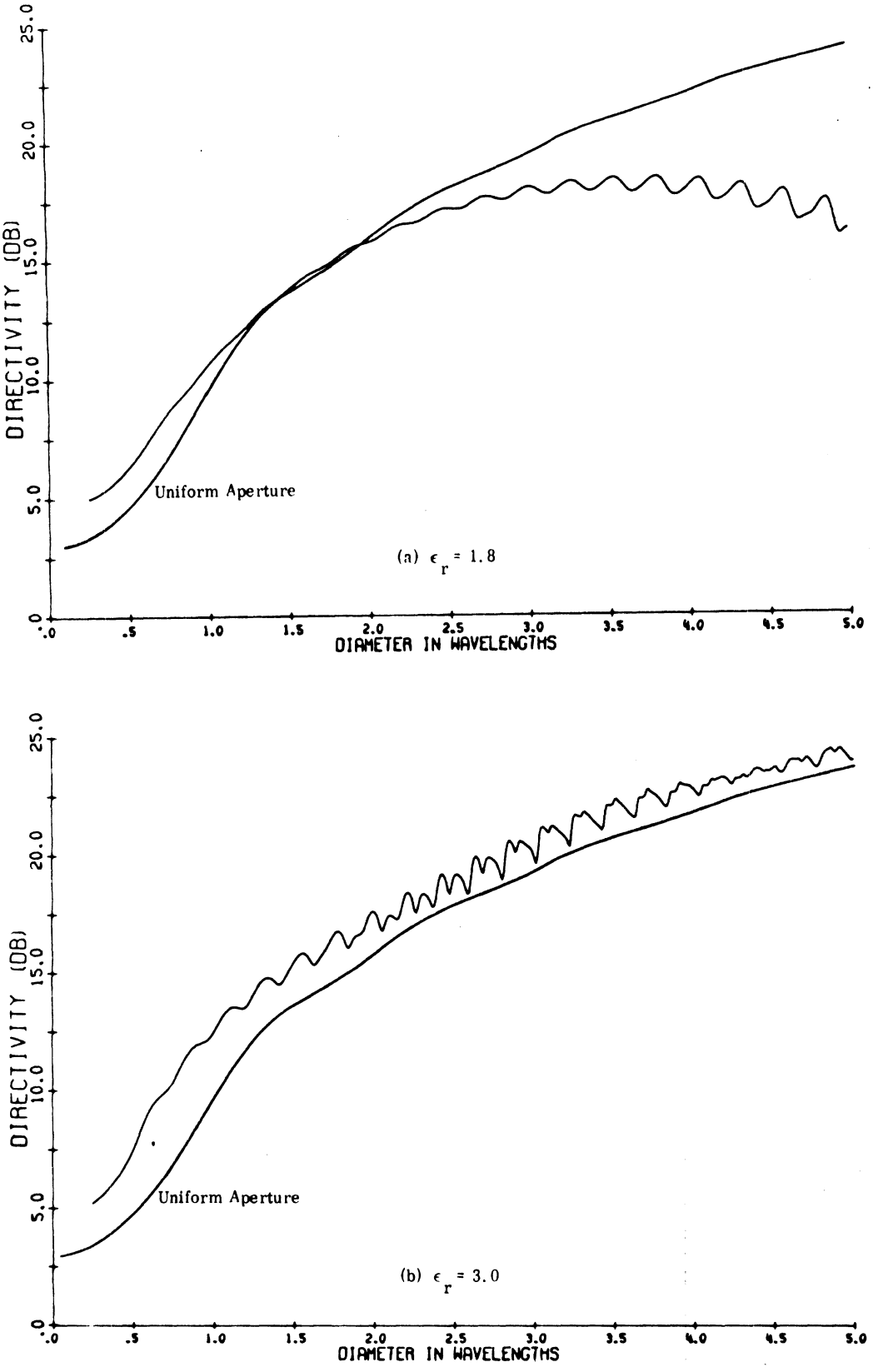

FIG. 6-9: DIRECTIVITY OF SPHERES WITH TAN δ = .0065.

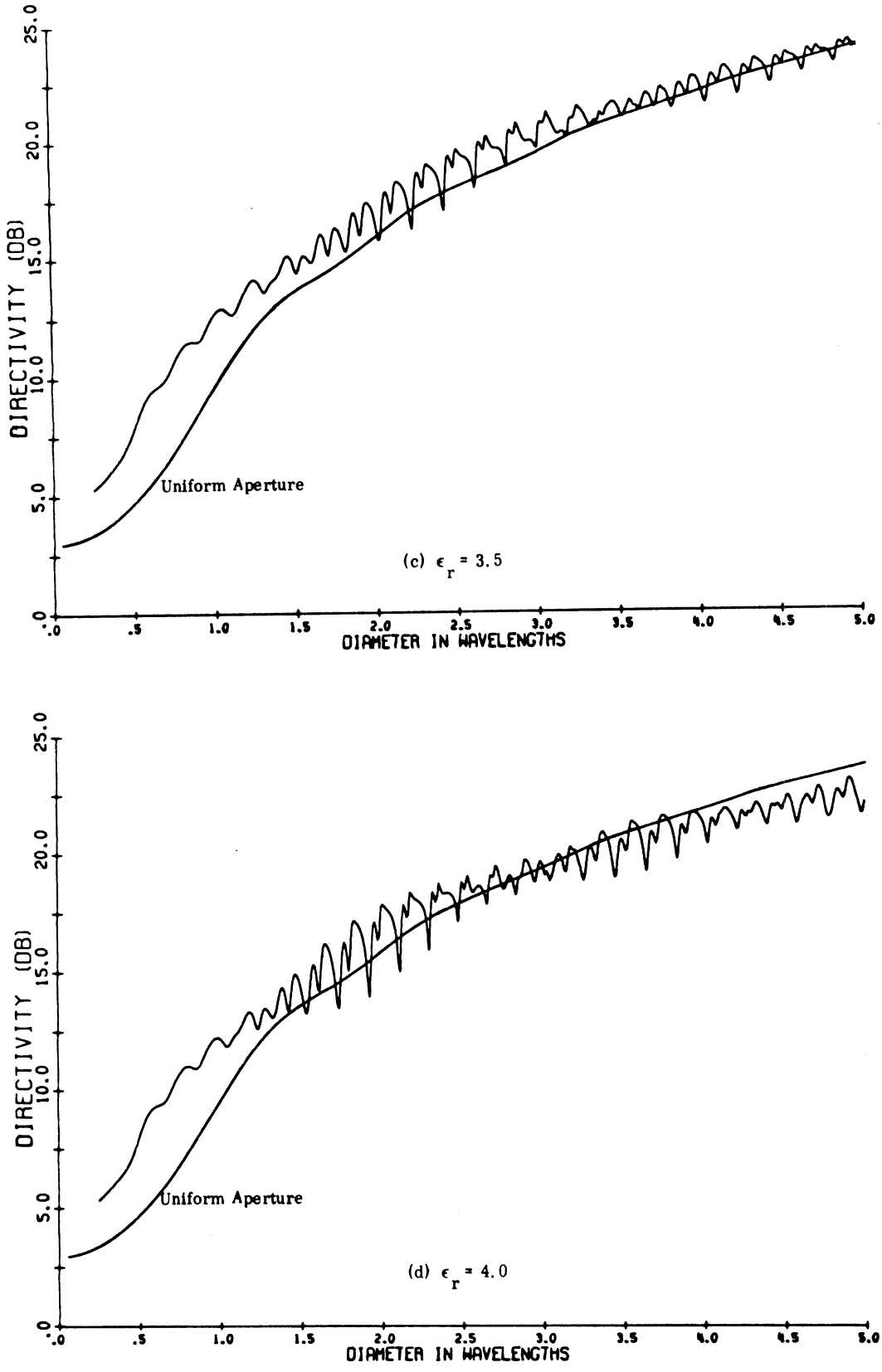

FIG. 6-9: DIRECTIVITY OF SPHERES WITH TANδ = .0065.

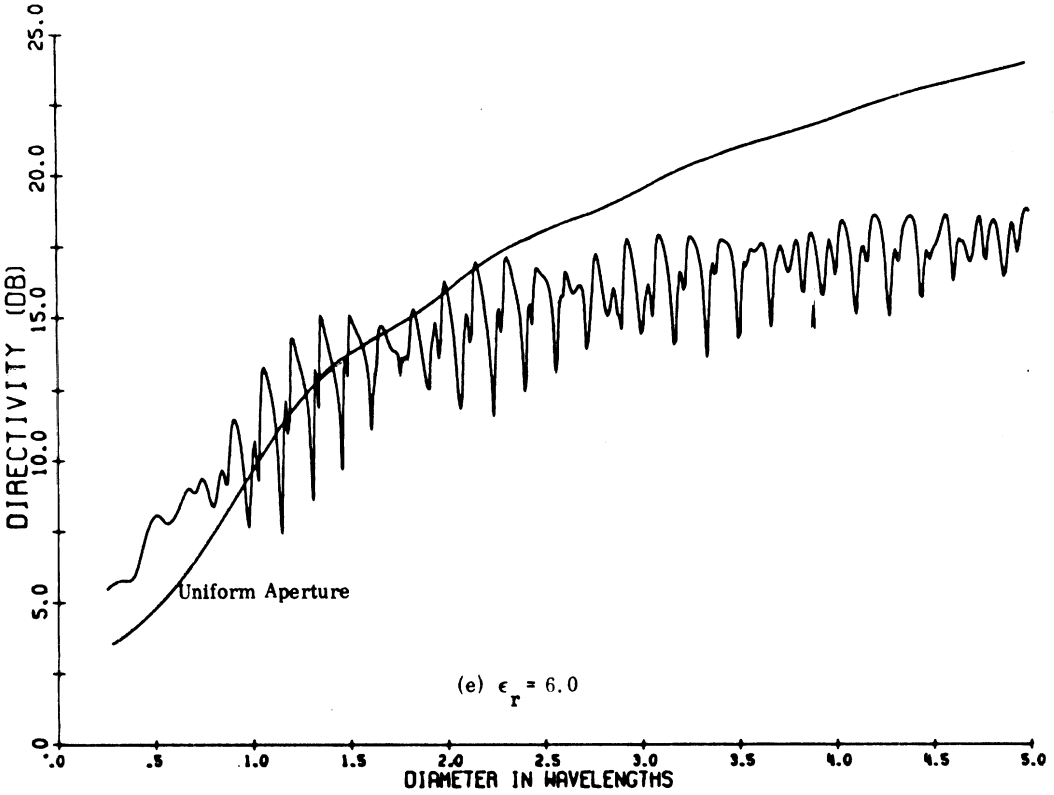

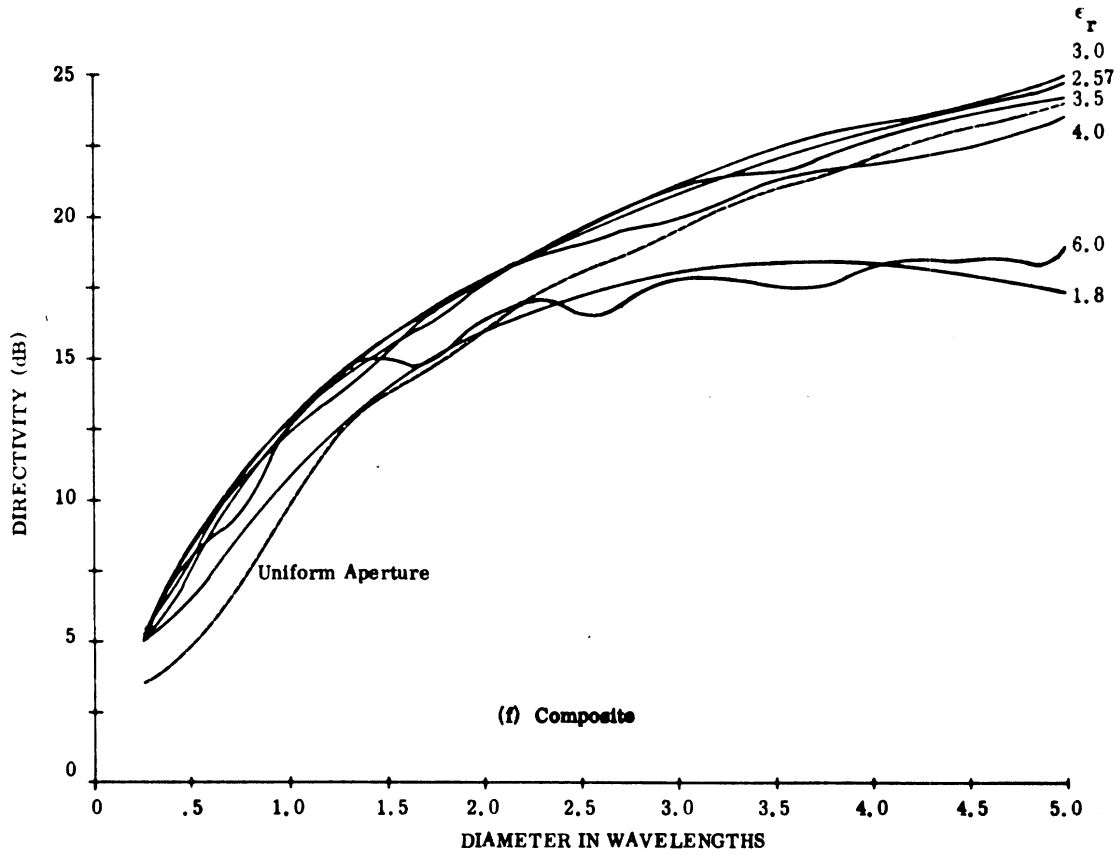

FIG. 6-9: DIRECTIVITY OF SPHERES WITH TAN δ = .0065.

6.4 Resonance and the Effect of Dielectric Loss

The resonance phenomenon noted in the directivity curves of Section 6.3 is now investigated. Figure 6-10 shows a detailed section computed using a diameter interval of .003λ. A pattern occurring in this curve is noted. For example, resonances occur at B, D, and then the pattern repeats starting at E with the nulls becoming stronger with increasing diameter.

Figure 6-11 shows the antenna patterns corresponding to points B, C and D of Fig. 6-10. The patterns of Fig. 6-11a (H-plane) and Fig. 6-11c (E-plane) each have ten complete lobes indicating that the resonance is due to a large tenth mode. It has been found that points A and F are caused by resonances in the 8th and 13th modes respectively. Hence, with increasing diameter, the resonance appears in the H-plane, then the E-plane, and again in the H-plane at the next higher mode.

Looking back at (5.1), it is seen that the far-zone field in the two planes may be expressed by

$$\bar{E}(\bar{R}) = \frac{-\omega\mu_1 C_e}{4\pi}\frac{e^{ik_1 R}}{R}\sum_{n=1}^{\infty}\frac{2n+1}{n(n+1)}(-i)^n \cdot \begin{cases} \left[\alpha_n \dfrac{P_n^1(\cos\theta)}{\sin\theta} + \beta_n \dfrac{\partial P_n^1(\cos\theta)}{\partial\theta}\right]\hat{\theta}\,, & \text{E-plane} \\ \left[\alpha_n \dfrac{\partial P_n^1(\cos\theta)}{\partial\theta} + \beta_n \dfrac{P_n^1(\cos\theta)}{\sin\theta}\right]\hat{\phi}\,, & \text{H-plane}\,. \end{cases} \qquad (6.1)$$

It has been found that when there is an ith mode resonance in the E-plane or H-plane the magnitude of β_i or α_i, respectively, is considerably larger than the other coefficients. It therefore can be seen from (6.1) that the radiation patterns will exhibit a strong resemblance to

$$\left(\frac{\partial P_i^1(\cos\theta)}{\partial\theta}\right)^2 \quad \text{in the plane of resonance}\,,$$

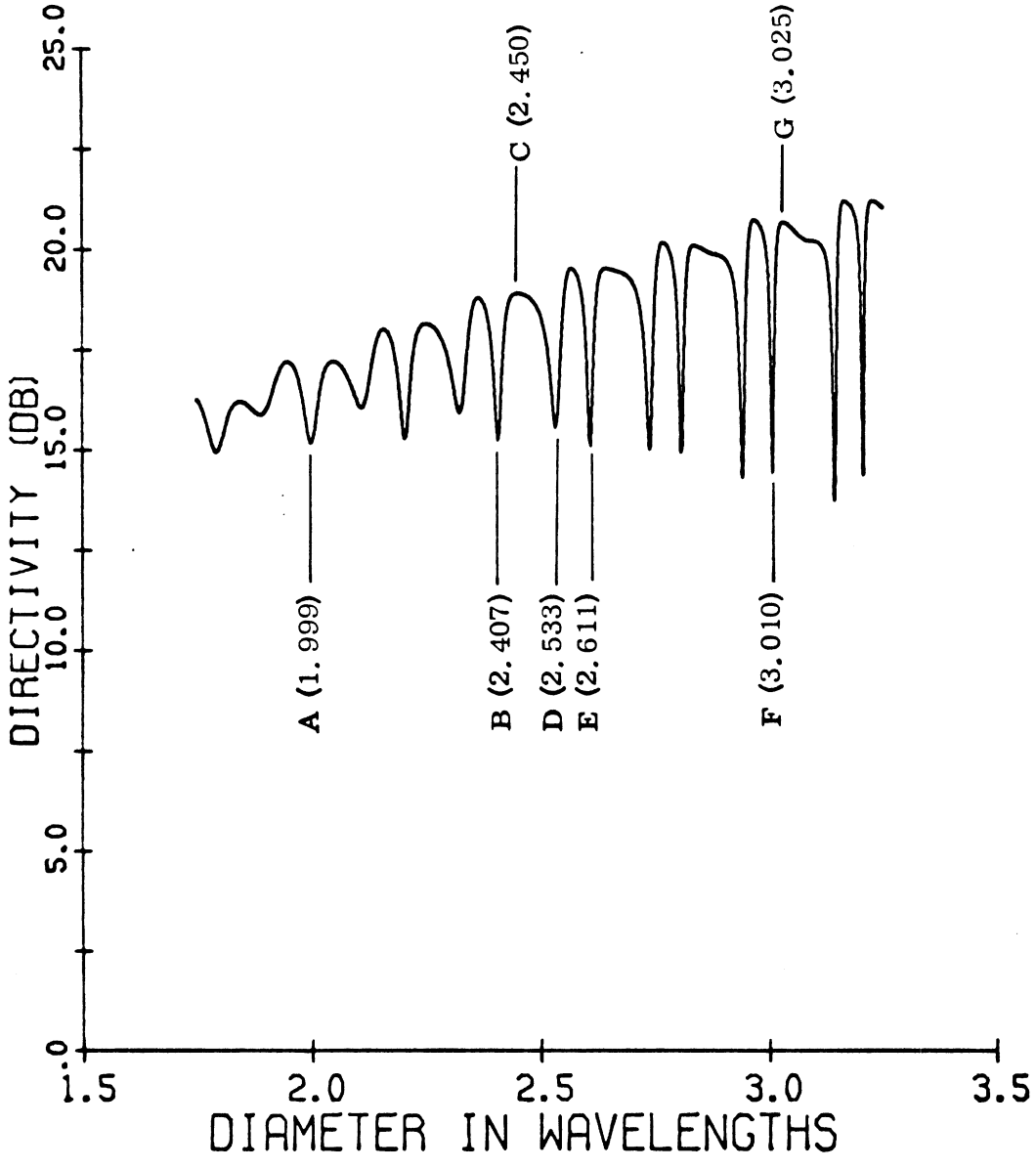

FIG. 6-10: DIRECTIVITY OF HUYGENS' SOURCE ON SPHERE SURFACE ($\epsilon_r = 3.2$, $\tan\delta = 0.0$)

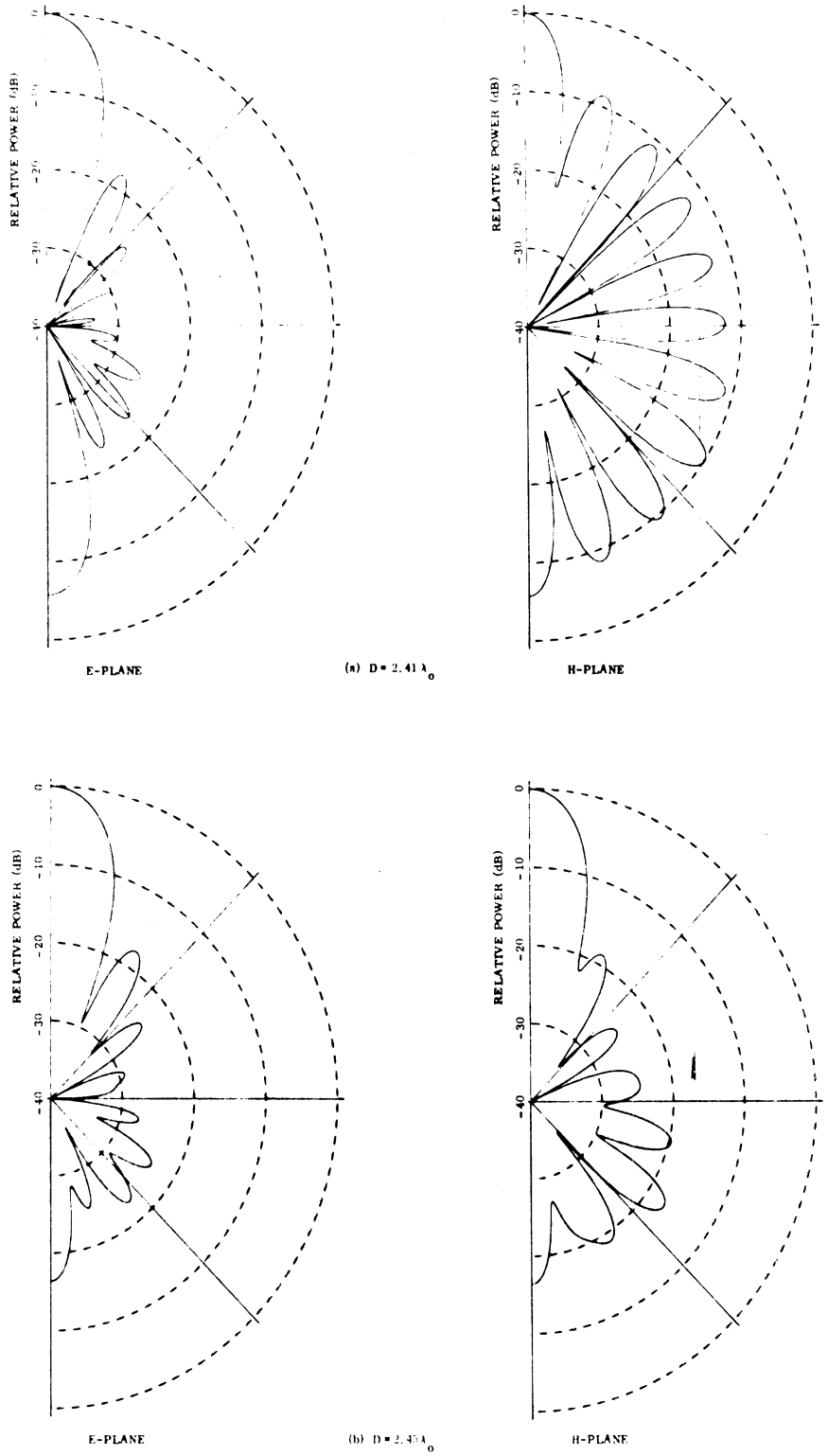

FIG. 6-11: RADIATION PATTERNS FOR VARIOUS SPHERE DIAMETERS ($\epsilon_r = 3.2$, $\tan\delta = 0.0$).

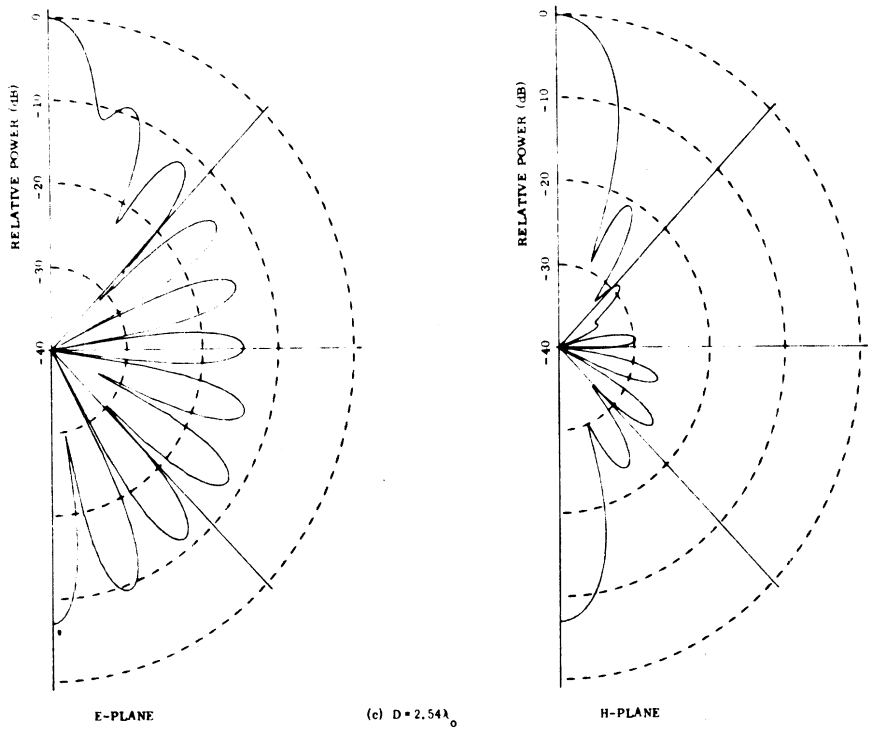

FIG. 6-11: RADIATION PATTERNS FOR VARIOUS SPHERE DIAMETERS ($\epsilon_r = 3.2$, $\tan\delta = 0.0$).

and $\left(\dfrac{P_i^1(\cos\theta)}{\sin\theta}\right)^2$ in the alternate plane.

This resonance phenomenon occurs when the denominators of β_i or α_i, which contain the respective factors $\epsilon_r\left[\rho_1 h_n(\rho_1)\right]' j_n(\rho_2) - \left[\rho_2 j_n(\rho_2)\right]' h_n(\rho_1)$ or $\left[\rho_1 h_n(\rho_1)\right]' j_n(\rho_2) - \left[\rho_2 j_n(\rho_2)\right]' h_n(\rho_1)$, become small. It has been shown by Stratton (1941, Sec. 9.25), however, that these factors never reach zero.

The total radiated power may be expressed as a summation over the power radiated in each mode, i.e.,

$$W = \sum_{n=1}^{\infty} P_n$$

as shown by (5.7). The quantity $\frac{P_n}{W} \cdot 100$ percent represents, therefore, the percent of the total power contributed by each mode. These power contributions are plotted for the modes with significant power for points B and C in Fig. 6-12a and F and G in Fig. 6-12b. Although the modes are discrete they have been connected for identification purposes.

From these figures it is noted that when the directivity is high, the power is distributed among the modes. At the points of resonance, however, most of the power is concentrated in a single mode; about 89 percent is in the 10th mode at B, and 98 percent is in the 13th mode at F.

Although it is not apparent from Fig. 6-12 because of the normalization, the total radiated power at resonance is considerable higher than at nonresonance, and hence the radiation resistance (see Fig. 6-13) shows strong peaks at the resonant points. This curve was computed using (5.10) in .001 diameter intervals.

It was noted from comparing the directivity curves for lossy spheres with the corresponding lossless curves that the attenuation had little effect on the points of high directivity. The dielectric loss did, however, significantly reduce the magnitude of the resonances with the effect being more pronounced for the larger diameter spheres. The reason for this may be explained with the aid of Fig. 6-14.

We define modal efficiency by

$$\text{Efficiency}_n = \frac{P_n(\text{radiated})}{P_n(\text{radiated}) + P_n(\text{loss})} \cdot 100 \text{ percent} ,$$

where P_n (radiated) and P_n (loss) are the nth terms of (5.7) and (5.32) respectively. In Fig. 6-14 this efficiency, using a loss tangent of .01, is plotted as a function of mode number for various resonant sphere diameters. Generally, as the sphere becomes larger, it is seen that the efficiency of the higher modes increases while that of the lower modes decreases slightly.

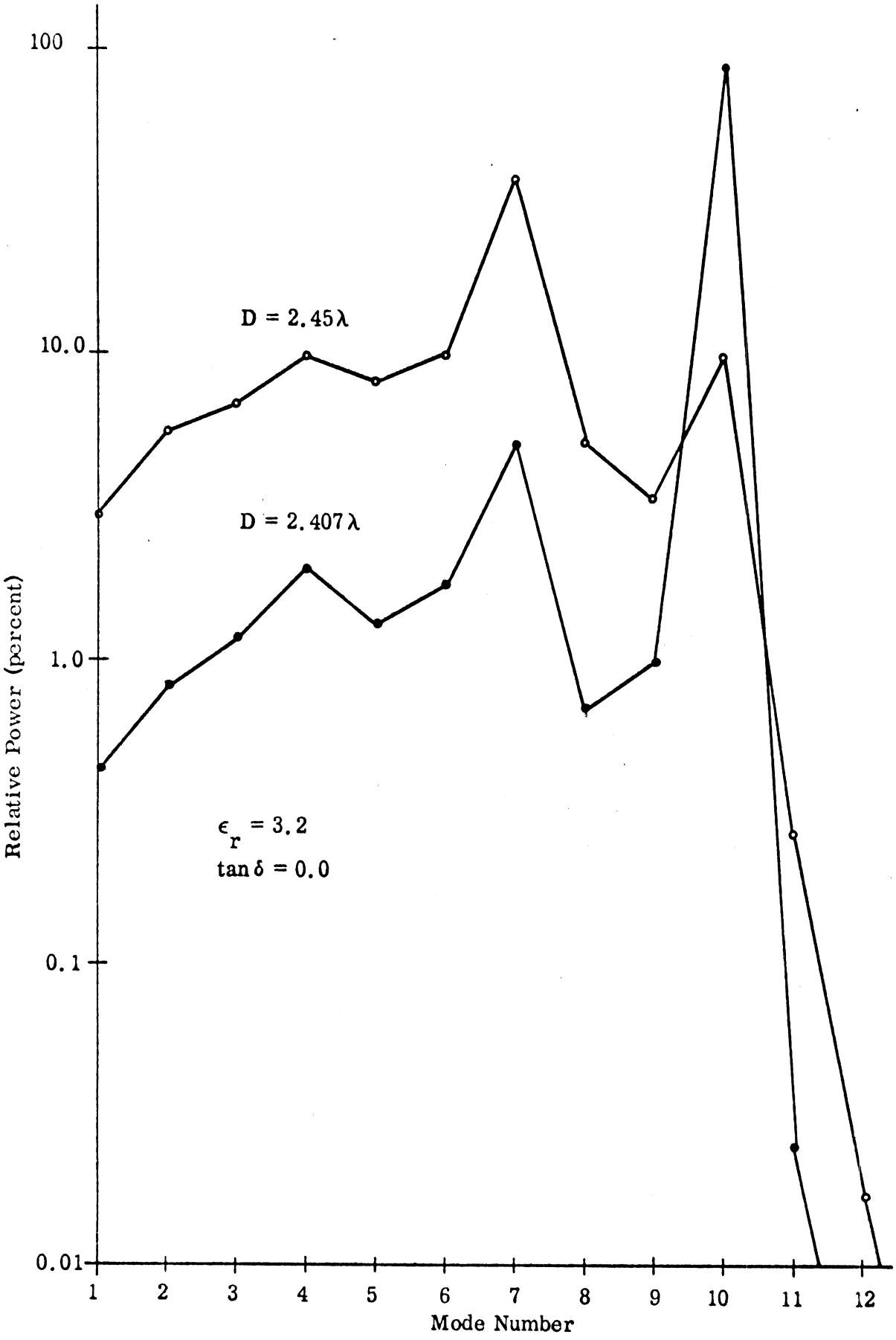

FIG. 6-12a: RELATIVE POWER DISTRIBUTION AMONG MODES.

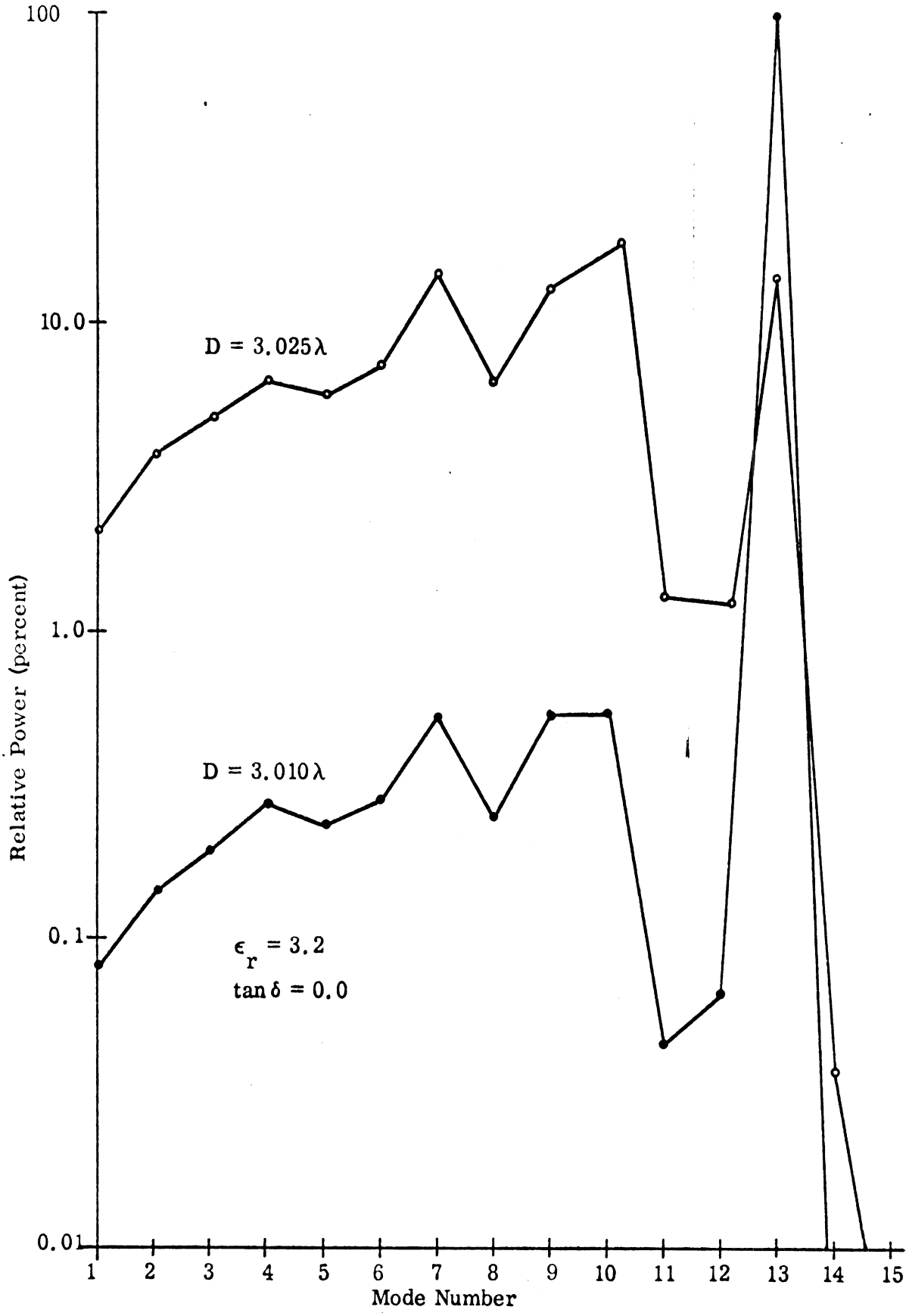

FIG. 6-12b: RELATIVE POWER DISTRIBUTION AMONG MODES

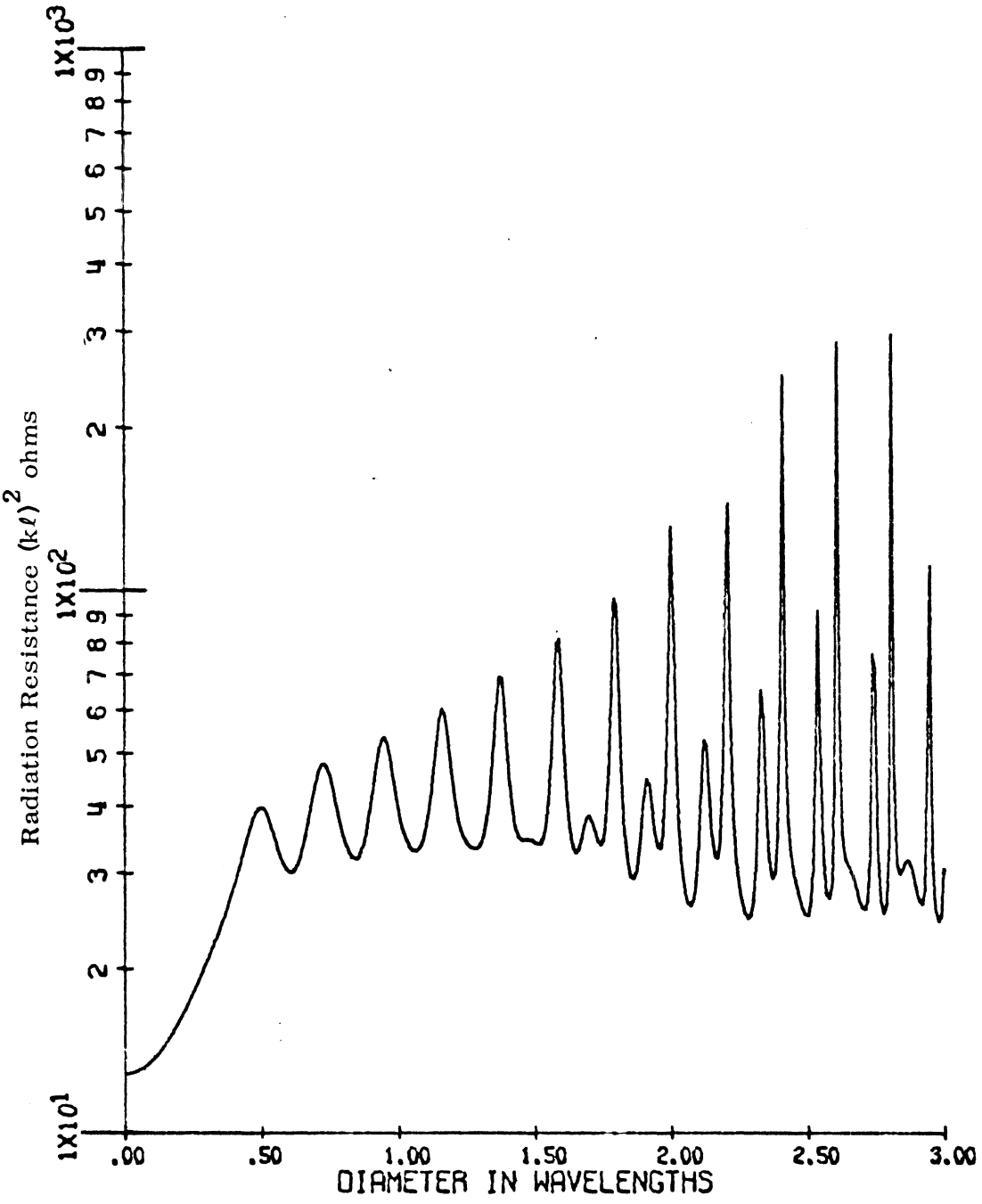

FIG. 6-13: RADIATION RESISTANCE FOR HUYGENS' SOURCE ON SURFACE OF DIELECTRIC SPHERE ($\epsilon_r = 3.2$, $\tan\delta = 0.0$).

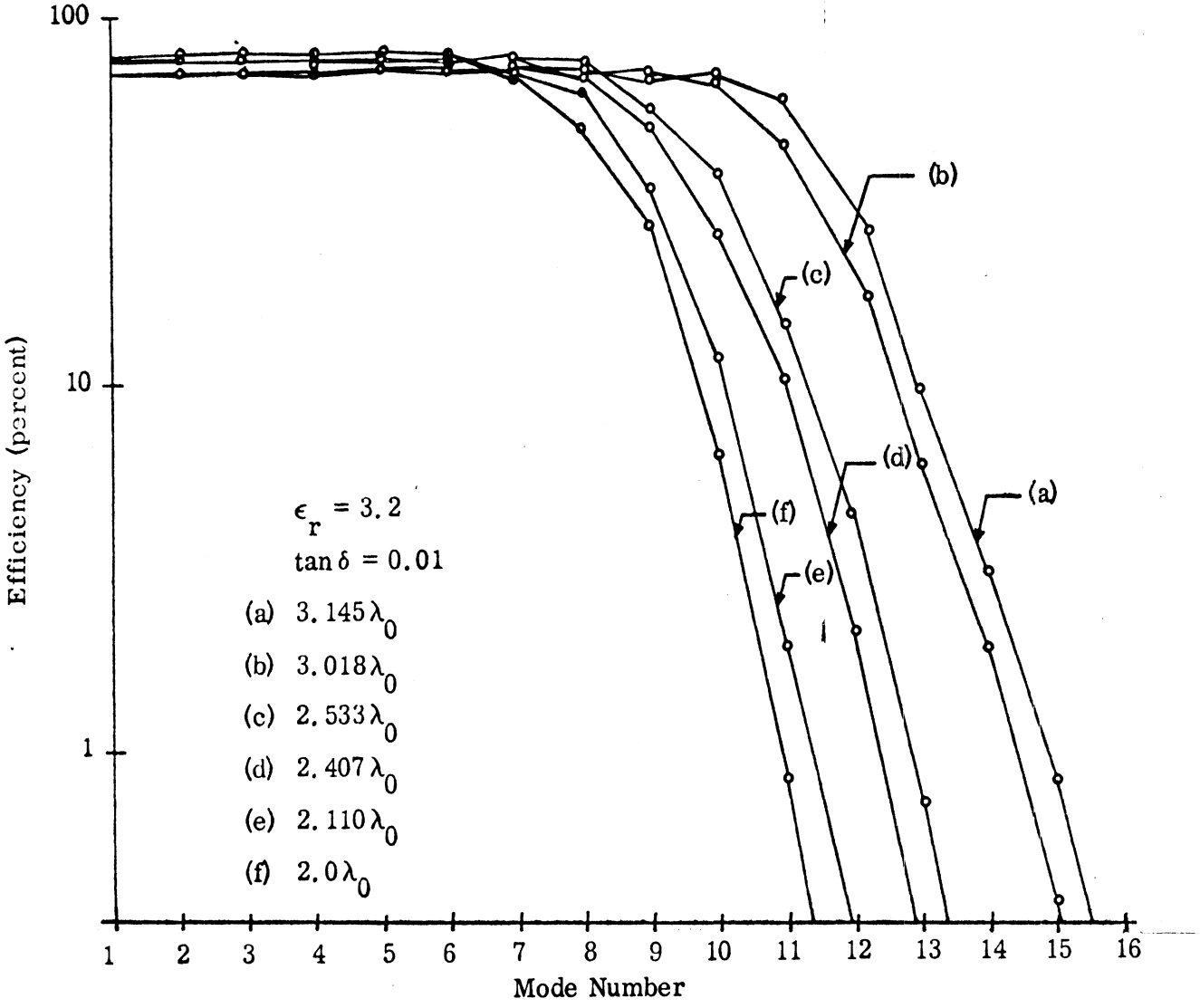

FIG. 6-14: MODAL EFFICIENCY AT VARIOUS RESONANT FREQUENCIES.

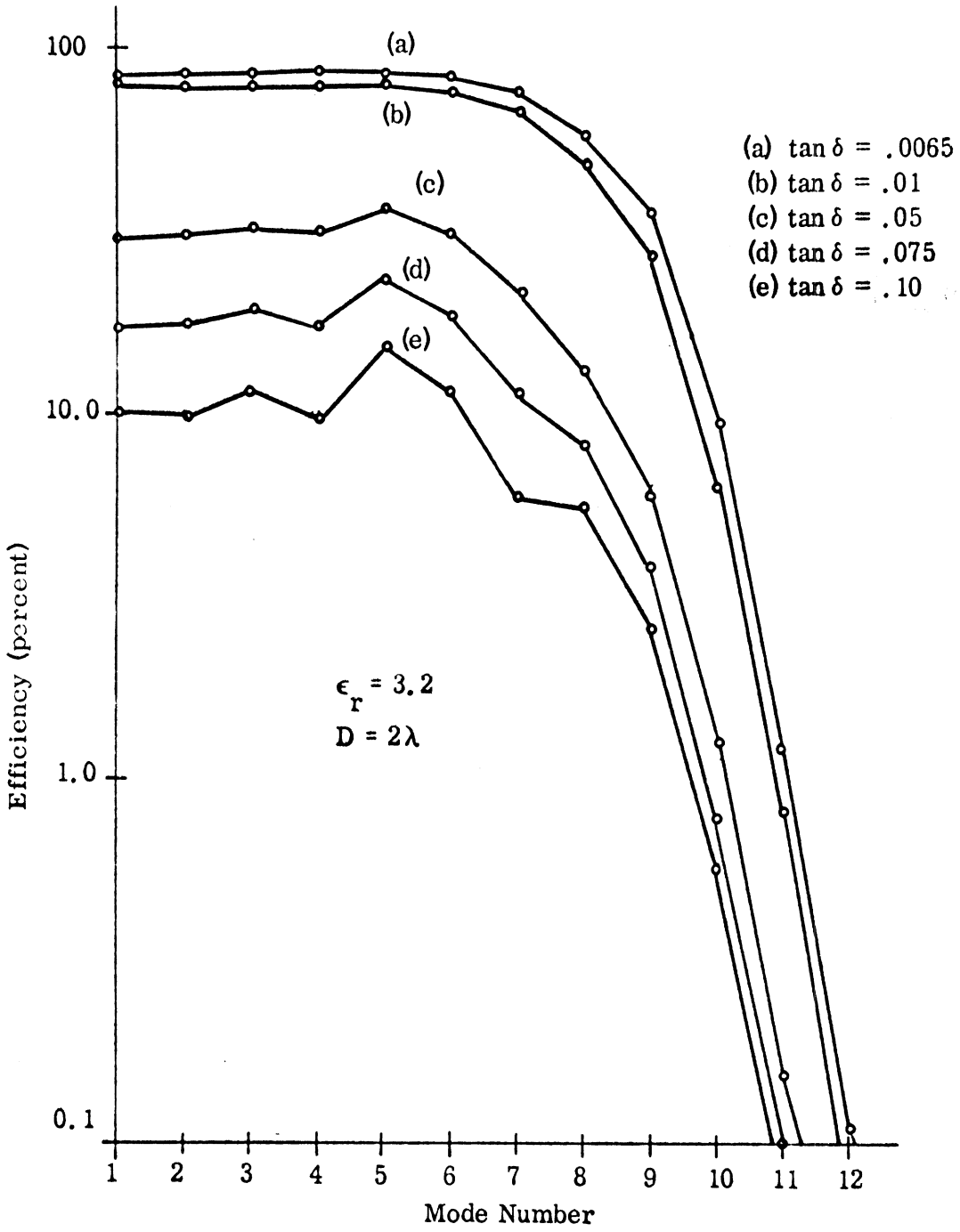

FIG. 6-15: MODAL EFFICIENCY FOR VARIOUS LOSS TANGENTS

Table 6-3 shows that each new resonant mode has an efficiency less than the previous one in the same plane. This, together with the fact that for a

TABLE 6-3

Modal Efficiency for Resonant Spheres
(loss tangent = .01; $\epsilon_r = 3.2$)

Diameter (λ_0)	Mode No. Number	Resonance Plane	Efficiency (%)
2.000	8	H	48.55
2.407	10	H	25.22
3.010	13	H	6.08
2.110	8	E	61.61
2.533	10	E	36.78
3.145	13	E	9.48

given diameter the resonant mode efficiency is less than that of the lower modes, accounts for the smoothing of the directivity curves with dielectric loss. These results also explain the reduction of the overall antenna efficiency, noted in Fig. 6-7, in the resonance region for the larger sphere diameters. The effect of other loss tangents on the modal efficiency is shown in Fig. 6-15.

The patterns of Figs. 6-16 and 6-17 were computed in 2-degree intervals using (4.13). Because of the high loss used in Fig. 6-16d, the internal reflections are greatly attenuated, and hence there is practically no radiation in the back direction. Finally, for a large sphere with constitutive parameters typical of plexiglas, Fig. 6-17c, the resonance is almost completely attenuated and therefore may not be noted in actual measurements.

6.5 Source Displaced from Sphere Surface

To examine the effect of moving the source away from the sphere, the curves of Fig. 6-18 were calculated using (4.30) in two-degree intervals. The dielectric constant was kept at 2.57 with a loss tangent of .0065. Since b is the

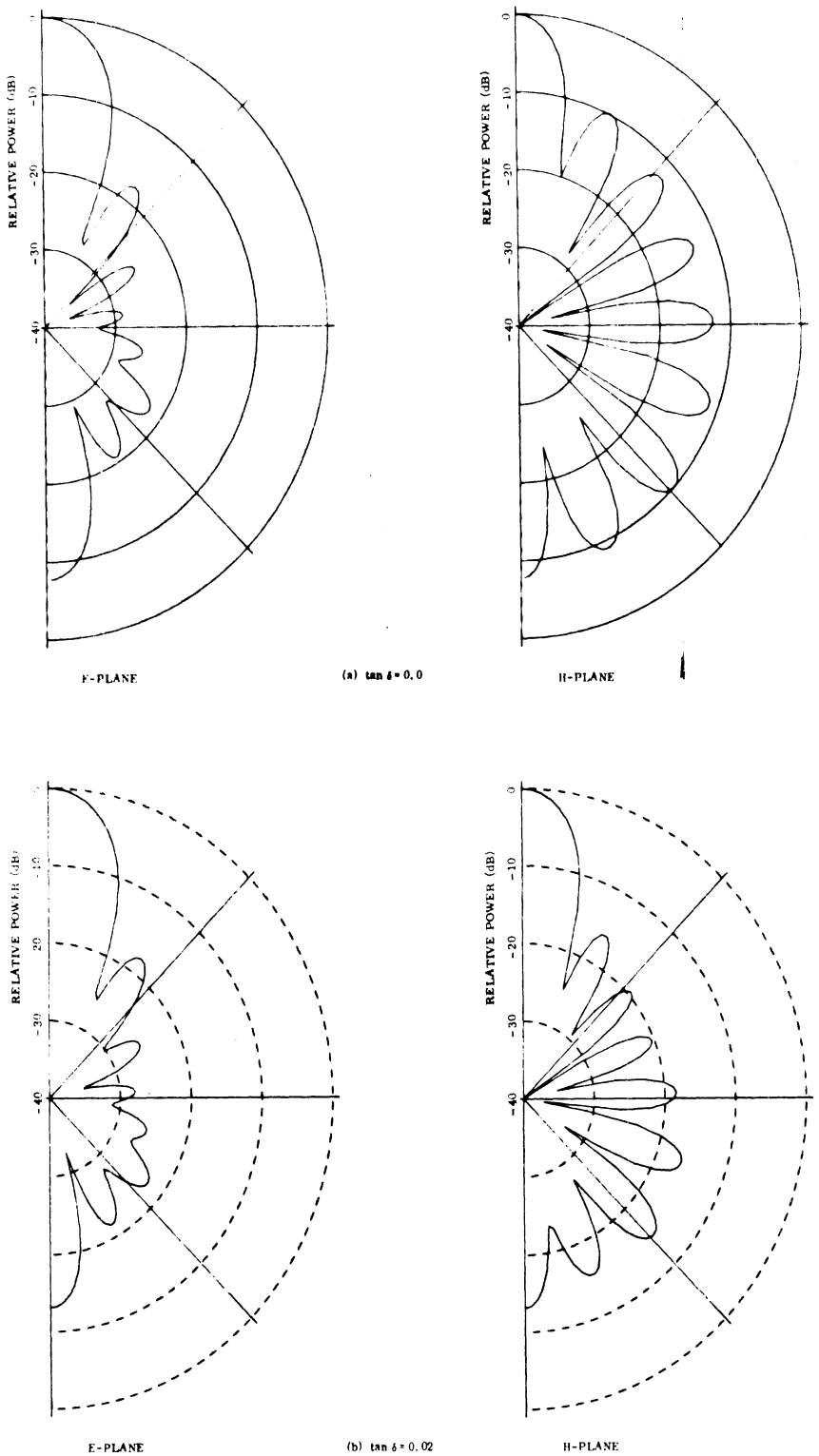

FIG. 6-16: RADIATION PATTERNS FOR SPHERES WITH VARIOUS LOSS TANGENTS ($D = 2\lambda_o$, $\epsilon_r = 3.2$).

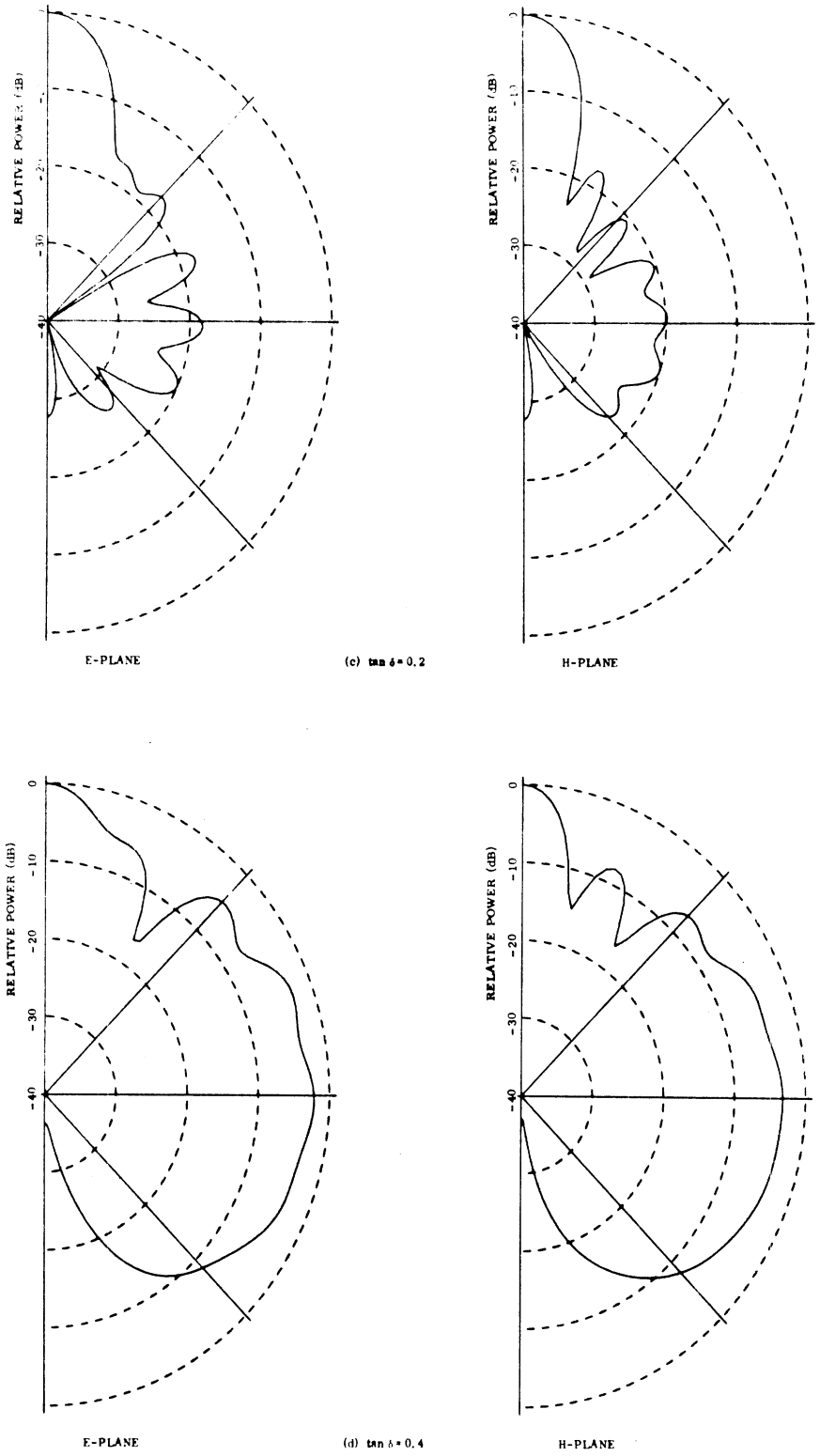

FIG. 6-16: RADIATION PATTERNS FOR SPHERES WITH VARIOUS LOSS TANGENTS ($D = 2\lambda_o$, $\epsilon_r = 3.2$).

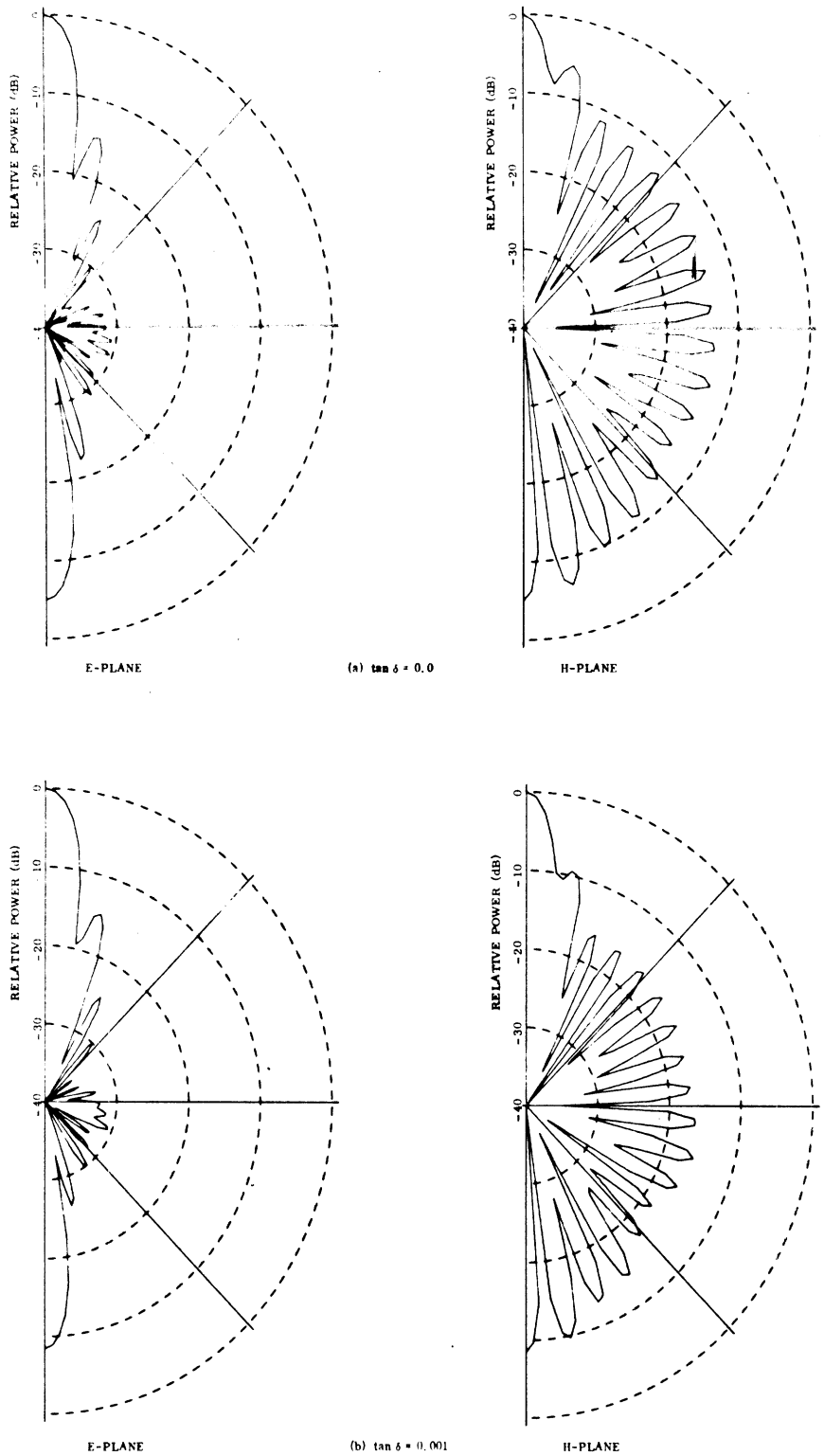

FIG. 6-17: RADIATION PATTERNS FOR SPHERES WITH VARIOUS LOSS TANGENTS ($D = 4.21\lambda_o$, $\epsilon_r = 2.57$).

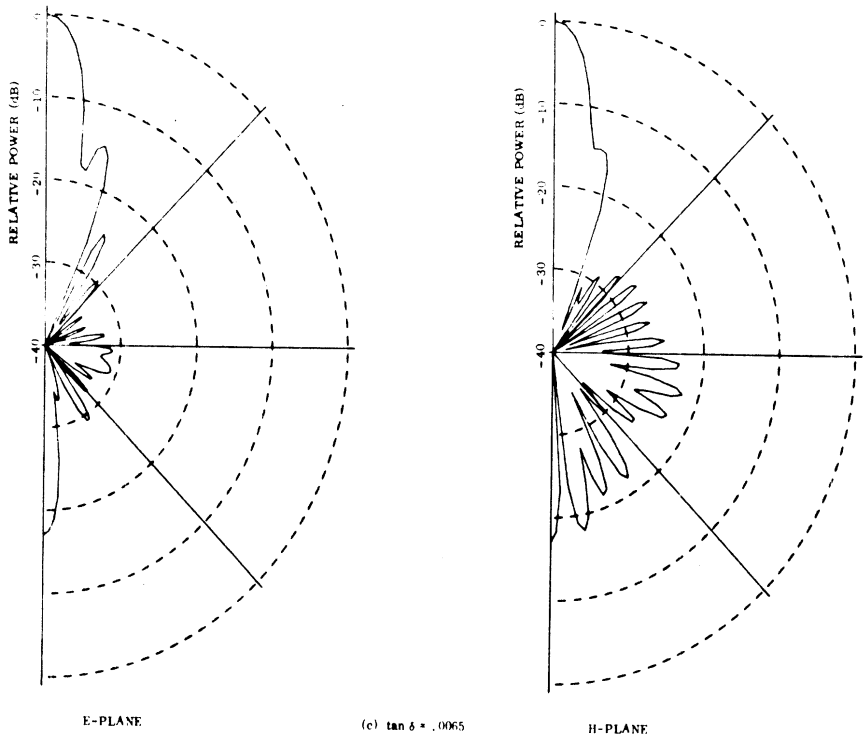

FIG. 6-17: RADIATION PATTERNS FOR SPHERES WITH VARIOUS LOSS TANGENTS ($D = 4.21\lambda_o$, $\epsilon_r = 2.57$).

distance from the origin to the source and a is the sphere radius, the ratios of b/a shown in Figs. 6-18a, b, c and d correspond to the source spaced 0.0, 0.25, 0.5 and 1.0 free-space wavelengths from the sphere surface. From these patterns it is seen that the main beam first narrows slightly and then becomes broader with increasing displacement. The sidelobe level also becomes considerably higher as the source is moved away from the sphere.

Without varying the dielectric constant, the curves shown in Fig. 6-19 were computed using (4.31). These patterns correspond to the source spaced 0.1, 0.5, 0.75 and $1.5\lambda_0$ inside the sphere surface. The theoretical patterns shown in Fig. 6-3 were also calculated using (4.31) for the source on the sphere surface, and may be compared to Fig. 6-18a which was computed from (4.30) using the same parameters.

From Fig. 6-19, it is seen that the antenna pattern continuously degrades as the source is moved into the sphere, and that the sphere shows very little focussing effect as the source approaches the center.

Directional patterns can, however, be obtained with the source located inside the sphere by appropriately adjusting the dielectric constant as shown in Figs. 6-20 and 6-21. The directivity of these patterns is about the same as that with the source located on the surface of a sphere with a lower dielectric constant.

Figure 6-22 shows the optimum ratio of source to sphere radius for various diameter spheres. These points were obtained by fixing the dielectric constant at 4, 6, 9, and 12 and varying the source position until the maximum directivity was found. The additional points corresponding to the source on the sphere surface were obtained by adjusting the dielectric constant. In each case a loss tangent of .0065 was used. For comparison, the upper curve shows the location of the geometrical optics paraxial focus (8.5).

It is seen from Fig. 6-22 that for a dielectric constant of 9 the source is located about half way between the center and back surface of the sphere. It is also noted that for a fixed source position a higher dielectric constant is necessary to obtain optimum directivity for the smaller spheres. In all cases, however, the best results were obtained for a dielectric constant less than that required for the paraxial focus.

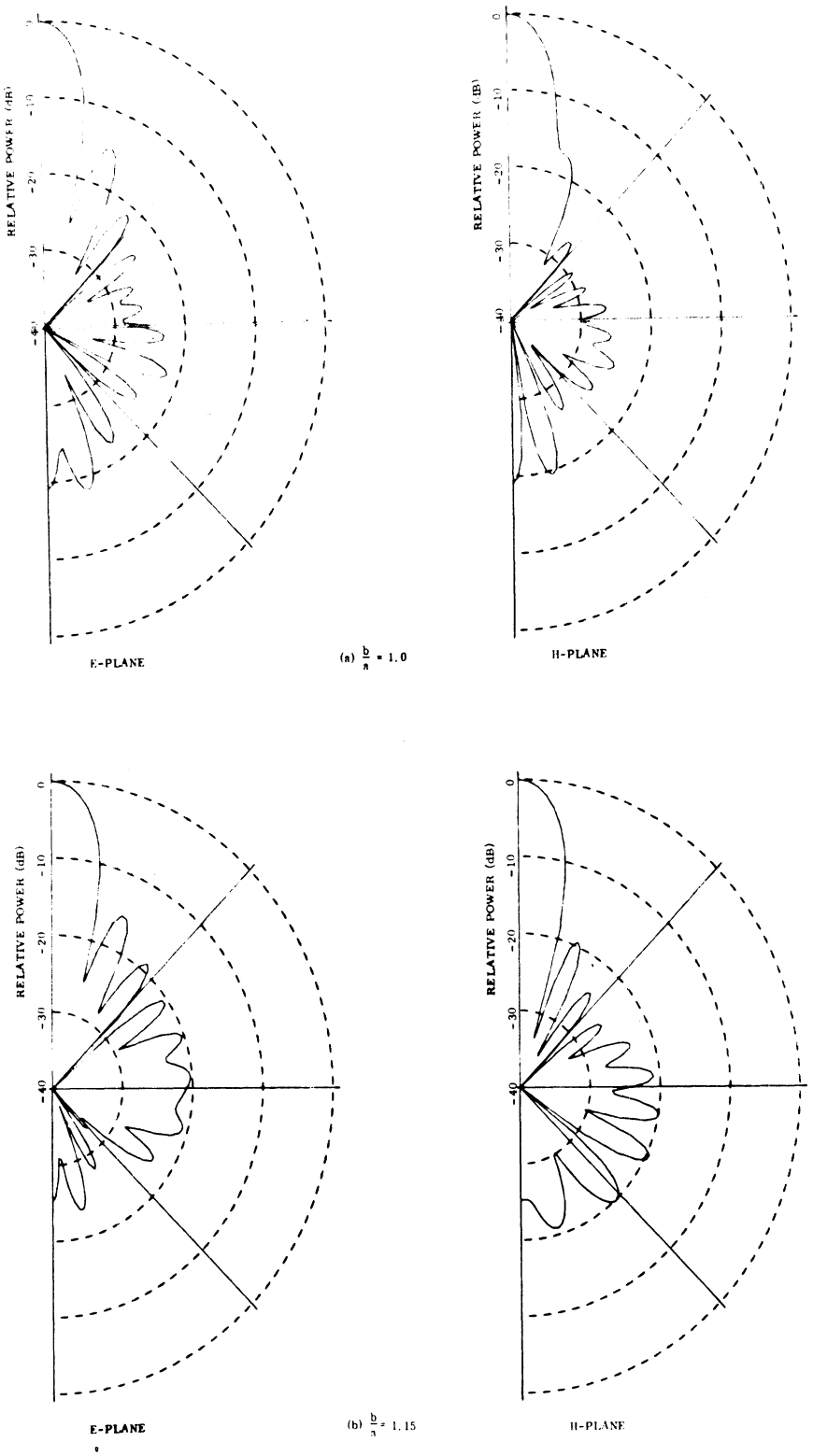

FIG. 6-18: RADIATION PATTERNS FOR SOURCE LOCATED OUTSIDE SPHERE ($D = 3.39\lambda_o$, $\epsilon_r = 2.57$, $\tan\delta = .0065$).

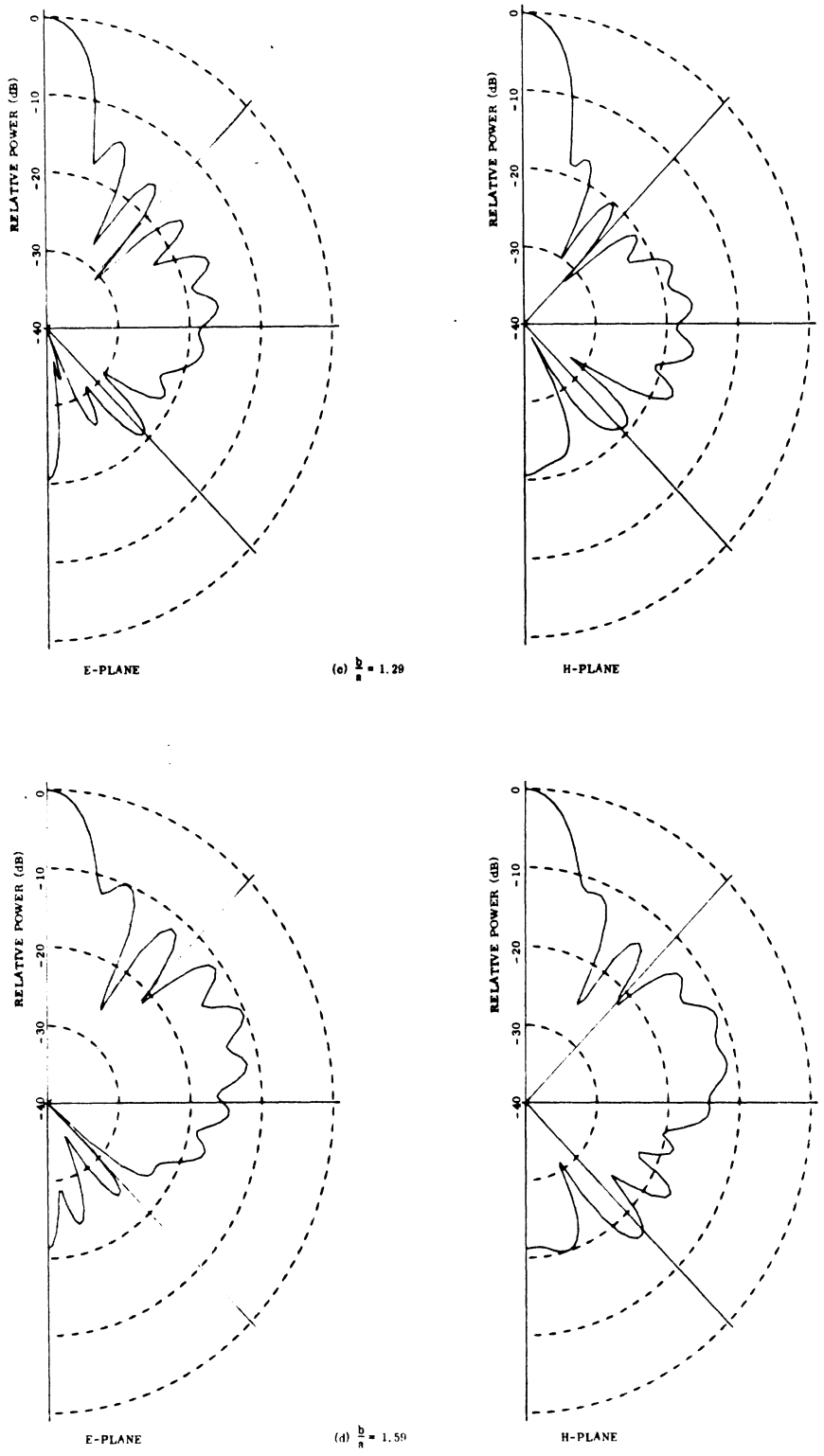

FIG. 6-18: RADIATION PATTERNS FOR SOURCE LOCATED OUTSIDE SPHERE ($D = 3.39\lambda_o$, $\epsilon_r = 2.57$, $\tan\delta = .0065$).

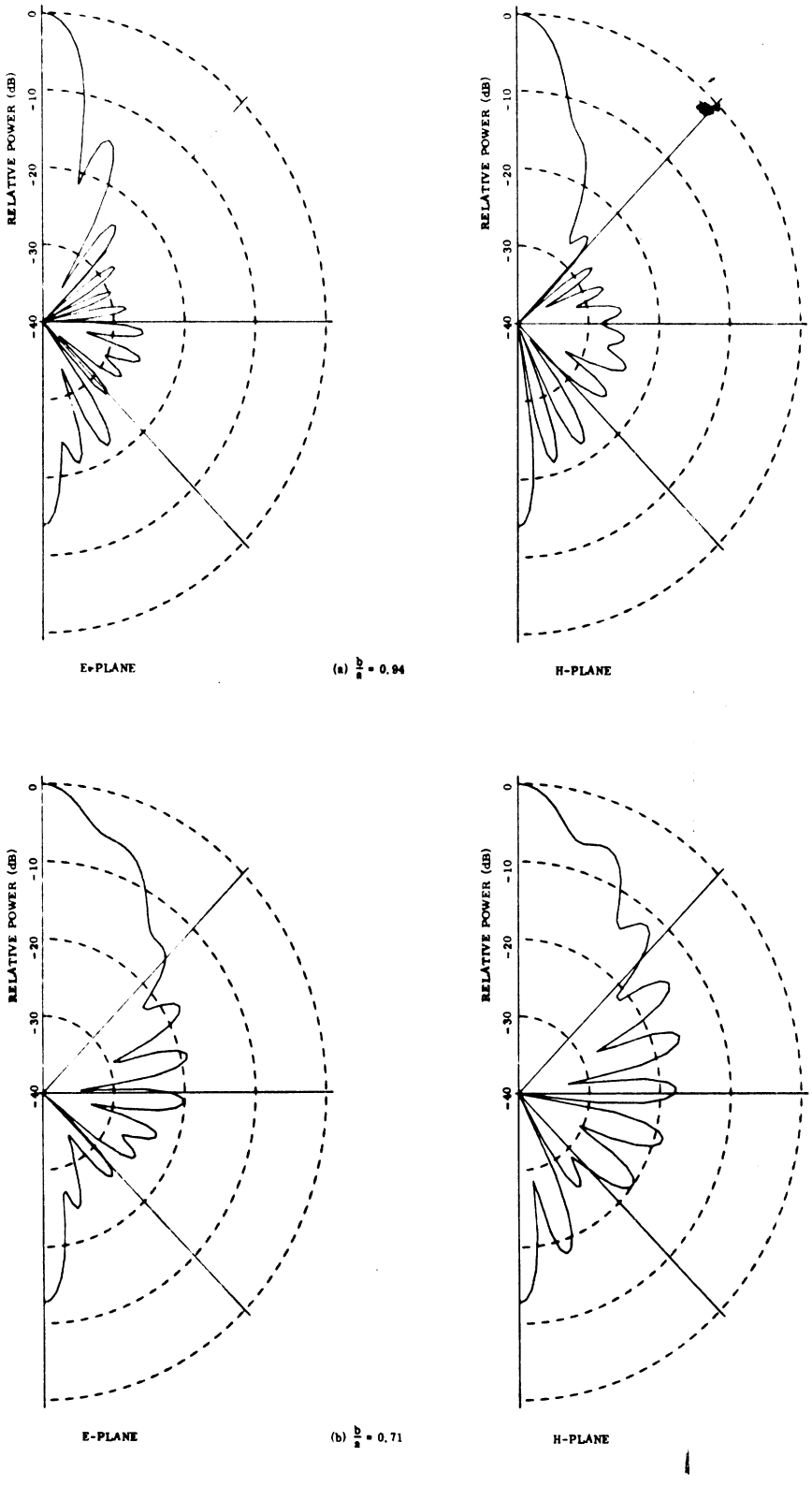

FIG. 6-19: RADIATION PATTERNS FOR SOURCE LOCATED INSIDE SPHERE ($D = 3.39\lambda_o$, $\epsilon_r = 2.57$, $\tan\delta = .0065$).

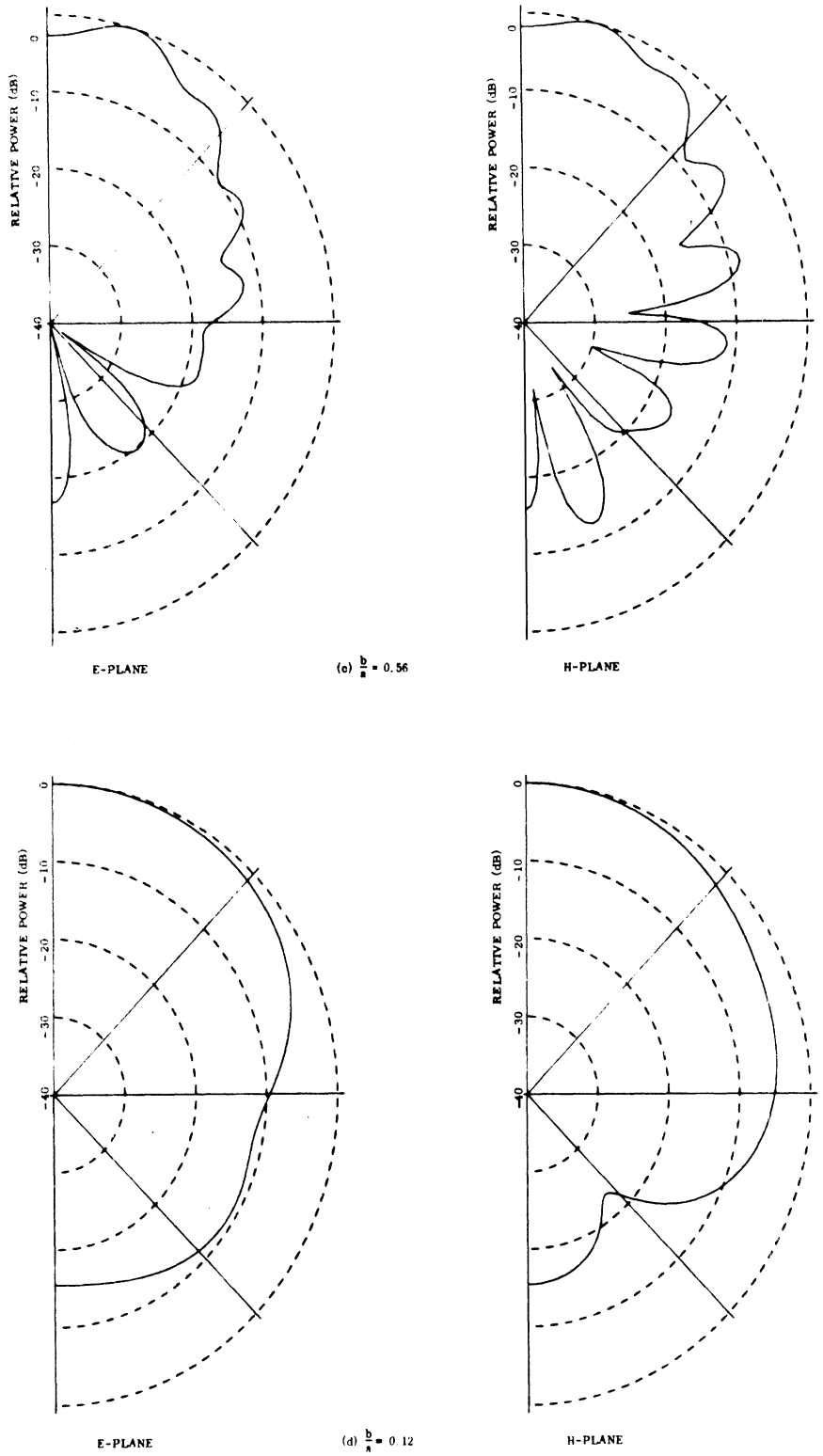

FIG. 6-19: RADIATION PATTERNS FOR SOURCE LOCATED INSIDE SPHERE ($D = 3.39\lambda_o$, $\epsilon_r = 2.57$, $\tan\delta = .0065$).

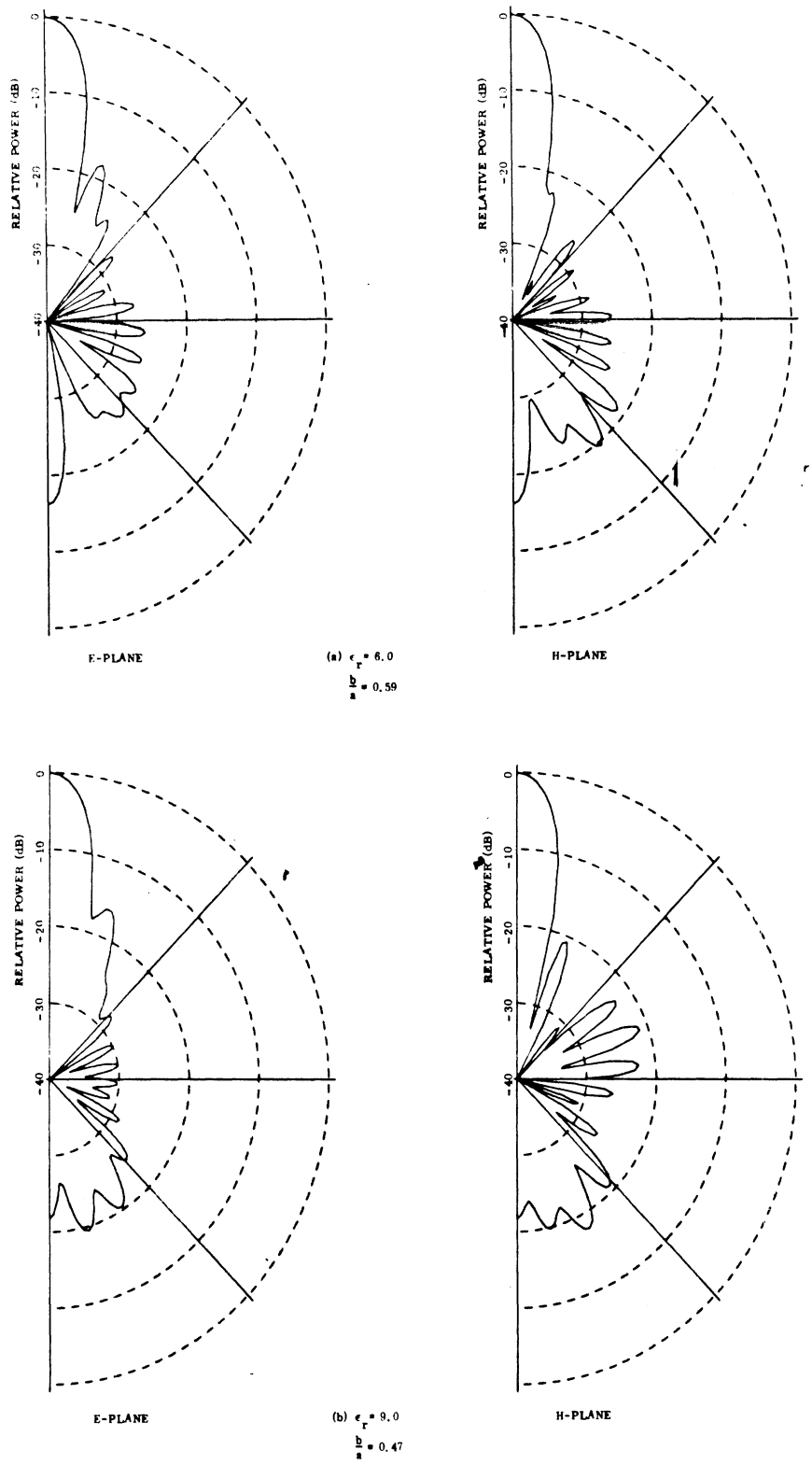

FIG. 6-20: RADIATION PATTERNS FOR SOURCE LOCATED INSIDE SPHERE ($D = 3.39\lambda_o$, $\tan\delta = .0065$).

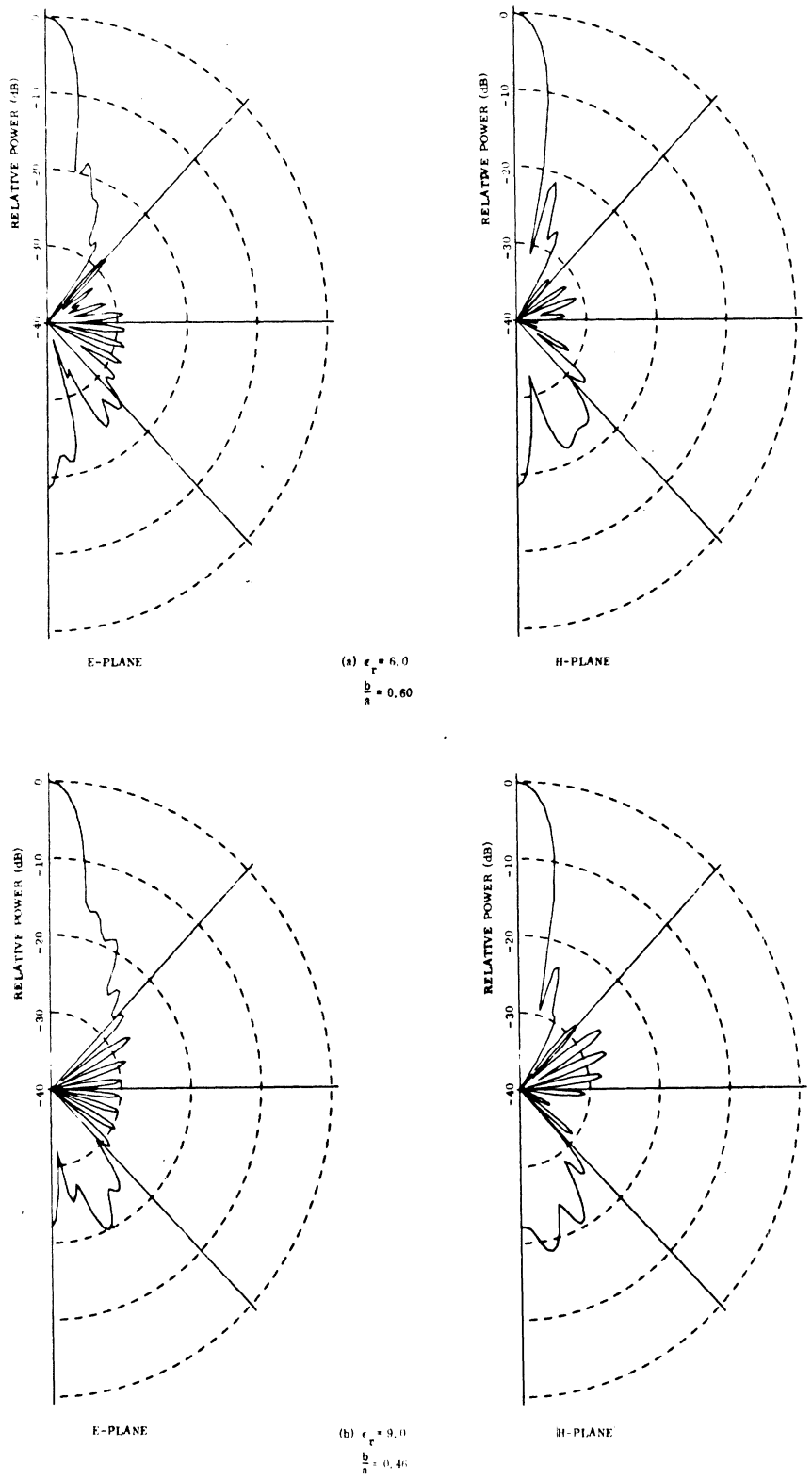

FIG. 6-21: RADIATION PATTERNS FOR SOURCE LOCATED INSIDE SPHERE ($D = 4.46\lambda_o$, $\tan\delta = .0065$).

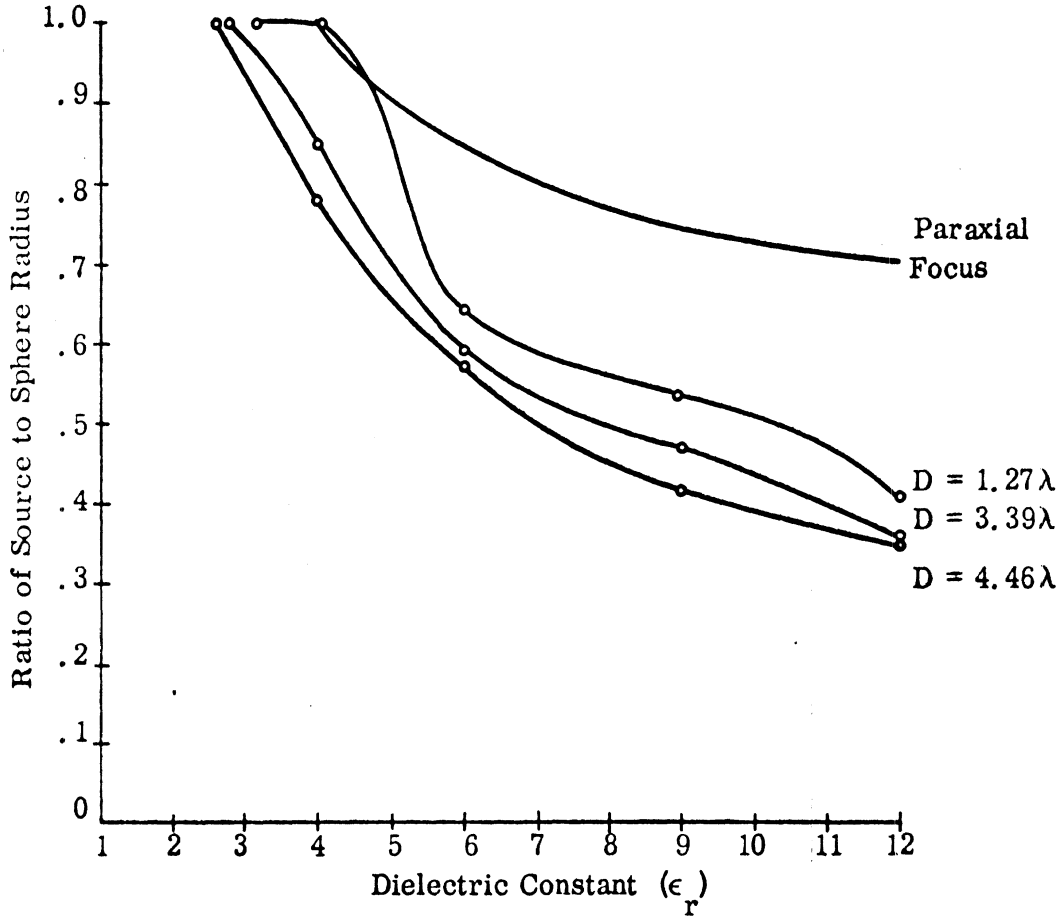

FIG. 6-22: SOURCE LOCATION AS A FUNCTION OF DIELECTRIC CONSTANT FOR OPTIMUM DIRECTIVITY.

Chapter VII

EXTENDED SOURCES

7.1 Introduction

The previous chapters were concerned with the effect of a dielectric sphere on the radiation from infinitesimal point sources. In this chapter the excitation is expanded into line sources concentric with the sphere.

Expressions for the far field radiated by curved electric dipoles are derived first, and then the results for a superposition of Huygens' sources in the presence of a dielectric sphere are presented. Finally, it will be shown that the patterns from these sources do not differ greatly from those of point sources.

7.2 Electric Field Due to a Curved Electric Dipole

Consider a dielectric sphere with a filament of current located in the x-z plane at R = b as shown in Fig. 7-1. It should be noted that in the $\phi = 0$

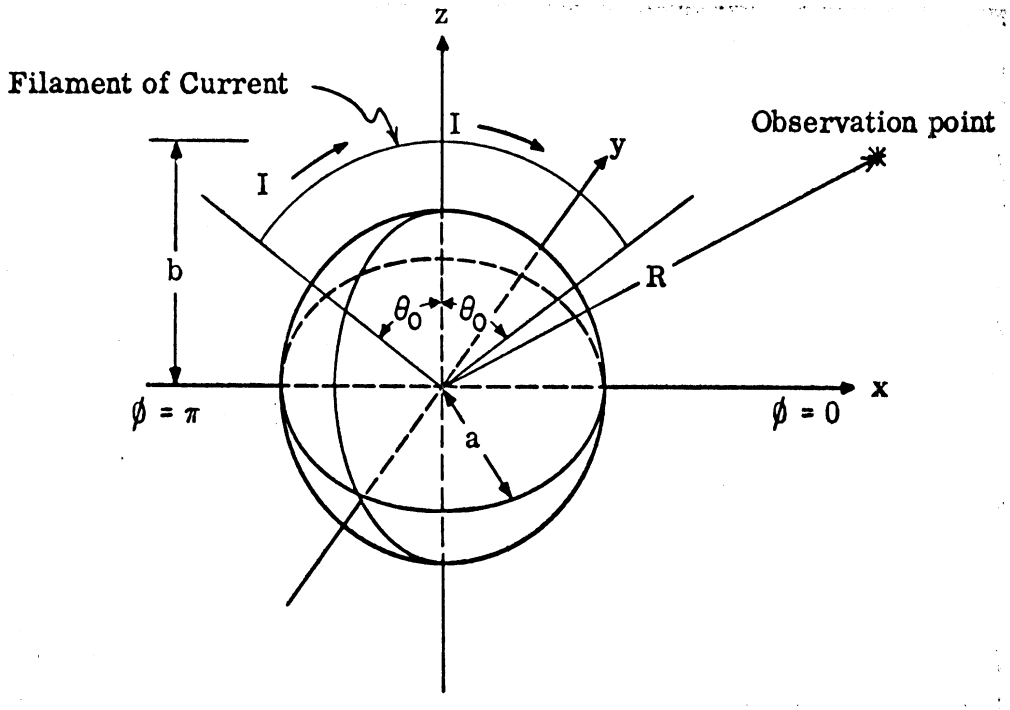

FIG. 7-1: CURVED FILAMENT OF CURRENT IN PRESENCE OF DIELECTRIC SPHERE (x-z PLANE).

and $\phi = \pi$ half-planes the current is defined to flow in the $+\hat{\theta}$ and $-\hat{\theta}$ directions respectively. This is because the θ coordinate variable is always measured in a downward direction from the +z-axis.

For the antenna located as shown in Fig. 7-1 we let

$$\bar{J}(\bar{R}') = I(\theta') \frac{\delta(R'-b)}{b \sin\theta'} \left[\delta(\phi) - \delta(\phi' - \pi)\right] \hat{\theta}' \tag{7.1}$$

where $I(\theta')$ is the current distribution on the antenna in the $\phi = 0$ half-plane and is only a function of the coordinate variable θ'.

To find the electric field in Region I, (7.1) is substituted into (2.1). Thus,

$$\bar{E}(\bar{R}) = i\omega\mu_1 \int_0^{\theta_0} \int_0^{\pi} \int_0^{\infty} \bar{\bar{G}}_3^{11}(\bar{R}|\bar{R}') \cdot \hat{\theta}' I(\theta') \frac{\delta(R'-b)}{b} \left[\delta(\phi') - \delta(\phi'-\pi)\right] R'^2 \, dR' d\phi' d\theta'. \tag{7.2}$$

Integration over the R' and ϕ' variables yields

$$\bar{E}(\bar{R}) = i\omega\mu_1 b \left\{ \int_0^{\theta_0} I(\theta') \bar{\bar{G}}_3^{11}(\bar{R}|\bar{R}') \cdot \hat{\theta}' d\theta' \Big|_{\substack{R'=b \\ \phi'=0}} - \int_0^{\theta_0} I(\theta') \bar{\bar{G}}_3^{11}(\bar{R}|\bar{R}') \cdot \theta' d\theta' \Big|_{\substack{R'=b \\ \phi'=\pi}} \right\}. \tag{7.3}$$

Following the same procedure for equations (7.1) and (2.2), a similar result is obtained for the electric field in Region II. Thus,

$$\bar{E}(\bar{R}) = i\omega\mu_1 b \left\{ \int_0^{\theta_0} I(\theta') \bar{\bar{G}}_3^{21}(\bar{R}|\bar{R}') \cdot \hat{\theta}' d\theta' \Big|_{\substack{R'=b \\ \phi'=0}} - \int_0^{\theta_0} I(\theta') \bar{\bar{G}}_3^{21}(\bar{R}|\bar{R}') \cdot \hat{\theta}' d\theta' \Big|_{\substack{R'=b \\ \phi'=\pi}} \right\}. \tag{7.4}$$

The expression $\bar{\bar{G}}_3(\bar{R}\,|\,\bar{R}')\cdot\hat{\theta}$ must now be examined. From equations (2.8) and (2.9) it is seen that at $R' = b$

$$\bar{M}'_{emn}(k)\cdot\hat{\theta}' = \bar{N}'_{omn}(k)\cdot\hat{\theta}' = 0\begin{cases}\phi' = 0 & \text{or}\\ \phi' = \pi\end{cases},$$

$$\left.\begin{aligned}\bar{M}'_{omn}(k)\cdot\hat{\theta}' &= mj_n(\rho_3)\,\frac{P_n^m(\cos\theta')}{\sin\theta'}\\ \bar{N}'_{emn}(k)\cdot\hat{\theta}' &= \frac{[\rho_3 j_n(\rho_3)]'}{\rho_3}\,\frac{\partial P_n^m(\cos\theta')}{\partial\theta'}\end{aligned}\right\}\ \phi' = 0 \qquad (7.5)$$

$$\bar{M}'_{omn}(k)\cdot\hat{\theta}'\Big|_{\phi'=\pi} = (-1)^m\,\bar{M}'_{omn}(k)\cdot\hat{\theta}'\Big|_{\phi'=0}$$

$$\bar{N}'_{emn}(k)\cdot\hat{\theta}'\Big|_{\phi'=\pi} = (-1)^m\,\bar{N}'_{emn}(k)\cdot\hat{\theta}'\Big|_{\phi'=0}\ , \qquad (7.6)$$

where ρ_3 denotes $k_1 b$.

Substitution of (2.16) through (2.18) into (7.3) and (7.4) yields the following expression for the electric field in the various regions:

$$\bar{E}(\bar{R}) = \frac{-k_1\omega\mu_1 b}{\pi}\sum_{n=1}^{\infty}\sum_{m=1}^{n}{}'\,\frac{2n+1}{n(n+1)}\,\frac{(n-m)!}{(n+m)!}\cdot$$

$$\left\{\bar{M}^{(1)}_{omn}(k_1)\,A^{(1)}_n I_{mn}(\theta_0) + \bar{N}^{(1)}_{emn}(k_1)\,B^{(1)}_n I'_{mn}(\theta_0)\right\} \quad R > b \geq a \qquad (7.7)$$

$$\bar{E}(\bar{R}) = \frac{-k_1\omega\mu_1 b}{\pi}\sum_{n=1}^{\infty}\sum_{m=1}^{n}{}'\,\frac{2n+1}{n(n+1)}\,\frac{(n-m)!}{(n+m)!}\cdot$$

$$\left\{\left[\bar{M}_{omn}(k_1) + a^{(1)}_n\bar{M}^{(1)}_{omn}(k_1)\right]h_n(\rho_3)I_{mn}(\theta_0)\right.$$

$$\left.+\left[\bar{N}_{emn}(k_1) + b^{(1)}_n\bar{N}^{(1)}_{emn}(k_1)\right]\frac{[\rho_3 h_n(\rho_3)]'}{\rho_3}\,I'_{mn}(\theta_0)\right\} \quad a \leq R < b \qquad (7.8)$$

$$\bar{E}(\bar{R}) = \frac{-k_1 \omega \mu_1 b}{\pi} \sum_{n=1}^{\infty} \sum_{m=1}^{n}{}' \frac{2n+1}{n(n+1)} \frac{(n-m)!}{(n+m)!} \cdot$$

$$\left\{ \bar{M}_{omn}(k_2) c_n^{(1)} h_n(\rho_3) I_{mn}(\theta_0) + \bar{N}_{emn}(k_2) d_n^{(1)} \frac{[\rho_3 h_n(\rho_3)]'}{\rho_3} I'_{mn}(\theta_0) \right\} ,$$

$$0 \leq R \leq a \qquad (7.9)$$

where

$$I_{mn}(\theta_0) = \int_0^{\theta_0} \frac{m P_n^m(\cos\theta')}{\sin\theta'} I(\theta') d\theta' ,$$

$$I'_{mn}(\theta_0) = \int_0^{\theta_0} \frac{\partial P_n^m(\cos\theta')}{\partial\theta'} I(\theta') d\theta' \qquad (7.10)$$

and $\sum'$ is used to denote that the summation is over the odd integers only. The scattering coefficients are given in Section 2.2.

The far-zone field of (7.7) is easily found with the aid of (4.27). Hence in this region

$$\bar{E}(\bar{R}) = \frac{-\omega \mu_1 b}{\pi} \frac{e^{ik_1 R}}{R} \sum_{n=1}^{\infty} \sum_{m=1}^{n}{}' \frac{2n+1}{n(n+1)} \frac{(n-m)!}{(n+m)!} (-i)^n \cdot$$

$$\left\{ -i\bar{m}_{omn} A_n^{(1)} I_{mn}(\theta_0) + \bar{n}_{emn} B_n^{(1)} I'_{mn}(\theta_0) \right\} , \qquad (7.11)$$

where $A_n^{(1)}$ and $B_n^{(1)}$ are given by (4.20).

For computational purposes, it is often desirable not to have the associated Legendre functions within the integrals of (7.10). It will now be shown that by locating the source in the x-y plane, the integration will be over the ϕ' variable, and hence the integrand will contain only trigonometric functions.

Consider a curved filament of electric current oriented as shown in Fig. 7-2. In this case, let

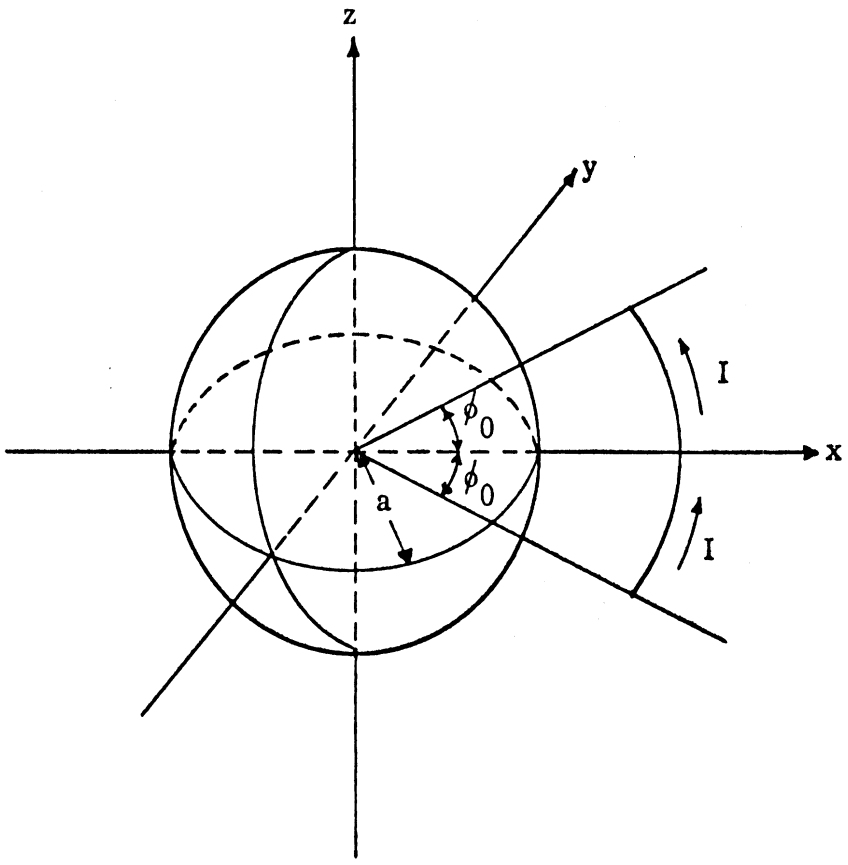

FIG. 7-2: CURVED FILAMENT OF CURRENT IN PRESENCE OF DIELECTRIC SPHERE (x-y plane).

$$\bar{J}(\bar{R}') = I(\phi') \frac{\delta(R'-b)}{b} \delta\left(\theta' - \frac{\pi}{2}\right)\hat{\phi}' \tag{7.12}$$

and assume that the current distribution $I(\phi')$ is an even function of the coordinate variable ϕ'.

To solve for the fields in Region I, (7.12) is substituted into (2.1) and on performing the R' and θ' integration one finds

$$\bar{E}(\bar{R}) = i\omega\mu b \int_0^{\phi_0} \bar{\bar{G}}_3^{11}(\bar{R}|\bar{R}') \cdot \hat{\phi} I(\phi')\, d\phi' \Big|_{\substack{R'=b \\ \theta'=\pi/2}}$$

$$+ i\omega\mu b \int_{-\phi_0}^{0} \bar{\bar{G}}_3^{11}(\bar{R}|\bar{R}') \cdot \hat{\phi} I(\phi')\, d\phi \Big|_{\substack{R'=b \\ \theta'=\pi/2}} . \tag{7.13}$$

Alternately, since $I(\phi')$ is an even function, this result may be expressed in the form

$$\bar{E}(\bar{R}) = 2i\omega\mu b \int_0^{\phi_0} \bar{\bar{G}}_{3\text{even}}^{11}(\bar{R}|\bar{R}) \cdot \hat{\phi} \cdot I(\phi') d\phi \Big|_{\substack{R'=b \\ \theta'=\pi/2}} , \tag{7.14}$$

where $\bar{\bar{G}}_{3\text{even}}^{11}$ is an even function of ϕ'. Taking the even parts of the spherical wave functions (2.8) and (2.9) results in

$$\bar{M}'_{omn} \cdot \hat{\phi}' = \bar{N}'_{emn} \cdot \hat{\phi}' = 0$$

and

$$\bar{M}'_{emn} \cdot \hat{\theta}' \Big|_{\substack{R'=b \\ \phi'=\pi/2}} = -j_n(\rho_3) \frac{\partial P_n^m(0)}{\partial\theta} \cos m\phi' ,$$

$$\bar{N}'_{omn} \cdot \hat{\phi} \Big|_{\substack{R'=b \\ \phi'=\pi/2}} = \frac{[\rho_3 j_n(\rho_3)]'}{\rho_3} m P_n^m(0) \cos m\phi' .$$

It is known (Smythe, 1950, p. 153) that

$$P_n^m(0) = \begin{cases} (-1)^{\frac{n-m}{2}} \dfrac{1\cdot 3\cdot 5\ldots(n+m-1)}{2\cdot 4\cdot 6\ldots(n-m)}, & n+m \text{ even} \\ 0, & n+m \text{ odd} \end{cases}$$

and also

$$\frac{\partial P_n^m(0)}{\partial \theta} = -P_n^{m+1}(0) \quad .$$

Using these relations in (7.14) the result is obtained

$$\bar{E}(\bar{R}) = \frac{-k_1 \omega\mu b}{2\pi} \sum_{n=1}^{\infty} \sum_{m=0}^{n} (2-\delta_0) \frac{2n+1}{n(n+1)} I_m(\phi_0) \cdot$$

$$\begin{cases} \bar{M}_{emn}^{(1)}(k_1) A_n^{(1)} P_n^{m+1}(0), & n+m \text{ odd} \\ \bar{N}_{omn}^{(1)}(k_1) B_n^{(1)} m P_n^m(0), & n+m \text{ even} \end{cases} \qquad R>b \qquad (7.16)$$

where

$$I_m(\phi_0) = \int_0^{\phi_0} I(\phi') \cos m\phi' d\phi' \quad .$$

7.3 A Superposition of Huygens' Sources

Consider two lines of crossed electric and magnetic current sources located on the surface of a dielectric sphere as shown in Fig. 7-3.

In the x-z plane, there is a filament of $\pm\hat{\theta}$ directed electric current,

$$\bar{J}_e(\bar{R}') = X(\theta') \frac{\delta(R'-a)}{a \sin\theta'} \left[\delta(\phi') - \delta(\phi'-\pi)\right] \hat{\theta} ,$$

together with a $-\hat{y}$ directed magnetic dipole strip,

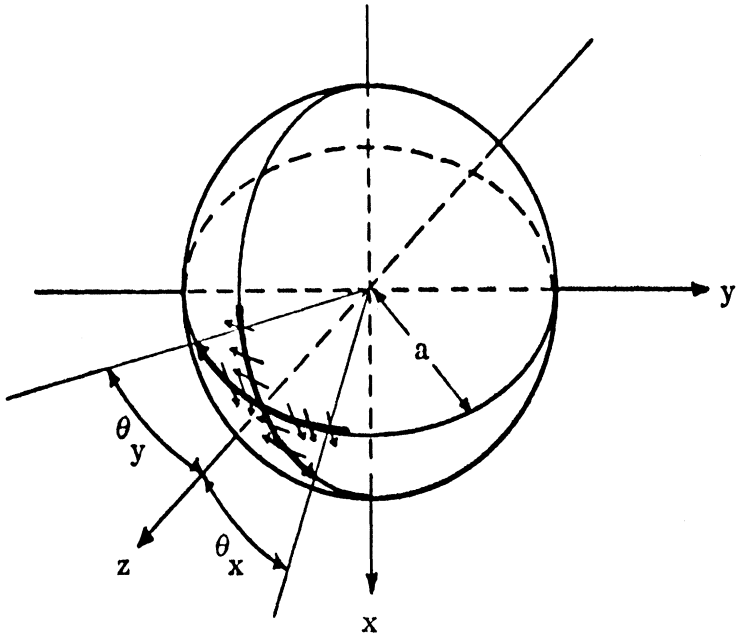

FIG. 7-3: A SUPERPOSITION OF HUYGENS' SOURCES ON THE SURFACE OF A DIELECTRIC SPHERE.

$$\bar{J}_m(\bar{R}') = -\eta_2 X(\theta') \frac{\delta(R'-a)}{a\sin\theta'} \left[\delta(\phi') + \delta(\phi'-\pi)\right]\hat{y} \ ,$$

where $X(\theta')$ is the electric current distribution in the $\phi = 0$ half-plane. Note that at any value of θ', $\bar{J}_m = -\eta_2 \bar{J}_e$, and hence there is a continuous line of approximate Huygens' sources.

In a similar manner, in the y-z plane the line of Huygens' sources consists of an $\hat{x}$ directed electric dipole strip,

$$\bar{J}_e(\bar{R}) = Y(\theta') \frac{\delta(R'-a)}{a\sin\theta'} \left[\delta(\phi'-\tfrac{\pi}{2}) + \delta(\phi'+\tfrac{\pi}{2})\right]\hat{x} \ ,$$

together with a filament of $\pm\hat{\theta}$ directed magnetic current

$$\bar{J}_m(\bar{R}') = \eta_2 Y(\theta') \frac{\delta(R'-a)}{a\sin\theta'} \left[\delta(\phi'+\tfrac{\pi}{2}) - \delta(\phi'-\tfrac{\pi}{2})\right]\hat{\theta}' \ .$$

Here $Y(\theta')$ represents the electric current distribution in the $\phi = \pi/2$ half-plane.

Proceeding in a manner similar to that used in Sec. 7.2, it is found that the far-zone field radiated by this superposition of sources may be expressed by

$$\bar{E}(\bar{R}) = \frac{i\omega\mu_1 a}{\pi R} e^{ik_1 R} \sum_{n=1}^{\infty} \sum_{m=1}^{n}{}' \frac{2n+1}{n(n+1)} (-i)^n \frac{(n-m)!}{(n+m)!} \cdot$$

$$\left\{ \left(A_n^{(1)} + \frac{D_n^{(1)}}{\sqrt{\epsilon_r}} \right) \left[X_{mn}(\theta_x) + Y'_{mn}(\theta_Y) \right] \bar{m}_{omn} \right.$$

$$\left. + i \left(B_n^{(1)} + \frac{C_n^{(1)}}{\sqrt{\epsilon_r}} \right) \left[X'_{mn}(\theta_x) + Y_{mn}(\theta_y) \right] \bar{n}_{emn} \right\} , \qquad (7.17)$$

where

$$X_{mn}(\theta_x) = \int_0^{\theta_x} m \frac{P_n^m(\cos\theta')}{\sin\theta'} X(\theta')d\theta'$$

$$Y_{mn}(\theta_y) = \int_0^{\theta_y} (-1)^{\frac{m+3}{2}} m \frac{P_n^m(\cos\theta')}{\sin\theta'} Y(\theta')d\theta'$$

$$X'_{mn}(\theta_x) = \int_0^{\theta_x} \frac{\partial P_n^m(\cos\theta')}{\partial\theta'} X(\theta')d\theta'$$

$$Y'_{mn}(\theta_y) = \int_0^{\theta_y} (-1)^{\frac{m+3}{2}} \frac{\partial P_n^m(\cos\theta')}{\partial\theta'} Y(\theta')d\theta' \quad .$$

7.4 Numerical Results

The dipole patterns shown in Figs. 7-4 and 7-5 were computed using (7.11) with the sinusoidal current distribution

$$I(\theta') = \sin k_0 a(\theta_0 - \theta') \quad . \qquad (7.18)$$

The upper patterns in these figures show the effect of bending the dipoles into arcs with no sphere present. In Fig. 7-4a, the dipole is in the form of a semi-circle, i.e., $\theta_0 = \pi/2$, and similarly in Fig. 7-5a, the dipole subtends a half-angle of $\pi/10$ radians. It is noted that these patterns are the same in both the forward and back directions and that arcing the dipole tends to reduce the nulls in the E-plane patterns occurring at $\theta = \pi/2$.

The patterns of Figs. 7-4b and 7-5b show the effect of adding a dielectric sphere with $\epsilon_r = 3.2$. Here the sphere tends to focus the energy into the forward direction.

The current distribution of (7.18) was also used in calculating the patterns of Fig. 7-6. They illustrate that directional patterns can be produced with a small sphere constructed of a material with a relatively high ($\epsilon_r = 7.5$) dielectric constant.

The patterns shown in Fig. 7-7 were calculated using (7.17) in 2-degree intervals with sinusoidal current distributions in both planes. The crossed sources each subtended half-angles of $\pi/6$ radians corresponding to a 3-inch sphere against the aperture of a C-band circular waveguide. In a comparison of Figs. 7-7 and 6-1, it is seen that extending the source had very little effect on the resulting patterns.

Using (7.17), the patterns of Fig. 7-8 were calculated with a) a point Huygens' source and b) an extended crossed source with sinusoidal currents, each subtending half-angles of $\pi/10$ radians. This would correspond to a 5-inch sphere operating at 5.6 GHz. Here it is noted that with the extended source the sidelobes are slightly reduced.

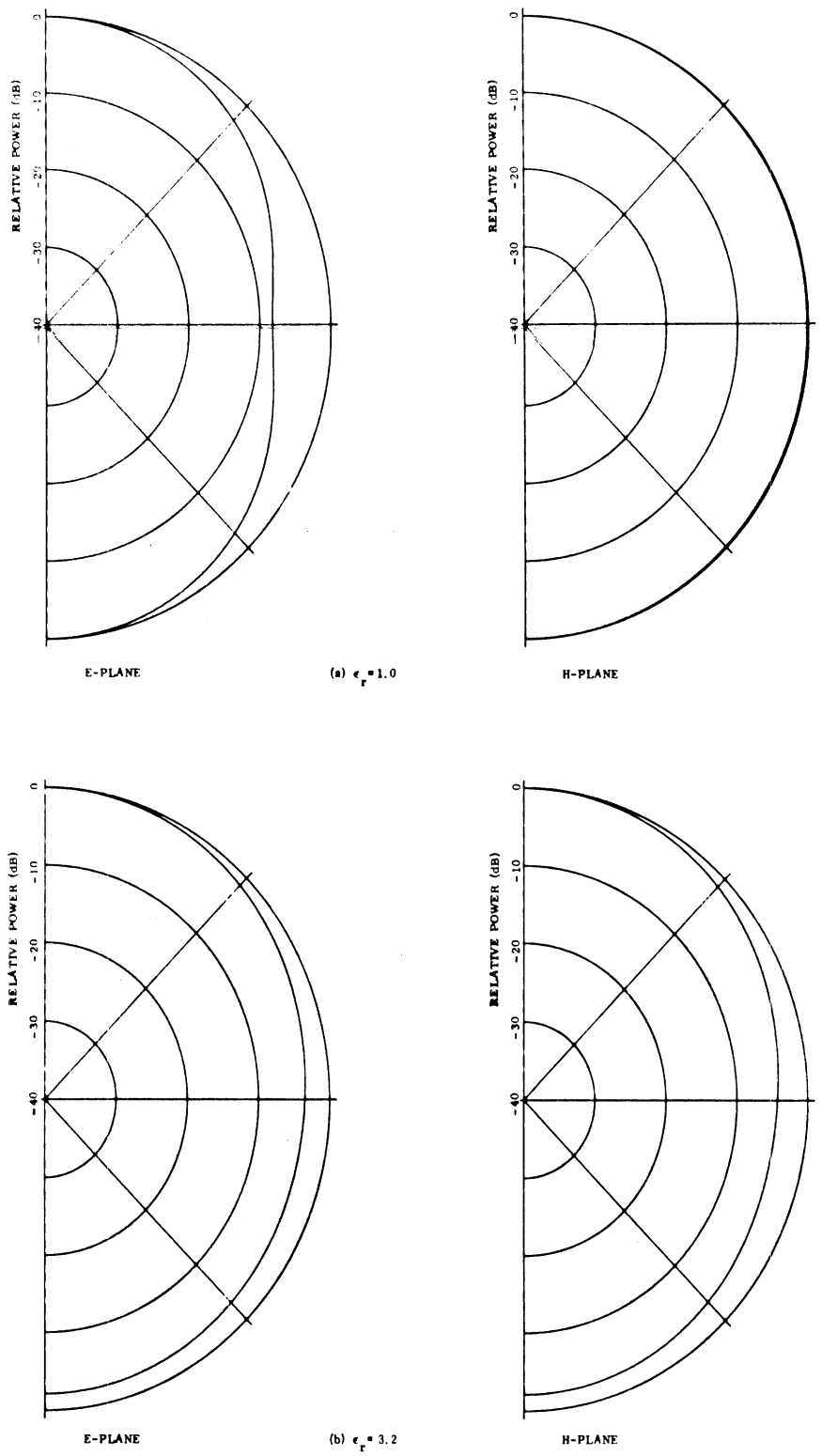

FIG. 7-4: RADIATION PATTERNS FOR CURVED HALF-WAVE DIPOLE ON SPHERE SURFACE ($D = \lambda_o/\pi$, $\tan \delta = 0.0$).

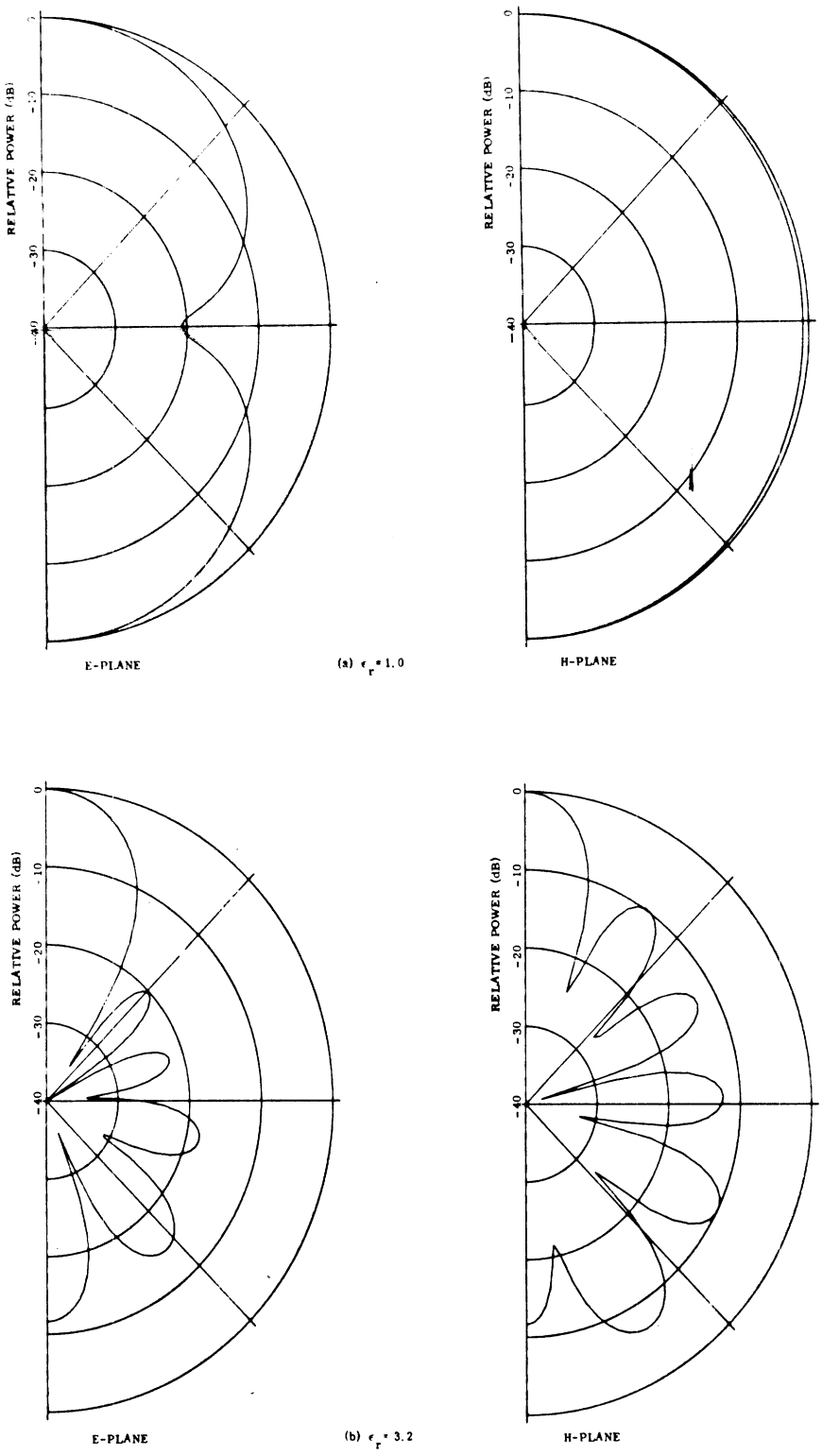

FIG. 7-5: RADIATION PATTERNS FOR CURVED HALF-WAVE DIPOLE ON SPHERE SURFACE ($D = 5\lambda_o/\pi$, $\tan\delta = 0.0$).

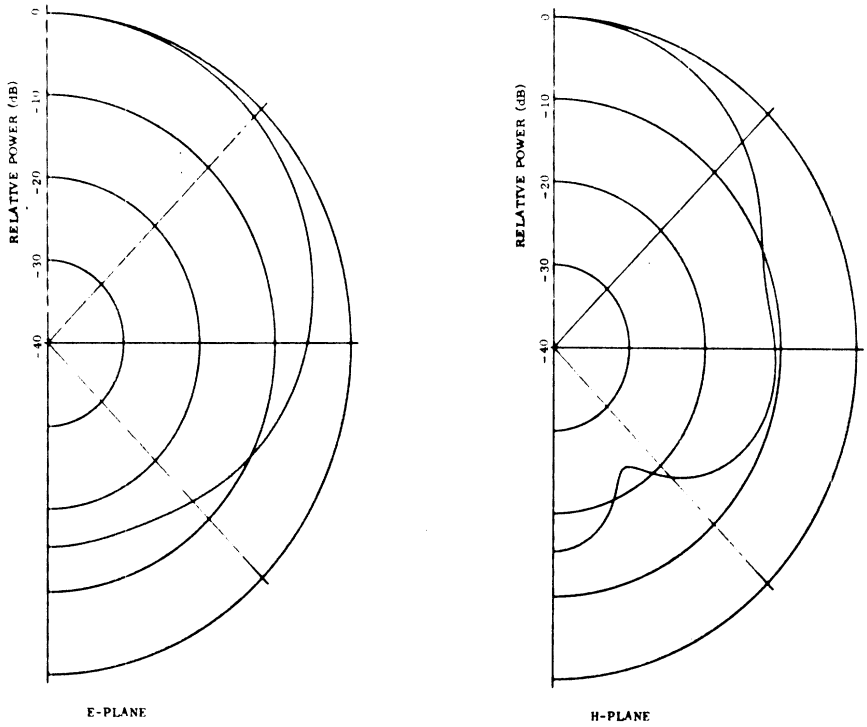

FIG. 7-6

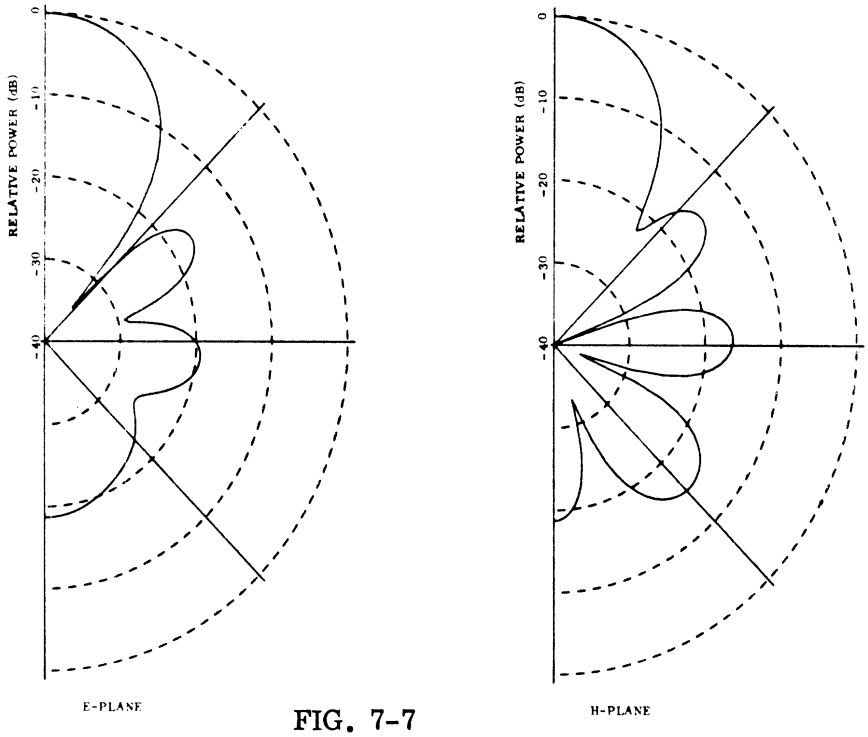

FIG. 7-7

FIG. 7-6: RADIATION PATTERNS FOR CURVED HALF-WAVE DIPOLE ON SPHERE SURFACE ($D = .4\lambda_o$, $\epsilon_r = 7.5$, $\tan\delta = 0.0$).

FIG. 7-7: RADIATION PATTERNS FOR EXTENDED SOURCE ($D = 1.27\lambda_o$, $\epsilon_r = 2.57$, $\tan\delta = 0.0$, $\theta_o = \pi/6$).

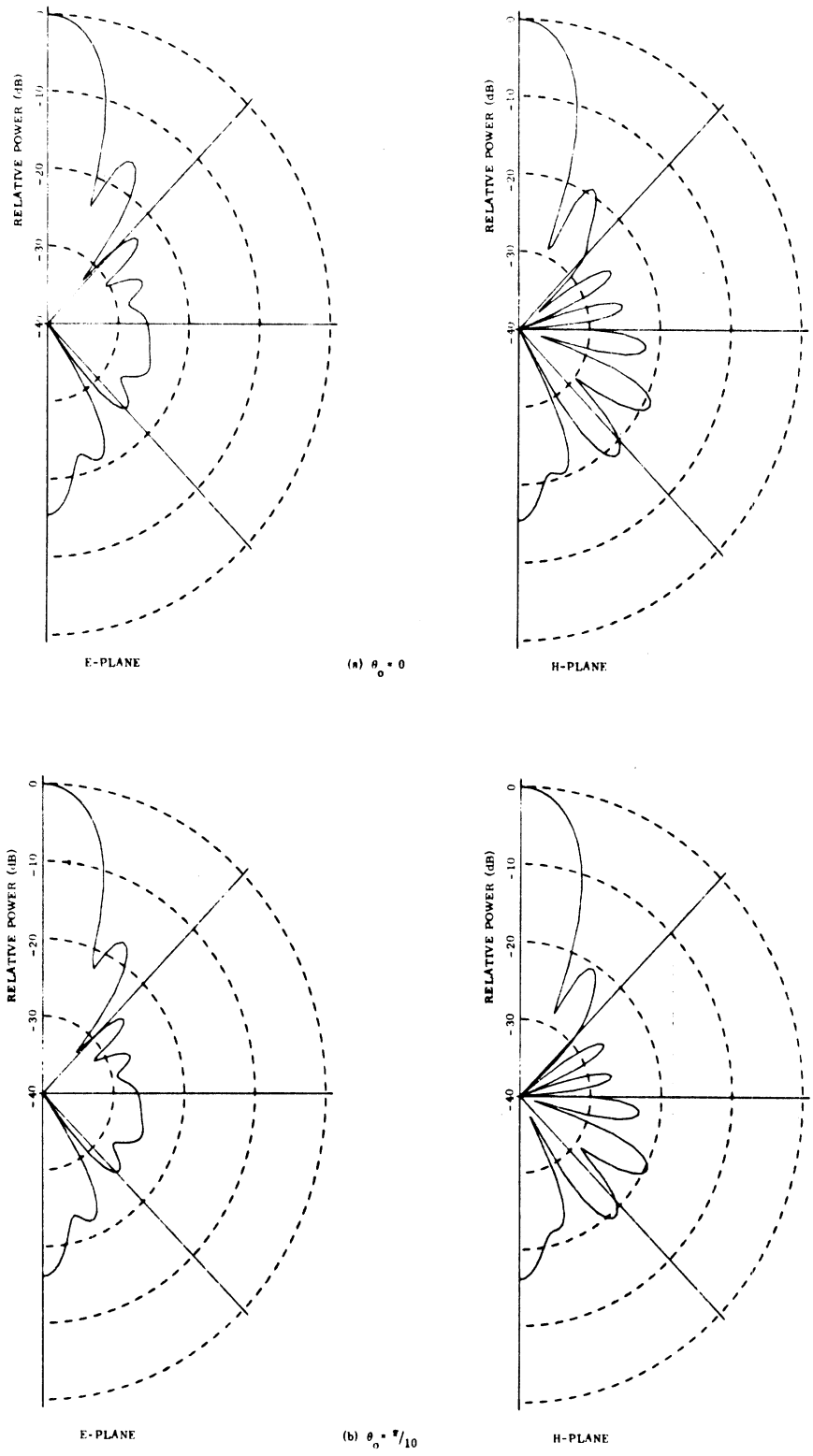

FIG. 7-8: RADIATION PATTERNS FOR EXTENDED SOURCE ($D = 2.37\lambda_o$, $\epsilon_r = 2.57$, $\tan\delta = .0065$).

Chapter VIII

INTERPRETATION BASED ON GEOMETRICAL OPTICS

8.1 Introduction

Physical insight into the way in which the homogeneous dielectric sphere focusses the energy from a point source to form the relatively directive antenna patterns shown in Chapter 6, may be obtained using the ray-tracing techniques of geometrical optics. With this method, it is assumed that the wavelength is infinitesimally small, i.e., $ka \rightarrow \infty$, and the paths of the electromagnetic wave propagation are determined using elementary geometry.

In this chapter, the trajectory of ray paths leaving the sphere are determined for various dielectric constants. Next, the amplitude and phase across an equivalent plane through the center of the sphere is examined and used to explain some of the results of Chapter 6. Finally, we look at the reduction of aperture radius caused by the critical angle as a function of source position and dielectric constant.

8.2 Ray Paths

Figure 8-1 shows the cross section of a homogeneous dielectric sphere with an index of refraction n, where $n = \sqrt{\epsilon_r}$. Consider a typical ray path ABF eminating from a point source located at A; the ray originates at the angle θ_i and travels undeviated to B. Here the ray is refracted by the air-dielectric interface with the transmitted portion leaving the sphere at an angle θ' measured from the horizontal.

The plane of incidence is defined as the plane containing the incident ray and the normal to the surface. Since for this case the surface normal is the radius vector, the plane of the paper is the plane of incidence. It follows, therefore, from the law of refraction (Snell's law) that the refracted ray BF must remain in the plane of the paper. To find the angle θ', Snell's law is applied at the local point B,

$$\sin\theta_t = n\sin\theta_i \tag{8.1}$$

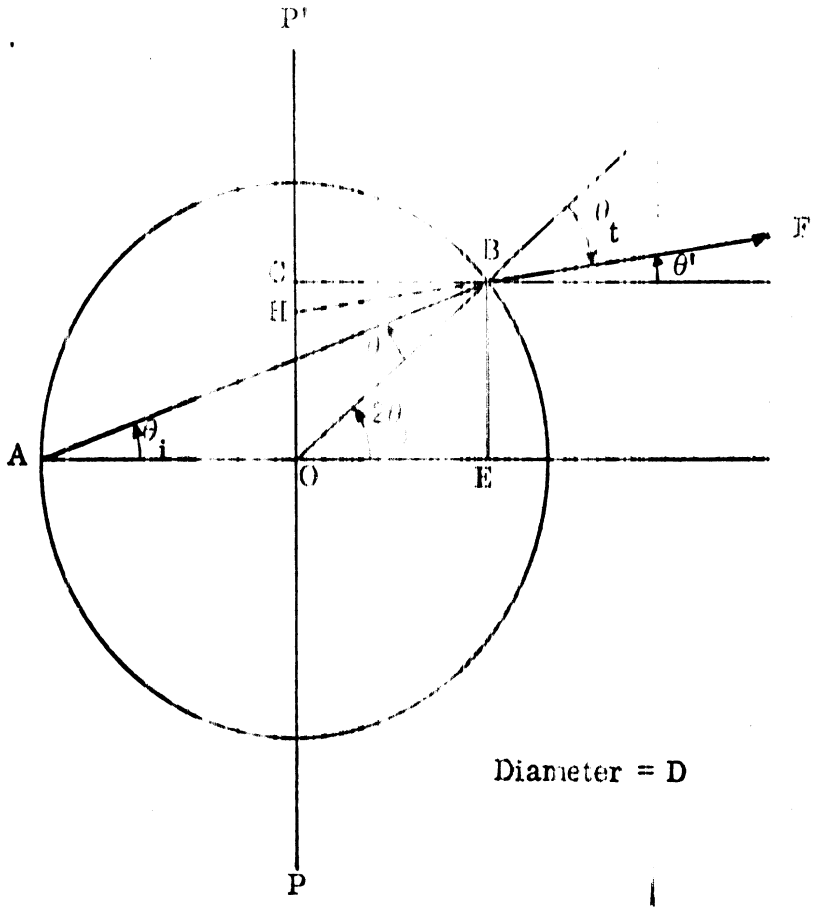

FIG. 8-1: GEOMETRY FOR RAY TRACING CALCULATIONS

and hence

$$\theta' = 2\theta_i - \sin^{-1}(n \sin\theta_i) \tag{8.2}$$

Since rays are traveling from a dielectric into a region of lower permittivity, there is a critical angle θ_c given by

$$\theta_c = \sin^{-1}(1/n) \ . \tag{8.3}$$

Rays incident at this angle, i.e. $\theta_i = \theta_c$, leave the sphere tangent to the surface. If $\theta_i > \theta_c$, the rays experience total internal reflection and will not be considered here.

Ideally one would like the dielectric sphere to transform the radiation from the point source into a plane wave. This would correspond to $\theta' = 0$ for all

values of θ_i. For small θ_i (8.2) becomes

$$\theta' = (2-n)\theta_i \quad , \tag{8.4}$$

and hence the emergent rays for this case are parallel to the axis when $n = 2$. This value of index is in agreement with Born and Wolf (1970, p. 162), since for a spherical lens of diameter D the paraxial focus is given by the formula

$$f = \frac{D}{4}\,\frac{n}{n-1} \tag{8.5}$$

and therefore lies on the surface when $n = 2$ corresponding to a dielectric constant of 4.

The deviation angle θ' as given by (8.2) is plotted in Fig. 8-2 as a function of incident angle for various dielectric constants. It is observed that except when $\theta_i = 0$, the deviation angle is strictly positive or strictly negative for for $\epsilon_r < 2$ or $\epsilon_r > 4$, respectively. It appears, therefore, that the sphere will have its maximum focussing effect when the dielectric constant is somewhere between these two values. Note also from Fig. 8-2 that the critical angle decreases with increasing dielectric constant. Figure 8-3 shows typical ray paths for a sphere with a dielectric constant of 3.0.

8.3 Amplitude and Phase Across an Equivalent Plane

Now an expression is derived for the amplitude and phase across an equivalent aperture plane, located at the center of the sphere, in a manner similar to that outlined by Bekefi and Farnell (1956).

In this analysis we consider incident rays in the range

$$\left\{ \begin{array}{ll} 0 \leq \theta_i \leq \theta_c \,, & \epsilon_r \geq 2 \\ 0 \leq \theta_i \leq \pi/4 \,, & \epsilon_r < 2 \end{array} \right\} \quad ,$$

since the critical angle occurs at $\pi/4$ for $\epsilon_r = 2$. Looking back at Fig. 8-1, a typical ray travels from A to B within the dielectric, and then leaves the

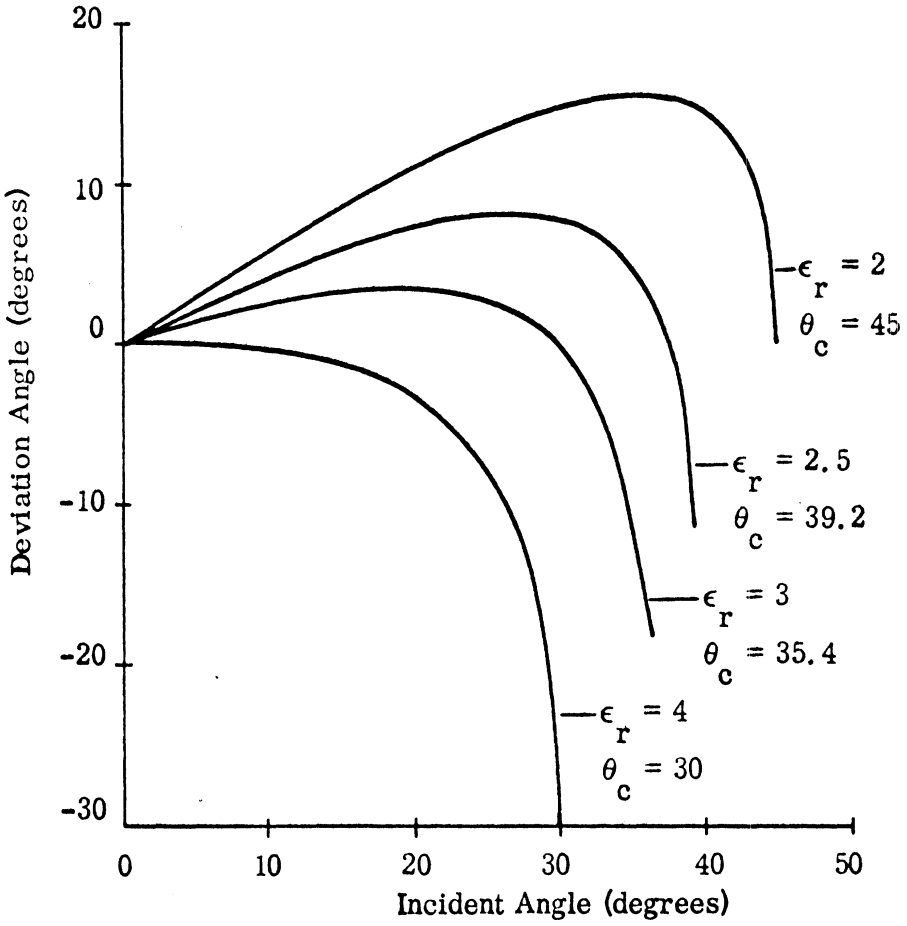

FIG. 8-2: ANGULAR DEVIATION OF RAYS FROM HORIZONTAL UPON EXIT FROM SPHERE.

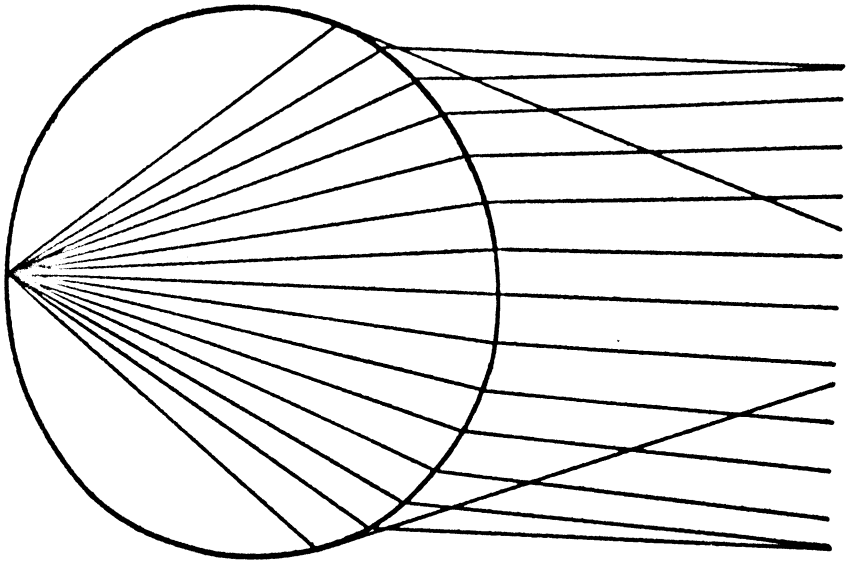

FIG. 8-3: RAY PATHS THROUGH DIELECTRIC SPHERE ($\epsilon_r = 3.0$).

sphere at the angle θ'. Reflection from the surface is being neglected. Now the sphere is removed and the ray BF is traced back as if it originated from point H on the plane .PP'.

The various angles and distances in Fig. 8-1 may be found as follows:

$$\theta_t = \sin^{-1}(n \sin\theta_i)$$

$$\theta' = 2\theta_i - \theta_t$$

$$AB = D\cos\theta_i$$

$$OE = CB = \frac{D}{2}\cos 2\theta_i$$

$$EB = OC = \frac{D}{2}\sin 2\theta_i$$

$$BH = CB \sec\theta'$$

$$CH = BH \sin\theta' \qquad (8.6)$$

Since the ray ABF suffers no phase reversal at B, the phase angle ϕ of the ray BF transformed back to H is given by

$$\phi = \left[nAB - BH - D(n - \tfrac{1}{2})\right] k_0 \text{ radians} , \tag{8.7}$$

where D is the sphere diameter, k_0 is the free space propagation constant, and the factor $k_0 D(n - \frac{1}{2})$ is used to normalize the phase to zero at the center of the sphere. Making use of (8.6) we obtain the desired phase expression

$$\phi = k_0 D\left[n(\cos\theta_i - 1) + \frac{1}{2}\left(1 - \frac{\cos 2\theta_i}{\cos\theta_i}\right)\right] . \tag{8.8}$$

It is apparent from Fig. 8-1 that the radius H of the intersection of the ray with the aperture plane is given by

$$H = OC - CH$$

and hence

$$H = \frac{D}{2}(\sin 2\theta_i - \cos 2\theta_i \tan\theta') . \tag{8.9}$$

The amplitude of the power density across the equivalent aperture plane remains to be examined. For the present we neglect the transmission coefficient associated with the surface of the sphere and consider two concentric cones of semi-angles θ and $\theta+d\theta$ as shown in Fig. 8-4. The power radiated by the

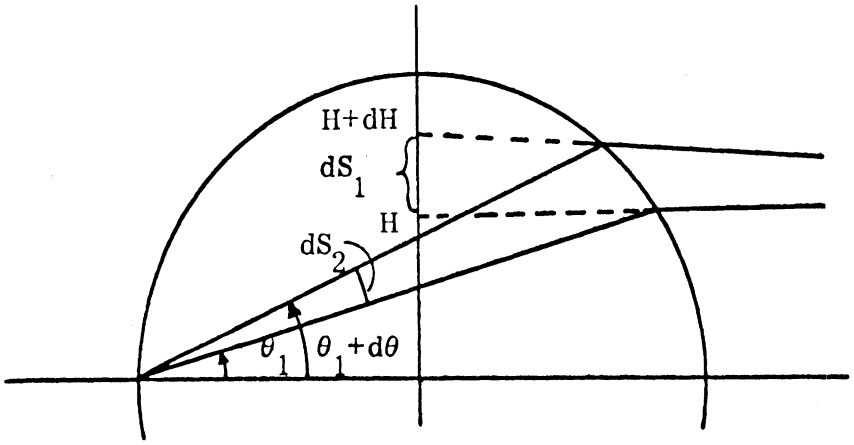

FIG. 8-4: GEOMETRY FOR APERTURE PLANE AMPLITUDE CALCULATION.

the source into the space enclosed by these cones appears over the equivalent plane in the annular ring of radius H and width dH.

The incremental areas of the annular rings located at unity radius and at the equivalent plane respectively are given by

$$dS_1 = \sin\theta d\theta d\phi$$

$$dS_2 = HdHd\phi \quad .$$

If $P(\theta)$ is the power radiated per unit solid angle and $P(H)$ is the power received per unit angle across the equivalent plane, conservation of energy requires (Born and Wolf, 1970, p. 116)

$$\frac{P(H)}{P(\theta)} = \frac{dS_1}{dS_2}$$

and thus

$$P(H) = P(\theta)\frac{\sin\theta}{H}\frac{d\theta}{dH} \quad . \tag{8.10}$$

Using (8.9) together with the relations (8.6) yields

$$P(H) = \frac{2\sin\theta_i}{HD}\left[2\cos 2\theta_i + 2\sin 2\theta_i \tan\theta' - \cos\theta_i \sec^2\theta'(2 - n\cos\theta_i \sec\theta_t)\right]^{-1} P(\theta). \tag{8.11}$$

Although only the primary rays are examined in this analysis, the above equation must now be modified to account for the amplitude reduction of these rays due to the energy reflected from the sphere surface.

Since the Huygens' source radiates a linearly polarized field, the two principal planes are considered where the electric field is either parallel or perpendicular to the plane of incidence corresponding to the E or H planes. The power transmission coefficients for these two planes are (Stratton, 1941, p. 496)

$$T_E = \frac{\sin 2\theta_i \sin 2\theta_t}{\sin^2(\theta_i+\theta_t)\cos^2(\theta_i-\theta_t)} \tag{8.12}$$

$$T_H = \frac{\sin 2\theta_i \sin 2\theta_t}{\sin^2(\theta_i+\theta_t)} \tag{8.13}$$

With this modification, the amplitude distribution A(H) across the line of intersection of the plane of incidence and the equivalent plane will thus be given by

$$A(H) = \left|P(H)T\right|^{1/2} , \tag{8.14}$$

where T is either T_E or T_H for the plane of incidence parallel to the E or H planes, respectively.

Comparing (8.12) with (8.13) it is seen that the former contains an additional cosine factor in the denominator, and hence the amplitude in the E-plane will, in general, be greater than the H-plane. Since the two transmission coefficients are identical for $\theta_i = \theta_t$, which would correspond to all rays for $\epsilon_r = 1$ or the on-axis ray for $\epsilon_r > 1$, the amplitude distribution will be continuous at the center of the aperture.

The results of this section are presented in Figs. 8-5 to 8-7 for a sphere of unity diameter. In Fig. 8-5, the phase shift (8.8) is plotted as a function of equivalent plane radius (8.9) for various dielectric constants. Here a dielectric constant of about 3.0 tends to yield the minimum phase deviation across the aperture. Looking back at Fig. 6-9f it is noted that this same value of dielectric constant produced the maximum directivity for the larger diameter spheres. That this should be the case is apparent from (8.8), where we see that the phase deviation is proportional to sphere diameter, and hence is a critical parameter for large spheres.

With $P(\theta) = (1+\cos\theta_i)^2$ in (8.11), the amplitude distribution across the equivalent plane (8.14) is plotted in Figs. 8-6 and 8-7 for various dielectric constants. We note that for $\epsilon_r > 2$, there is a greater tapering of the amplitude across the aperture in the H-plane than the E-plane. In the light of this one expects

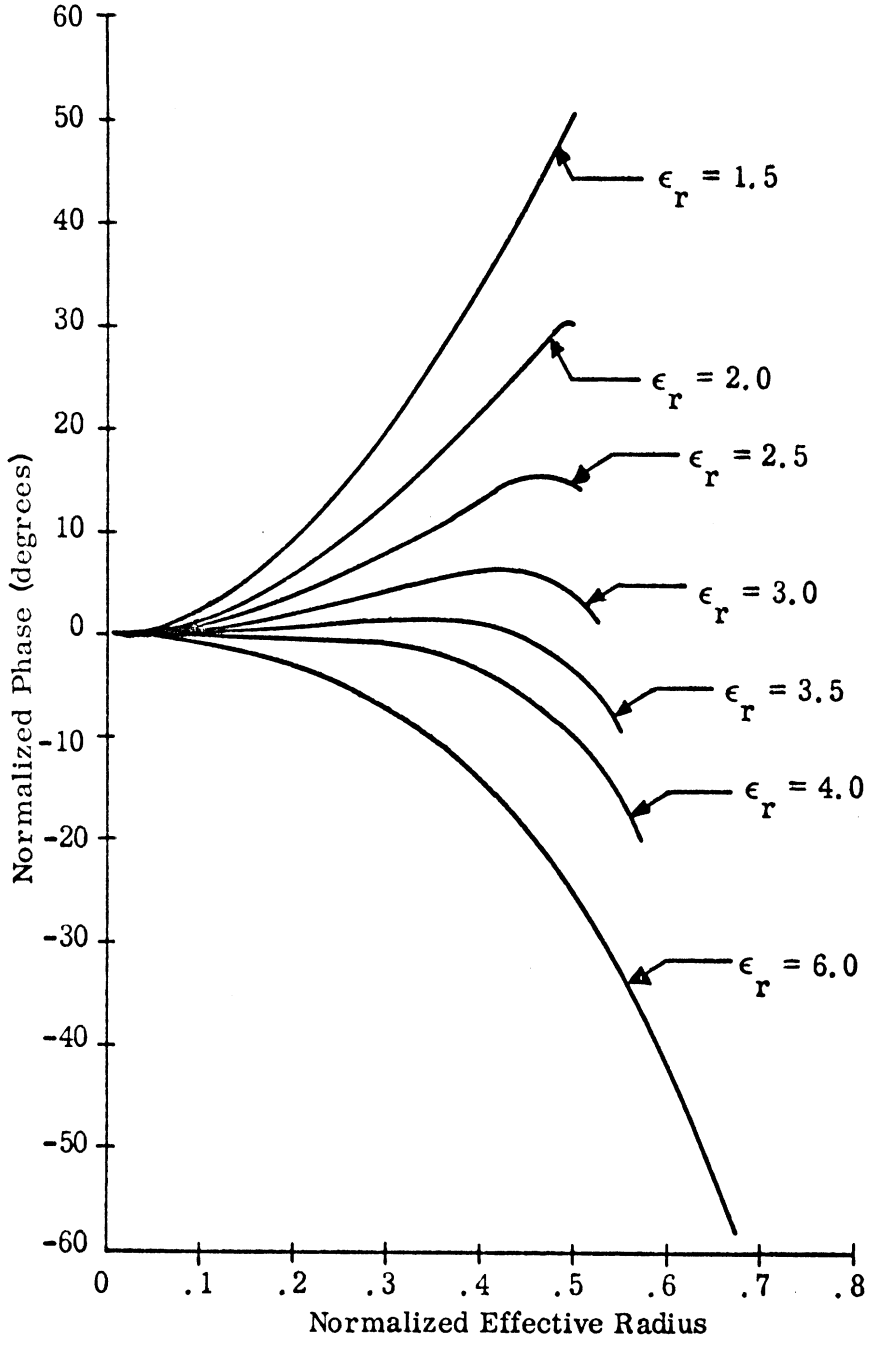

FIG. 8-5: PHASE ACROSS APERTURE FOR VARIOUS DIELECTRIC CONSTANTS.

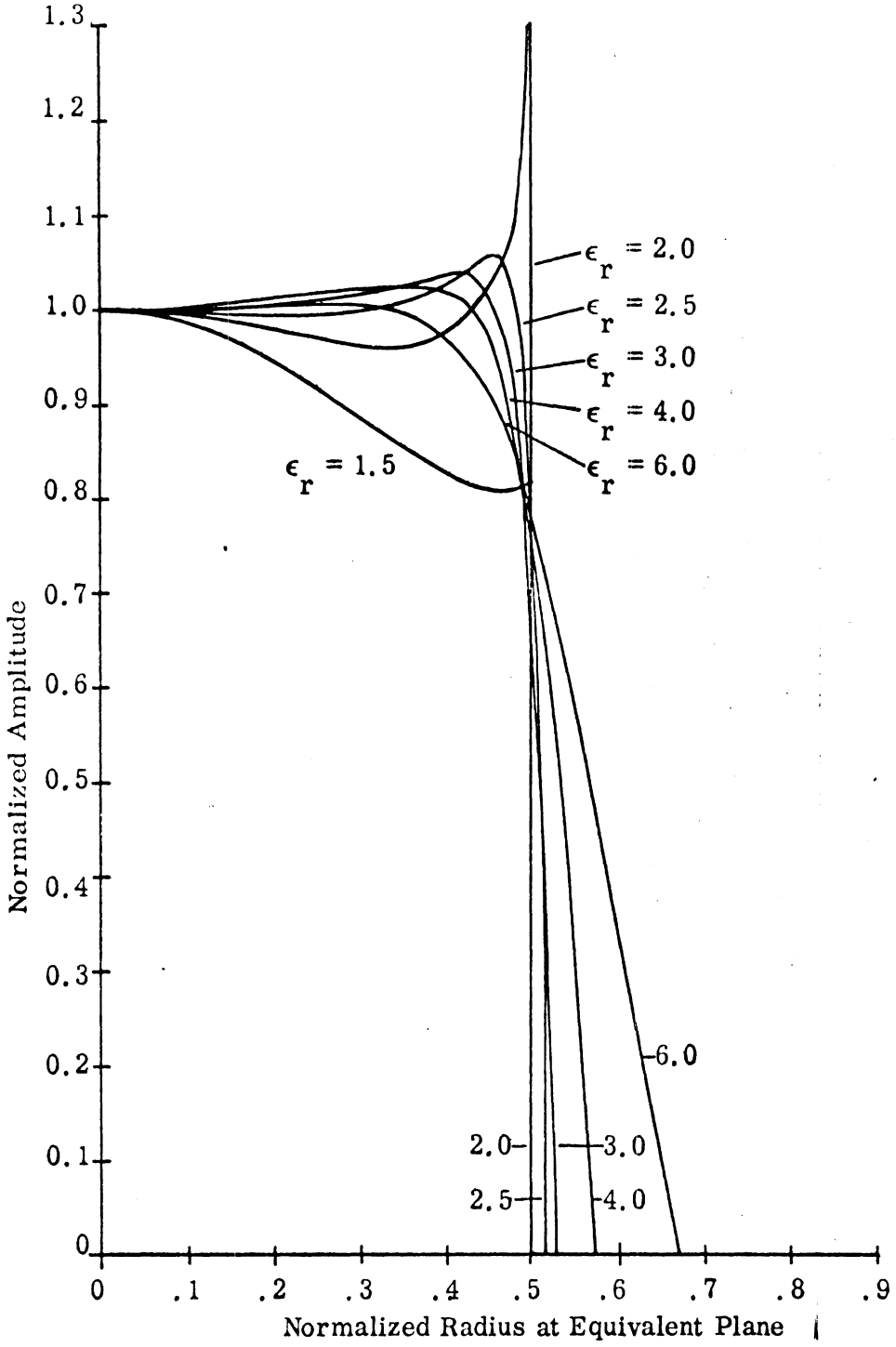

FIG. 8-6: E-PLANE APERTURE AMPLITUDE FOR VARIOUS DIELECTRIC CONSTANTS.

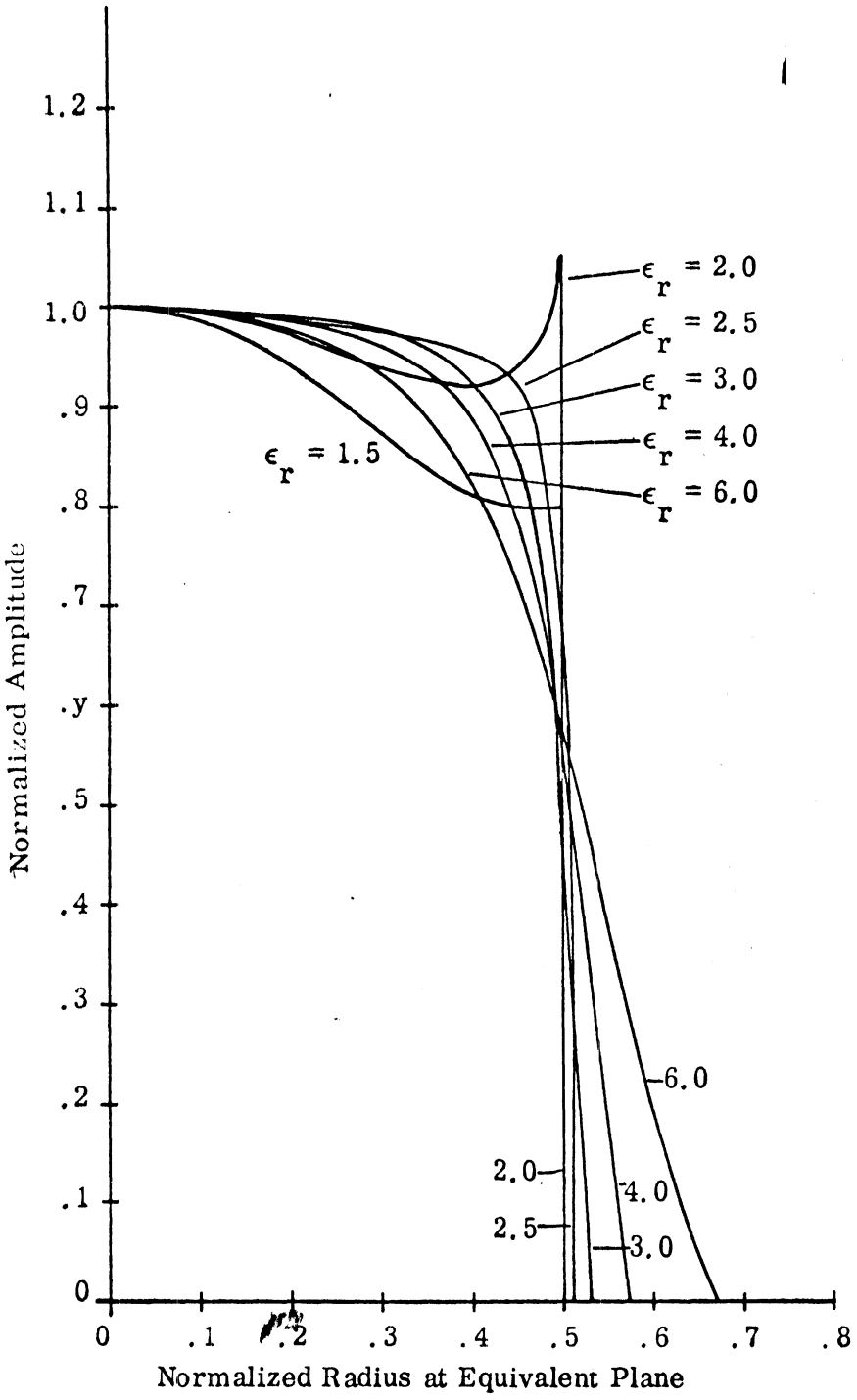

FIG. 8-7: H-PLANE APERTURE AMPLITUDE FOR VARIOUS DIELECTRIC CONSTANTS.

the far-field pattern in the H-plane to have a wider main beam and lower side lobes than the E-plane (Silver, 1963). In the patterns presented in Figs. 6-2 to 6-4, this tends to be the case.

8.4 Effective Aperture Radius

It was noted in Section 8.2 that rays incident at an angle equal to or greater than the critical angle experience total internal reflection. We now wish to investigate how the effective aperture radius, which is limited by this critical angle, varies as a function of the dielectric constant for the source located on the surface or inside the sphere.

Figure 8-8 shows the cross section of a sphere of radius a. Assuming

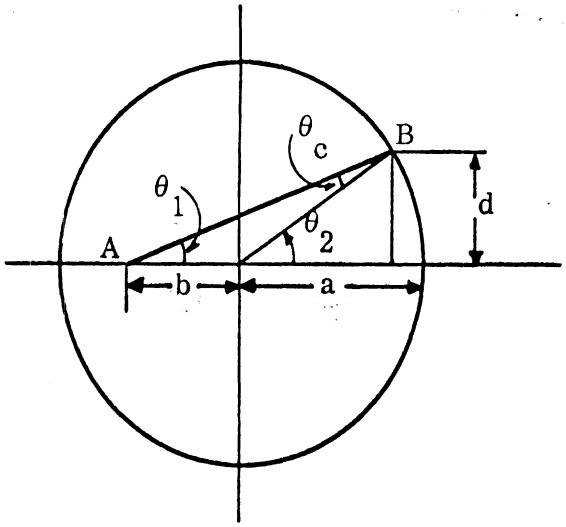

FIG. 8-8: GEOMETRY FOR APERTURE RADIUS AT CUTOFF.

the ray AB is incident on the surface at the critical angle θ_c, we seek the aperture radius d. As was shown in Section 8.2, the critical angle is given by

$$\sin\theta_c = \sqrt{1/\epsilon_r} = 1/n \qquad (8.15)$$

where n is the index of refraction. Also from the Law of Sines note

$$\frac{b}{\sin\theta_c} = \frac{a}{\sin\theta_1}$$

and hence

$$\sin\theta_1 = \frac{a}{nb} \quad . \tag{8.16}$$

Since

$$\theta_2 = \theta_1 + \theta_c \quad ,$$

$$\frac{d}{a} = \sin\theta_1\cos\theta_c + \sin\theta_c\cos\theta_1 \quad . \tag{8.17}$$

Using (8.15) and (8.16) in the above expression yields

$$\frac{d}{a} = \frac{1}{\epsilon_r}\left(\sqrt{\epsilon_r - \frac{a^2}{b^2}} + \frac{a}{b}\sqrt{\epsilon_r - 1}\right) \tag{8.18}$$

which is valid for $(a/b)^2 \leq \epsilon_r$.

Equation (8.18) is plotted in Fig. 8-9 together with the optimized directivity data of Fig. 6-22. Here the effective aperture radius is generally about nine-tenths of the sphere radius for the optimized points, and that locating the source at the paraxial focus would result in a considerable reduction of the of the effective aperture radius.

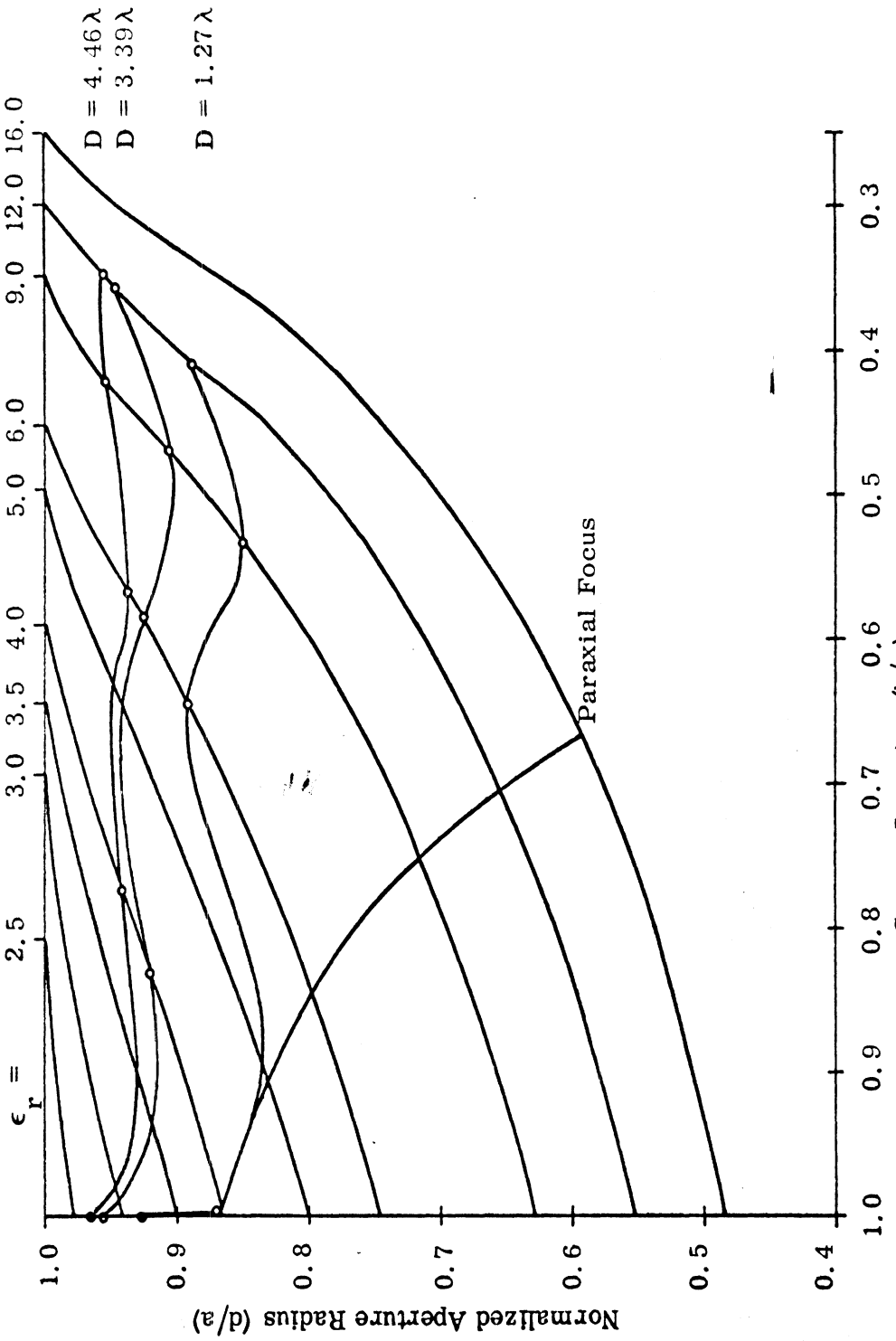

FIG. 8-9: NORMALIZED APERTURE RADIUS AT CUTOFF VS. SOURCE LOCATION FOR VARIOUS DIELECTRIC CONSTANTS.

Chapter IX

CONCLUSIONS AND RECOMMENDATIONS

9.1 Conclusions

This thesis has been devoted to the study of the radiation from simple sources in the presence of a homogeneous dielectric sphere. The dyadic Green's functions of the third and fourth kinds pertaining to this problem have been presented and should be applicable to most electromagnetic problems dealing with homogeneous spheres. Using the method of scattering superposition, exact representations for the electric fields excited by infinitesimal electric or magnetic dipole current sources located inside, outside, or on the surface of a dielectric sphere were formulated.

Because of the simplicity and directional characteristics of the Huygens' source, the antenna parameters using this source in the presence of a dielectric sphere were studied in detail. Expressions were developed for the radiated power, radiation resistance, directivity and antenna efficiency. These results may be easily reduced to that for individual electric or magnetic dipoles by letting the appropriate constants be zero.

When the calculated radiation patterns for the Huygens' source on the sphere surface were compared to measured patterns for plexiglas spheres on the end of waveguides, excellent agreement was found. These results confirm the findings of Croswell and Chatterjee (1972) that waveguide-excited dielectric spheres may be used to radiate patterns which are superior to those from optimized circular horns of the same cross-sectional area. Extending the point Huygens' source into crossed curved lines of sources did not significantly affect the radiation patterns.

Again using the point source, the directivity was plotted as a function of sphere diameter for various dielectric constants. It was found that for spheres greater than $2.5\lambda_0$ in diameter, a dielectric constant of about 3.0 tended to yield the optimum directivity.

The dielectric sphere exhibits a resonance phenomenon in which much of the energy is radiated into the side lobes with a commensurate decrease in the directivity. This effect was most pronounced for the larger, denser spheres. It was found that with increasing sphere diameter, the resonance alternates between the two principle planes with each new resonance in a particular plane being at the next higher mode. The resonance may not be apparent in the radiation pattern of a lossy sphere, but will be manifest as a reduction in the antenna efficiency. This is because the resonance occurs at a high order mode which is quickly attenuated by dielectric loss.

Using the Huygens' source model, it was shown that by appropriately adjusting the dielectric constant, radiation patterns with high directivity and low side lobes may be produced with the source located inside the sphere. This suggests that directional patterns may be radiated by a truncated sphere mounted on a waveguide, as shown in Fig. 9-1.

Expressions were developed for the radiation from a curved electric dipole in the presence of a dielectric sphere. The bending of the half-wave dipole into an arc tended to reduce the sharp nulls in the E-plane patterns. It was found that directional patterns may be radiated from a dipole partially wrapped around the meridian of a dielectric sphere. This, together with the previous results, suggests the use of a monopole mounted on a ground plane covered by a dielectric hemisphere as shown in Fig. 9-2.

Using the methods of geometrical optics, it was shown that a relatively small phase deviation occurs across an equivalent aperture plane when the dielectric constant of the sphere is about 3. This, together with the tapering of the field amplitude across the aperture, may be used to explain why the small sphere is able to focus the point source into a relatively directive pattern. Since the phase deviation is proportional to sphere size, this focussing effect should tend to degrade for large spheres.

9.2 Recommendations for Further Research

There is considerable room for future investigation, both theoretical and experimental, of sources in the presence of dielectric spheres.

According to Luneberg's original theory (1944), an inhomogeneous lens with the permittivity profile $\epsilon_r(R) = 2 - (R/a)^2$ will focus rays from a point source on the surface into a collimated beam. It would be interesting to perform a detailed numerical analysis of the expressions given by Tai (1956; 1971, Sec. 46) for the electromagnetic solution of the spherical Luneberg lens. The results could then be compared to those presented in this work for the homogeneous sphere.

Using the method of dyadic Green's functions, together with scattering superposition, exact expressions could be formulated for the radiation from stratified spheres. Numerical results could then be easily obtained with a computer program similar to that presented in Appendix B. since only the calculations of the scattering coefficients would need to be modified. Again, the data could be compared to that of a homogeneous sphere to see the effect of layering on the antenna parameters such as the radiation pattern, resonance, and dielectric loss.

It would be interesting to construct the models shown in Figs. 9-1 and 9-2 and measure their performance. The data presented in Fig. 6-22 could be used to provide the initial design parameters. The antenna of Fig. 9-1 has a smaller axial dimension than the full sphere, as well as providing a flat surface for mounting the waveguide.

The radiation patterns of the antenna shown in Fig. 9-2 should be the same as that of a dipole within a full sphere because of the imaging properties of the conducting ground plane. This structure is similar to that used by Meinke (1970), except that here the source is located inside the dielectric hemisphere. It could be easily mounted on the outside of an aircraft and would not require a radome.

As a final remark, antennas are frequently designed without consideration of the radome and then modified to reduce the often deleterious effects of this protective cap. In view of this work, perhaps the dielectric cover should be considered an integral part of the radiating system used to improve the beam-forming properties of the antenna.

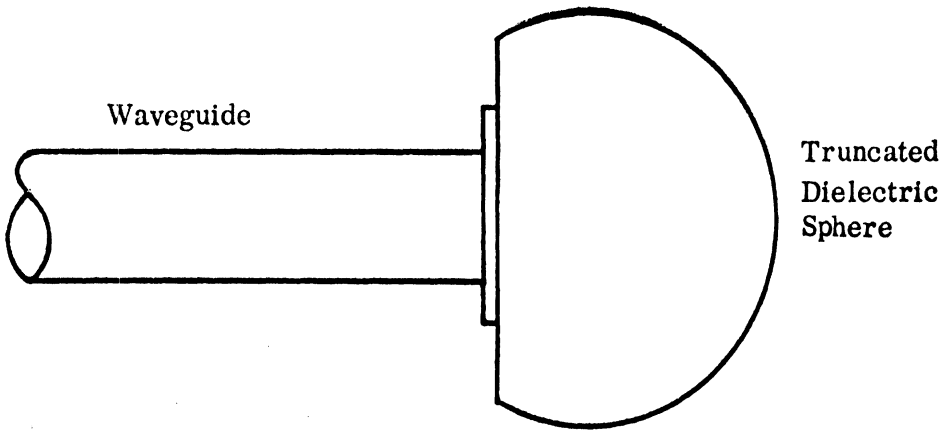

FIG. 9-1: PROPOSED ANTENNA FOR EXPERIMENTAL STUDY

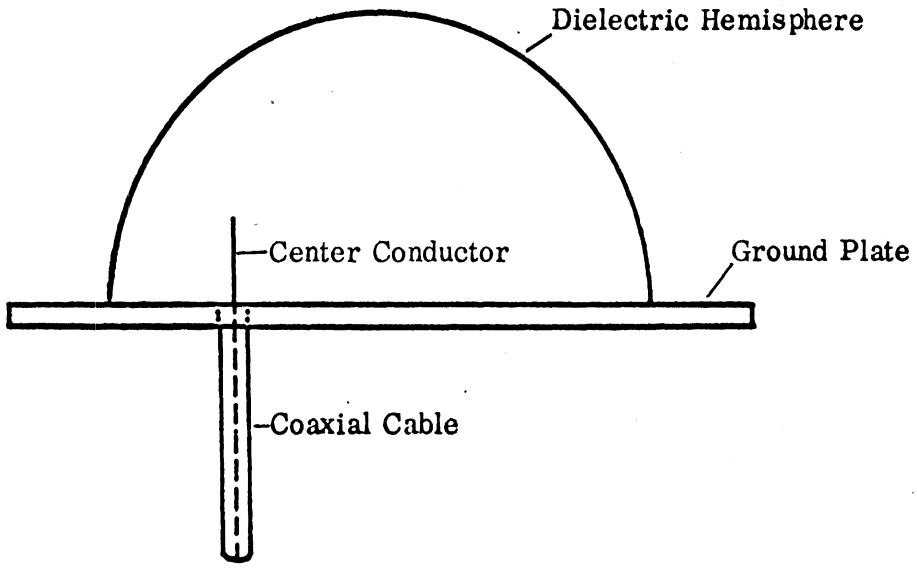

FIG. 9-2: PROPOSED ANTENNA FOR EXPERIMENTAL STUDY.

REFERENCES

Abrahamowitz, M. and I.A. Stegun (Eds.) (1964), Handbook of Mathematical Functions, NBS Appl. Math. Series No. 55.

Assaly, R.N. (1958), "Experimental Investigation of a Homogeneous Dielectric Sphere as a Microwave Lens," Can. J. Phys., 36, 1430-1435.

Barrick, D.E. (1970), "Spheres," in Radar Cross Section Handbook, Vol. 1 (G.T. Ruck, ed.), Plenum Press, New York, 141-204.

Bekefi, G. and G.W. Farnell (1956), "A Homogeneous Dielectric Sphere as a Microwave Lens," Can. J. Phys., 34, 790-803.

Born, M. and E. Wolf (1970), Principles of Optics, 4th Ed., Pergamon Press, London.

Cheston, T.C. and E.J. Luoma (1963), "Constant -k Lenses," APL Technical Digest, March-April.

Croswell, W.F. and J.S. Chatterjee (1972), "Waveguide Excited Dielectric Spheres as Feeds," Trans. IEEE, AP-20, 206-208.

Harrington, R.F. (1961), Time-Harmonic Electromagnetic Fields, McGraw-Hill, New York.

Inada, H. and M.A. Plonus (1970), "The Geometric Optics Contribution to the Scattering from a Large Dense Dielectric Sphere," Trans. IEEE, AP-18, 89-99.

Inada, H. and M.A. Plonus (1970), "The Diffracted Field Contribution to the Scattering from a Large Dense Dielectric Sphere," Trans. IEEE, AP-18, 649-660.

Jasik, H. (1961), Antenna Engineering Handbook, McGraw-Hill, New York.

Johnson, R.C. (1964), "Optical Scanners," in Microwave Scanning Antennas, Vol. 1 (R.C. Hansen, ed.), Academic Press, New York, 213-261.

Kraus, J.D. (1950), Antennas, McGraw-Hill, New York.

Luneberg, R.K. (1944), The Mathematical Theory of Optics, Brown University Press, Providence, R.I.

Meinke, H.H. (1970), "Research on Antennas - Progress Report No. 8," Institut fur Hochfrequenztechnik der Technischen Hochschule Munchen, 61-90.

Papas, C.H. (1965), Theory of Electromagnetic Wave Propagation, McGraw-Hill, New York.

Ryan, C.E. and F.L. Cain (1971), "Design Considerations for Constant-Index Lenses," Abstracts of the 21st Annual Symposium USAF Antenna Research and Development Program, University of Illinois, Monticello, Ill.

Ryan, C.E. and F.L. Cain (1972), "Final Report on Contract F33615-71-C-1497," Georgia Institute of Technology, Atlanta, Georgia.

Schelkunoff, S.A. (1943), Electromagnetic Waves, D. van Nostrand Co., Inc., New York.

Schelkunoff, S.A. and H.T. Friis (1952), Antennas: Theory and Practice, Wiley, New York.

Silver, S. (1963), Microwave Antenna Theory and Design, MIT Rad. Lab. Series, Boston Technical Lithographers, Inc., Lexington, Mass.

Smythe, W.R. (1950), Static and Dynamic Electricity, McGraw-Hill, New York.

Stratton, J.A. (1941), Electromagnetic Theory, McGraw-Hill, New York.

Tai, C.T. (1947), "Radiation of a Hertzian Dipole Immersed in a Dissipative Medium," Harvard University Cruft Laboratory Technical Report No. 21.

Tai, C.T. (1958), "The Electromagnetic Theory of the Spherical Luneberg Lens," Appl. Sci. Res., B7, 113-130.

Tai, C.T. (1971), Dyadic Green's Functions in Electromagnetic Theory, Intext, Scranton, Pa.

von Hippel, A.R. (1954), Dielectric Materials and Applications, Tech. Press of MIT and Wiley, New York.

Appendix A

EVALUATION OF $\left[\rho j_n(\rho)\right]' h_n(\rho) - \left[\rho h_n(\rho)\right]' j_n(\rho)$

Let $z_1(\rho)$ and $z_2(\rho)$ be two spherical Bessel functions which are particular solutions to the differential equation

$$\rho^2 z'' + 2\rho z' + \left[\rho^2 - n(n+1)\right] z = 0 \tag{A.1}$$

Since

$$\rho^2 z'' = \rho(\rho z)'' - 2\rho z'$$

(A. 1) may be in the form

$$\rho(\rho z_1)'' + \left[\rho^2 - n(n+1)\right] z_1 = 0 \tag{A.2}$$

$$\rho(\rho z_2)'' + \left[\rho^2 - n(n+1)\right] z_2 = 0 \quad . \tag{A.3}$$

On multiplying (A. 2) and (A. 3) by z_2 and z_1, respectively, and subtracting, it is found

$$\rho z_2(\rho z_1)'' - \rho z_1(\rho z_2)'' = 0 \quad . \tag{A.4}$$

We next form the integral

$$\int \left[\rho z_2(\rho z_1)'' - \rho z_1(\rho z_2)''\right] d\rho = 0 \tag{A.5}$$

and integrate by parts yielding

$$\rho^2 z_2 z_1' - \rho^2 z_1 z_2' = c \tag{A.6}$$

where c is a constant.

Letting $z_2 = h_n(\rho)$ and $z_1 = j_n(\rho)$, where $h_n(\rho) = j_n(\rho) + iy_n(\rho)$, (A. 6) becomes

$$\rho^2 j_n(\rho)' h_n(\rho) - \rho^2 h_n(\rho)' j_n(\rho) = c \quad . \tag{A.7}$$

Taking the limit as $\rho \longrightarrow 0$,

$$c = -i .$$

Using this result together with the relations

$$\rho j_n(\rho)' = \left[\rho j_n(\rho)\right]' - j_n(\rho)$$

$$\rho h_n(\rho)' = \left[\rho h_n(\rho)\right]' - h_n(\rho)$$

in (A.7) yields the result

$$\left[\rho j_n(\rho)\right]' h_n(\rho) - \left[\rho h_n(\rho)\right]' j_n(\rho) = -\frac{i}{\rho} . \qquad \text{(A.8)}$$

Appendix B

COMPUTER PROGRAM

Although numerous computer programs were used throughout this research, the one of primary significance, together with the necessary subroutines, is listed in this appendix. This program was written in standard IBM FORTRAN IV for use with the G level compiler, and was run on an IBM System 360/67 computer.

The MAIN program calculates and prints out the normalized far-zone radiation patterns (magnitude, phase, and intensity in dB) in the two principal planes for a Huygens' source on the surface or inside a lossy dielectric sphere. It also prints the coefficients of the $\bar{m}$ and $\bar{n}$ functions, the directivity, and provides the pattern data (truncated to -40 dB) in an array suitable for plotting. This program may easily be modified to compute data for only the electric or magnetic current source, or for the case where the source lies outside the dielectric sphere, by making the appropriate changes in the coefficient formulas of lines 35 to 39.

The input parameters to the MAIN program are defined as follows.

DIAM	Sphere diameter (λ_0)
PER	Dielectric constant
TAN	Dielectric loss tangent (X1000)
SP	Distance from source to sphere surface (λ_0)
THINC	Increment in θ variable (degrees).

Note: The parameter THINC should divide evenly into 180 degrees. If THINC = 1, for example, data is calculated from $\theta = 0$ to $\theta = 180$ in one-degree intervals.

Subroutine ASLEG is used to generate arrays of associated Legendre functions of the first order and their derivatives. The parameters are as follows:

NMAX	Maximum value of degree (N) desired
THINC	Increment in θ variable (degrees). See note above.

SLEGEN, DLEGEN — The names of single precision two-dimensional arrays in which the output functions are returned:

$$\text{SLEGEN}(N,M) = \frac{P_N^1(\cos M)}{\sin M}$$

$$\text{DLEGEN}(N,M) = \frac{\partial P_N^1(\cos M)}{\partial M} \quad ,$$

where $M = (N-1)\text{THINC}$.

Subroutine CBESS generates arrays of spherical Bessel and Hankel functions of complex arguments and their derivatives. The parameters are as follows.

BES, DBES, HANK, DHANK — Names of single-precision complex arrays in which the output functions are returned:

$$\text{BES}(N) = j_{N-1}(X)$$

$$\text{DBES}(N) = \frac{\partial}{\partial X}\left[X j_{N-1}(X)\right]$$

$$\text{HANK}(N) = h_{N-1}^{(1)}(X)$$

$$\text{DHANK}(N) = \frac{\partial}{\partial X}\left[X h_{N-1}^{(1)}(X)\right]$$

X — Double precision complex argument.

NMAX — Maximum value of order (N) desired.

Double precision arithmetic is used throughout these subroutines, with the final output converted to single precision.

```
C   ********** MAIN PROGRAM**********
C
      DIMENSION DLEGEN(45,181),R1(181),R2(181),TH(181),EHMAX(2)
      DOUBLE PRECISION SLEGEN(45,181)
      COMPLEX ANPN(181),BNPN(181),ANDPN(181),BNDPN(181),EH(181,2),B1(45)
     2,DB1(45),B2(45),DB2(45),B3(45),DB3(45),H1(45),DH1(45),H2(45),
     3DH2(45),H3(45),DH3(45),AN,BN,CNA,I,AX,ANA,BNA,SER,CER,DN
      COMPLEX*16 RO1,RO2,RO3
    1 READ 500,DIAM,PER,TAN,SP,THINC
      LK=2
      X=.0001*TAN
      PI=3.14159265358979
      CONV=180./PI
      I=(0.,1.)
      MA=180./THINC+1
      CER=PER*(1.+I*X)
      SER=CSQRT(CER)
      RO1=DIAM*PI
      RK1=RO1
      RO2=SER*RO1
      RO0=RO2
      RO3=(DIAM-2.*SP)*PI*SER
C  RO1=K1A,RO2=K2A,RO3=K2B
      NMAX=2.*RO1+6.5
      NSUM=NMAX+1
      CALL ASLEG(NSUM,THINC,SLEGEN,DLEGEN)
      CALL CBESS(B1,DB1,H1,DH1,RO1,NMAX)
      CALL CBESS(B2,DB2,H2,DH2,RO2,NMAX)
      CALL CBESS(B3,DB3,H3,DH3,RO3,NMAX)
      SDAV=0.
      DO 20 J=1,MA
      ANPN(J)=0
      BNPN(J)=0
      ANDPN(J)=0
      BNDPN(J)=0
   20 CONTINUE
```

```
0032            PRINT 200
0033            DO 22 N=1,NMAX
0034            M=N+1
0035            ANA=-I/(RO2*(H1(M)*DB2(M)-DH1(M)*B2(M)))
0036            BNA=-I/(RO2*(H1(M)*DB2(M)/SER-SER*DH1(M)*B2(M)))
0037            CNA=B3(M)-I*DB3(M)/RO3
0038            BN=-BNA*CNA
0039            AN=ANA*CNA
C   AN AND BN ARE THE COEFFICIENTS OF THE M AND N FUNCTIONS.
0040     21     CONTINUE
0041            PRINT 198,AN,BN
0042            Y=N
0043            AX=((2.*Y+1.)/(Y*(Y+1.)))*(0.-I)**N
0044            BX=(2*Y+1.)/2.
0045            SDAN=SDAN+BX*(CABS(AN)**2+CABS(BN)**2)
C   SDAN IS THE DENOMINATOR OF THE DIRECTIVITY EXPRESSION
0046            DO 22 L=1,MA
0047            ANPN(L)=ANPN(L)+AX*SLEGEN(N,L)*AN
0048            BNPN(L)=BNPN(L)+AX*SLEGEN(N,L)*BN
0049            ANDPN(L)=ANDPN(L)+AX*DLEGEN(N,L)*AN
0050            BNDPN(L)=BNDPN(L)+AX*DLEGEN(N,L)*BN
0051         22 CONTINUE
0052            DO 25 K=1,2
0053         25 EHMAX(K)=0
0054            DO 50 L=1,MA
0055            EH(L,1)=ANPN(L)+BNDPN(L)
0056            EH(L,2)=-ANDPN(L)-BNPN(L)
0057            DO 50 K=1,2
0058         40 EHMAX(K)=AMAX1(EHMAX(K),CABS(EH(L,K)))
0059         50 CONTINUE
0060            DIRH=10.*ALOG10((CABS(EH(MA,1))**2)/SDAN)
0061            DO 55 K=1,2
0062            DO 55 L=1,MA
0063         55 EH(L,K)=EH(L,K)/EHMAX(K)
0064            PRINT 302,DIAM,PER,RK1,ROO,N,X
0065            PRINT 305
```

```
0066            PRINT 303,SP
0067            PRINT 304,DIRH,LK
0068            DO 75 L=1,MA
0069            ANGLE=(L-1)*THINC
0070            TH(L)=ANGLE
0071            AMAG1=CABS(EH(L,1))
0072            AMAG2=CABS(EH(L,2))
0073            ANG1=ATAN2(AIMAG(EH(L,1)),REAL(EH(L,1)))*CONV
0074            ANG2=ATAN2(AIMAG(EH(L,2)),REAL(EH(L,2)))*CONV
0075            R1(L)=20.*ALOG10(AMAG1)
0076            R2(L)=20.*ALOG10(AMAG2)
0077            PRINT 310,ANGLE,AMAG1,ANG1,R1(L),ANGLE,AMAG2,ANG2,R2(L)
0078            IF (R1(L).LT.-40.) R1(L)=-40.
0079            IF (R2(L).LT.-40.) R2(L)=-40.
0080          75 CONTINUE
0081          77  PRINT 213,EHMAX(1),EHMAX(2)
0082          100 CONTINUE
0083            WRITE(10,114) MA,(R1(L),R2(L),L=1,MA)
              C  THIS STATEMENT PRINTS ON DEVICE 10 THE NUMBER OF POINTS TO BE
              C *PLOTTED AND THEN THE E- AND H-PLANE INTENSITY ARRAYS.
0084            GO TO 1
0085          114 FORMAT(I4,(24F10.4))
0086          302 FORMAT('1',21X,'NORMALIZED FAR ZONE ELECTRIC FIELD FROM SOURCE LOC
                 1ATED ON SURFACE OF DIELECTRIC SPHERE'/'0***** SOURCE: HUYGEN
                 2        DIAMETER IN WAVELENGTHS: ',F6.3,5X,'DIELECTRIC CONSTANT: '
                 3,F6.3/52X,'AIR KA: ',F6.3,11X,'DIELECTRIC KA: ',F6.3/
                 4                          28X,'NUMBER OF TERMS USED IN SERIES: ',I2,19X
                 5,'LOSS TAN: ',F8.6)
0087          303 FORMAT(17X,'SOURCE DISTANCE FROM SPHERE IN WAVELENGTHS: ',F7.4)
0088          305 FORMAT(52X,'SOURCE INSIDE SPHERE SURFACE')
0089          304 FORMAT(              //, 6X,'PHI: 0 DEGREES     ',46X,'PHI: 90 DEGREES
                 6    DIRECTIVITY: ',F6.3,' DB'/'0       THETA      ELECTRIC FIELD
                 7 INTENSITY          ',16X,'THETA      ELECTRIC FIELD      INTENSITY
                 8         '/'     (DEGREES)  MAGNITUDE  ANGLE         (DB)
                 9',12X,'(DEGREES)  MAGNITUDE  ANGLE ',7X,'(DB)              ',3X,I2)
0090          310 FORMAT(5X,2(F7.2,2X,E10.4,1X,F7.2,3X,F9.3,24X))
```

```
0091          198 FORMAT(10X,2E12.4,5X,2E12.4,5X,2E12.4,5X,2E12.4)
0092          200 FORMAT('0',14X,'M COEFFICIENT',14X,'N COEFFICIENT',/15X,'REAL',6X,
             1'IMAGINARY',10X,'REAL',6X,'IMAGINARY')
0093          213 FORMAT('0NORMALIZATION CONSTANT: ',E12.4,36X,'NORMALIZATION CONSTA
             1NT: ',E12.4)
0094          500 FORMAT(5E10.3,I1)
0095              END
```

```
0001            SUBROUTINE ASLEG(NMAX,THINC,SLEGEN,DLEGEN)
                C
0002            DIMENSION DLEGEN(45,181)
0003            DOUBLE PRECISION SLEGEN(45,181),X,TH,RAD,CONV,PI
0004            MMAX=180./THINC
0005            MA=MMAX+1.
0006            PI=3.14159265358979
0007            CONV=PI/180.
0008            RAD=THINC*CONV
0009            DO 10 N=1,NMAX
0010            A=N
0011            SLEGEN(N,1)=A*(A+1.)/2.
0012            DLEGEN(N,1)=SLEGEN(N,1)
0013            DLEGEN(N,MA)=A*(A+1.)/2.*(-1)**N
0014            SLEGEN(N,MA)=-DLEGEN(N,MA)
0015         10 CONTINUE
0016            DO 20 M=2,MMAX
0017            L=M-1
0018            TH=L*RAD
0019            X=DCOS(TH)
0020            SLEGEN(1,M)=1.
0021            DLEGEN(1,M)=X
0022            SLEGEN(2,M)=1.5*DSIN(2.*TH)/DSIN(TH)
0023            DLEGEN(2,M)=3.*DCOS(2.*TH)
0024            DO 20 N=3,NMAX
0025            SLEGEN(N,M)=((2.*N-1)*X*SLEGEN(N-1,M)-N*SLEGEN(N-2,M))/(N-1)
0026            DLEGEN(N,M)=N*X*SLEGEN(N,M)-(N+1)*SLEGEN(N-1,M)
0027         20 CONTINUE
0028            RETURN
0029            END
```

```
0001            SUBROUTINE CBESS(BES,DBES,HANK,DHANK,X,NMAX)
                C
                C       INDEX IS ONE GREATER THAN ORDER OF THE FUNCTION
0002            COMPLEX BES(1),DBES(1),HANK(1),DHANK(1),I
0003            COMPLEX*16 X,JO,J(90),P,Y(75)
0004            I=(0.,1.)
0005            NN=NMAX+16
0006            NO=NN-1
0007            NP=NN-2
0008            NQ=NMAX+1
0009            NR=NMAX+2
0010            J(NN)=(0.,0.)
0011            J(NO)=(1.,1.)
0012            JO=CDSIN(X)/X
0013            Y(1)=-CDCOS(X)/X
0014            Y(2)=Y(1)/X-JO
0015            DO 10 M=1,NP
0016            N=NO-M
0017         10 J(N)=(2*(N-1)+3)*J(N+1)/X-J(N+2)
0018            DO 12 N=3,NR
0019         12 Y(N)=((2*(N-1)-1)/X)*Y(N-1)-Y(N-2)
0020            P=JO/J(1)
0021            BES(1)=J(1)*P
0022            HANK(1)=BES(1)+I*Y(1)
0023            DO 20 L=1,NQ
0024            K=L+1
0025            BES(K)=J(K)*P
0026            HANK(K)=BES(K)+I*Y(K)
0027            DBES(L)=L*BES(L)-X*BES(K)
0028         20 DHANK(L)=L*HANK(L)-X*HANK(K)
0029            RETURN
0030            END
```